UNIVERSIDADE DE LISBOA
FACULDADE DE CIÊNCIAS
DEPARTAMENTO DE QUÍMICA E BIOQUÍMICA

Modulation of Calcitonin Amyloid Formation by Anionic Lipid Membranes

Paulo Renato dos Santos Caldas

Dissertação

Mestrado em Bioquímica

Especialização em Bioquímica Médica

2014

UNIVERSIDADE DE LISBOA
FACULDADE DE CIÊNCIAS
DEPARTAMENTO DE QUÍMICA E BIOQUÍMICA

Modulation of Calcitonin Amyloid Formation by Anionic Lipid Membranes

Paulo Renato dos Santos Caldas

Dissertação

Mestrado em Bioquímica

Especialização em Bioquímica Médica

Orientador

Professora Doutora Ana Coutinho

2014

Knowledge, like air, is vital to life.
Like air, no one should be denied it.

Alan Moore

FOREWORD

This dissertation describes the work performed under the supervision of Dr. Ana Coutinho at the Biological Fluorescence group from Centro de Química-Física Molecular (CQFM)/Instituto de Nanociência e Tecnologia (IN) at Instituo Superior Técnico (IST) in Lisbon, from September 2013 to September 2014.

The studies presented here were targeted on elucidating the interaction mechanism of both salmon and human calcitonin polypeptides with anionic lipid membranes. This work was performed under the framework of the project "Modulation of calcitonin amyloid formation by lipid membranes and extracellular matrix: implications for the mechanism of cytotoxicity of amyloidogenic polypeptides" (Project PTDC/BBB-BQB/2661/2012) financed by Fundação para Ciência e Tecnologia (FCT) from Ministério da Educação e Ciência. Paulo Renato dos Santos Caldas was the recipient of a research fellowship.

ACKNOWLEDGMENTS

I take this opportunity to express my sincere gratitude to my mentor and supervisor Dr. Ana Coutinho for accepting me in this project, for sharing her knowledge with me and for the time and attention that she gives to her students every day. Together with Professor Manuel Prieto, his great humour and willingness, they gave a superb and relaxed environment in the laboratory and offered me freedom to plan my own experiences, which gave me enthusiasm and confidence in my work. I am really thankful to both of them for their constant support and encouragement.

I would also like to thank to my colleague and friend Joana Ricardo who has helped me in learning the experimental procedures in the laboratory and how to work with all kind of apparatus during my initial days of research. I want to give a word of appreciation to Dr. Aleksander Fedorov for his help with the time-resolved fluorescence measurements, and his patience with the "new guy", and to thank my colleagues Tânia Sousa, Maria João Sarmento, Marina Monteiro, Fábio Fernandes, Raquel Varela and of course my great friend Samuel Jacob for the outstanding environment created on the work place and for the hilarious coffee breaks we had during this year.

As it should be, I want to thank my parents, Isabel and Paulo, my sister Renata and my brother-in-law Tiago, for their support during these last five years, for never questioning my decisions and objectives and for helping me in everything they could. And a special thanks to my beautiful lady Rita Garcia, for her love, constructive suggestions and patience to my evening schedules and little time for everything.

Finally, but not the least, I want to thank all my friends and colleagues who have accompanied me through these five years of biochemistry. They made this journey a fantastic and unforgettable experience. I cannot name everyone, but each of them was important from time to time. Especially, I need to give a huge and very special acknowledgment to my two friends and partners Denys Holovanchuk and Samuel Jacob for their combined friendship, intellect and joking in all works and projects developed during these last five years. My success in this journey would not have been the same without both of them. It is a privilege when our colleagues are also our best friends. I thank you all for everything.

To finish, I dedicate this thesis to the memory of my grandparents, who always helped me more than they could and I know they would give anything to be here right now.

ABSTRACT

Recent studies have suggested that biological membranes can stimulate the pathological conversion of amyloidogenic proteins/peptides into toxic aggregates by providing a soft surface that can promote their misfolding and self-assembly. These interactions can be controlled by a range of biophysical features arising from the specific lipid composition of the membrane. In this work, both salmon and human calcitonins (sCT and hCT) were used as model polypeptides to study the role that negatively-charged lipid membranes can play in modulating their aggregation pathway. Specifically, a multi-parametric study based on steady-state and time-resolved fluorescence intensity and anisotropy measurements was carried out to study the interaction of both unlabelled and HiLyte Fluor 488-labelled sCT and hCT polypeptides (sCT-HL488 and hCT-HL488, respectively) with liposomes prepared with a variable anionic lipid content.

The influence of a small set of solvents, namely several aliphatic and fluoro alcohols, on the photophysical properties of both the free HL488 dye and both HL488-labeled CT variants was first characterized. The changes in the fluorescence intensity decay kinetics displayed by the fluorescently-labelled peptides with the solvent used were assigned to an intramolecular photon-induced electron transfer mechanism dependent on the conformational dynamics of the polypeptide chain. In the second part of this work, the interaction of sCT-HL488 with lipid membranes was found to be critically dependent on the method used to prepare the samples (direct injection vs solvent evaporation). CT binding to liposomes was also established to be dominantly driven by electrostatic interactions. Furthermore, a coupled partition/oligomerization model was used to describe the biphasic fluorescence intensity data obtained when high sCT-HL488 concentrations were used in the partition studies. The excitonic band detected in the absorption spectra of sCT-HL488 at a high P/L molar ratio (low phospholipid concentrations) revealed the formation of parallel (H-type) dimers between the HL488 chromophores covalently linked to sCT, which were non-fluorescent.

Keywords

Salmon Calcitonin, Human Calcitonin, Hilyte Fluor 488, Fluorescence spectroscopy, Amyloid fibril formation, Lipid-protein-interaction, Membrane model system

RESUMO DO TRABALHO

A acumulação *in vivo* de agregados proteicos insolúveis, genericamente designados por fibras amilóides, são o principal fenótipo de várias doenças graves categorizadas como patologias amilóides, onde se incluem a doença de Alzheimer, Parkinson e diabetes Mellitus tipo II. Estas doenças representam um problema de saúde alarmante a nível mundial pelo que há um interesse clínico urgente e significativo em compreender os factores que desencadeiam a formação destas estruturas para se poder desenvolver meios farmacológicos adequados que possam diminuir, ou atenuar, estas patologias. A maioria destas doenças são predominantemente esporádicas e resultam de problemas no *folding* de proteínas específicas que levam à sua agregação, e consequente formação de depósitos/placas, criando condições patológicas em determinados tecidos humanos. Deste modo, uma das chaves fundamentais para se perceber o desenvolvimento destas doenças reside no estudo dos mecanismos moleculares que levam ao *misfolding* e agregação destas proteínas *in vitro*.

Estudos recentes mostraram que o estabelecimento de interacções lípido-péptido/proteína podem induzir um decréscimo na barreira de energia associada ao *unfolding* proteico, conduzindo à destabilização da estrutura nativa das proteínas/péptidos, e consequente *misfolding*. Com efeito, tem sido demonstrado que as membranas biológicas são capazes de promover a conversão de proteínas/péptidos em agregados tóxicos actuando como catalisadores do seu processo de fibrilhação, dependendo da composição lipídica da membrana (características estruturais dos seus lípidos componentes). No entanto, os mecanismos detalhados através dos quais a acumulação destes agregados compromete a integridade das membranas lipídicas ainda permanecem por esclarecer.

Uma importante linha de investigação desenvolvida ao longo dos últimos anos no laboratório de acolhimento tem estado, precisamente, focada no estudo dos mecanismos que podem levar à formação de estruturas amilóides desencadeados pelo estabelecimento de interacções entre proteínas não amiloidogénicas e membranas carregadas negativamente, sob condições próximas das fisiológicas. O objectivo deste trabalho, que visou dar continuidade a este tópico, centrou-se no uso da calcitonina (CT) como polipéptido modelo para se estudar a capacidade das membranas lipídicas aniónicas em modularem a sua via de agregação em solução. Neste estudo foram empregues ambas as variantes humana (hCT) e de salmão (sCT) desta hormona polipeptídica.

A CT é uma hormona com 32 resíduos de aminoácidos libertada pela glândula tiróide e que tem um papel importante no metabolismo do cálcio, sendo por isso administrada no tratamento da osteoporose e hipercalcemia. Nos últimos anos, a variante humana da calcitonina (hCT) tem sido cada vez menos utilizada neste tipo de tratamentos devido à sua tendência elevada em formar agregados que podem conduzir, eventualmente, à formação de depósitos de placas amilóides. Recentemente, a calcitonina de salmão (sCT) tem sido usada como uma alternativa clínica à hCT devido à sua maior potência farmacológica e menor tendência em sofrer agregação. Com efeito, a hCT é geralmente considerada um péptido amiloidogénico, o que a torna um modelo peptídico ideal para este tipo de estudo. Por outro lado, a sCT é útil devido ao facto de sua cinética de fibrilhação em solução ser muito mais lenta do que a da hCT permitindo, eventualmente, estudar em detalhe estados intermediários da cinética.

Neste trabalho, os polipéptidos sCT e hCT foram utilizados quer na sua forma nativa (não derivatizada), quer conjugados com o fluoróforo HiLyte Fluor 488 (HL488) nos seus resíduos *N*-terminal (hCT-HL488 e sCT-HL488, respectivamente). A escolha desta posição de derivatização da CT visou minimizar a possibilidade de o fluoróforo conjugado interferir na formação de estruturas β, já que é conhecido que esta envolve a sequência *C*-terminal destes polipéptidos (resíduos 25-32). Deste modo, através da realização de medidas de fluorescência em estado estacionário e resolvidas no tempo, com o fim de caracterizar as propriedades de emissão de fluorescência intrínsecas e extrínsecas destes polipéptidos, procurou-se obter informação sobre (i) o seu estado de agregação em solução, e (ii) sobre o modo como a sua interacção com lipossomas era condicionada pela sua composição lipídica, nomeadamente pelo seu conteúdo em fosfolípidos aniónicos.

Os estudos de partição foram realizados utilizando-se vesículas unilamelares grandes (LUVs) como sistema modelo de membranas, preparadas com uma composição lipídica variável, nomeadamente misturas de 1-palmitoil-2-oleoil-*sn*-glicero-3-fosfocolina (POPC), um fosfolípido *zwitteriónico*, com 0, 10, 20 ou 30 mol% de 1-palmitoil-2-oleoil-*sn*-glicero-3-fosfoserina (POPS), um fosfolípido aniónico. Este tipo de vesiculas têm sido maioritariamente usadas para estudar interacções de péptidos com as membranas devido ao seu tamanho adequado (100 nm) e grau de curvatura, por comparação com outros sistemas vesiculares como, por exemplo, as vesículas unilamelares pequenas (SUVs) e gigantes (GUVs).

Numa primeira fase do trabalho, explorou-se a fluorescência intrínseca da sCT e hCT devida à presença de um resíduo de tirosina na estrutura primária de cada uma destas formas de calcitonina (Tyr22 e Tyr12, respectivamente). Foi realizada uma caracterização espectroscópica sumária das suas propriedades de emissão de fluorescência em solução tampão e efectuou-se ainda um estudo da sua partição para LUVs de POPC contendo 20 mol% de POPS através da monitorização da sua anisotropia de fluorescência em estado estacionário. Após se ter minimizado experimentalmente o impacto da dispersão da radiação (*scattering*) causada pelas suspensões de lipossomas no valor deste parâmetro, recuperou-se um valor de $K_p = (5.5 \pm 0.3)\text{x}10^5$ para a sCT. Curiosamente, a variante humana, hCT, não mostrou qualquer tipo de interacção com os lipossomas preparados com uma composição lipídica idêntica, não havendo variações significativas em nenhum dos parâmetros espectroscópicos estudados com o aumento da concentração de fosfolípido no sistema.

Este tipo de metodologia oferece a vantagem de não ser necessário usar fluoróforos extrínsecos ligados covalentemente à sequência peptídica, o que pode causar perturbações na estrutura nativa em solução. Contudo, a fluorescência intrínseca de ambas as variantes CT é pouco eficiente devido aos baixos coeficientes de absorção molar e rendimentos quânticos dos seus resíduos de Tyr, tornando a realização de medidas de fluorescência na presença de vesiculas lipídicas problemática uma vez que, aos comprimentos de onda usados, estas provocam um elevado nível de *scatter* no sistema. Por outro lado, as propriedades espectroscópicas deste fluoróforo intrínseco das proteínas são ainda caracteristicamente pouco sensíveis a pequenas alterações na polaridade do seu microambiente directo.

Deste modo, o trabalho prosseguiu com o estudo das duas variantes de calcitonina derivatizadas, sCT-HL488 e hCT-HL488, respectivamente. Devido ao facto de a sonda fluorescente utilizada ter sido comercializada recentemente, não há muita informação disponível na literatura. A segunda fase do trabalho iniciou-se então com a realização de um estudo da variação das propriedades espectroscópicas da sonda livre HL488 e de ambas as variantes CT derivatizadas numa série de solventes para apurar o seu comportamento em meio homogéneo em função das propriedades do solvente. Neste estudo, foi usada uma variedade de álcoois com diferentes tamanhos de cadeia alifática (metanol, etanol, propanol, butanol) e fluoro álcoois (trifluoroetanol (TFE) e hexafluoroisopropanol (HFIP)), além de soluções tampão preparadas com força iónica variável.

Relativamente à sonda livre, os seus espectros de absorção e de emissão de fluorescência apresentaram um desvio batocromático progressivo com a diminuição da constante diéletrica dos álcoois alifáticos estudados. Contudo, na presença dos dois fluoro álcoois, ambos os espectros da sonda livre apresentaram um desvio hipsocromático significativo relativamente ao seu comportamento em solução aquosa, o que poderá ser devido à capacidade conhecida destes solventes em estabelecerem pontes de hidrogénio. Por outro lado, a sonda apresentou sempre um decaimento de intensidade de fluorescência mono-exponencial, com um tempo de vida próximo de 3.9ns em todos os solventes estudados, excepto em glicerol. A medição de espectros de emissão resolvidos no tempo (TRES) confirmou que os decaimentos complexos apresentados pelo fluoróforo livre em glicerol eram devidos a um efeito de relaxação do solvente devido à sua viscosidade elevada. Ainda nesta fase, o espectro de excitação da anisotropia em estado estacionário da sonda foi medido em glicerol para se obter o valor da sua anisotropia fundamental em função do comprimento de onda de excitação. Com os dados obtidos, foi possivel (i) concluir que os momentos dipolares das transições $S_1 \leftarrow S_o$ e $S_2 \leftarrow S_o$ da sonda HL488 estão orientados perpendicularmente entre si, e (ii) prever assim o impacto da necessidade de se usar diferentes comprimentos de onda de excitação nas medidas de anisotropia em estado estacionário e resolvidas no tempo nos estudos que foram realizados posteriormente.

O comportamento obtido para a variação das propriedades espectrais de ambos os péptidos derivatizados com o solvente usado foi muito idêntica à descrita anterioremente para a sonda livre HL488. No entanto, os péptidos sCT-HL488 e hCT-HL488 apresentaram agora um decaimento de intensidade de fluorescência complexo na maioria dos solventes estudados, embora sempre com uma componente dominante com ~3.9ns (com contribuição variável para a intensidade de fluorescência total consoante o solvente). Este comportamento foi discutido em termos da possibilidade de ocorrência de um mecanismo de extinção de fluorescência (*quenching* estático ou dinâmico) da sonda usada devido a um processo de transferência electrónica fotoinduzida (PET) por possíveis resíduos de aminoácidos presentes no esqueleto polipeptídico das CTs. A conformação adoptada pelos polipéptidos, assim como as flutuações dinâmicas da cadeia polipeptídica, são altamente dependentes da polaridade e viscosidade do solvente, influenciando a eficiência dos mecanismos PET, que caracteristicamente decorrem do estabelecimento de interacções de curto alcance. Finalmente, constatou-se que o estado de agregação de ambos os péptidos em solução aquosa não variava numa gama alargada de concentrações (1nM to ~8μM) pois a sua anisotropia de fluorescência em estado estacionário era constante.

A redução da ponte persulfureto também não influenciou de modo dramático a dinâmica rotacional de ambos os polipéptidos derivatizados em solução aquosa, tendo-se concluído que estes adoptavam uma conformação relativamente compacta a partir da realização de medidas de anisotropia resolvidas no tempo.

Por último, os péptidos derivatizados foram usados em estudos de partição através da realização de medidas da sua fluorescência extrínseca em estado estacionário e resolvidas no tempo. Foi avaliado o impacto da concentração de péptido no sistema, assim como da composição lipídica das membranas: usaram-se lipossomas compostos por POPC com proporções variáveis de POPS (0, 10, 20 e 30 mol%), que foram adicionados a uma concentração fixa de sCT-HL488 ou hCT-HL488 em tampão HEPES-KOH, pH 7.4. Tal como se verificou nos estudos em que se explorou as propriedades de fluorescência intrínseca da hCT, não houve qualquer tipo de alteração espectral nas medidas de absorção UV-VIS ou emissão fluorescência, assim como na variação da anisotropia em estado estacionário, com o aumento da concentração de vesiculas de POPC:POPS 70:30 nos estudos realizados com o péptido humano (1μM hCT-HL488). Mesmo aumentando a carga negativa das vesiculas para 50% (POPC:POPS 50:50) não se observou qualquer interacção do péptido com as membranas. Mostrou-se assim que carga negativa promovida pelo POPS não é suficiente para desencadear uma ligação do péptido humano às membranas, e que os mecanismos de interacção descritos na literatura se devem provavelmente a variações na composição lipídica, como a inclusão de colesterol e/ou gangliósidos nas membranas, que têm a capacidade de potenciar as interacções membrana-péptido.

O mesmo desenho experimental, utilizando-se agora sCT-HL488 (0.2, 1μM e 3.4μM) mostrou um desvio para o vermelho no seu espectro de absorção UV-VIS com o aumento da concentração de vesiculas contendo proporções variáveis de POPS (10, 20 e 30 mol%) associado à mudança de polaridade do microambiente da sonda covalentemente ligada. Em concordância, o valor de anisotropia em estado estacionário e da anisotropia residual revelaram também um aumento em função da adição de vesiculas ao meio, revelando assim adsorção do péptido às membranas aniónicas. O coeficiente de partição estimado a partir da variação do valor de anisotropia em estado estacionário mostrou aumentar em função da percentagem de POPS presente nas vesiculas, indicando que as interacções electrostáticas são as principais responsáveis pela interacção membrana-péptido. Recuperou-se ainda um valor de $K_p = (3.1 \pm 0.2)\text{x}10^5$ e $K_p = (2.9 \pm 0.3)\text{x}10^5$ nos estudos realizados com 1.0 e 3.4μM de sCT-HL488, respectivamente, na interacção com vesiculas de POPC:POPS 80:20.

Sendo este valor muito semelhante ao valor recuperado anteriormente nos estudos com a fluorescência intrínseca, é um indicativo de que a ligação da sonda ao péptido não altera significativamente a sua partição para as membranas.

A emissão de fluorescência em estado estacionário de 1 e 3.4μM de sCT-HL488 em interacção com LUVs de POPC contendo 20mol% de POPS mostrou um comportamento bifásico, com um decréscimo acentuado para ~80 e ~60%, respectivamente, do valor inicial em solução aquosa, quando baixas concentrações de lípido foram adicionadas ao sistema. Com o aumento da concentração de vesiculas em solução, o valor de emissão de fluorescência foi progressivamente recuperado. Concomitantemente, o valor médio do tempo de vida de sCT-HL488, para ambas as concentrações utilizadas, não variou significativamente com o aumento da concentração de lípido. Estes resultados mostraram que, para concentrações de péptido em solução elevadas (relativamente à concentração de vesiculas aniónicas), a sCT-HL488 sofre quenching estático, indicando a formação de complexos escuros na superfície membranar. Adicionalmente, foi ainda possível identificar o estabelecimento de interacções excitónicas (formação de agregados tipo H) sob as mesmas condições experimentais, corroborando a formação de agregados de sCT-HL488 na membrana.

Utilizando concentrações mais baixas de sCT-HL488 (0.2μM), observámos ainda que o método de preparação das amostras influenciava criticamente a sua cinética de interacção com as membranas lipídicas aniónicas. Apesar de debatida, a razão por detrás deste comportamento não foi completamente esclarecida.

Em resumo, mostrou-se que, apesar de a calcitonina humana não interactuar com membranas aniónicas, estas têm a capacidade de induzir a partição de sCT-HL488 acoplada a um mecanismo de oligomerização dependente da concentração de péptido e de lípido no sistema, como já descrito na literatura para outros tipos de péptido. Concentrações de péptido críticas levam à agregação de monómeros na superfície das membranas aniónicas que não são fluorescentes. A identificação deste tipo de intermediários oligoméricos pode ter um papel importante na via de fibrilhação da CT mediada por membranas e/ou contribuir directa ou indirectamente para a sua toxicidade celular.

Palavras-chave

Calcitonina de salmão, Calcitonina humana, Hilyte Fluor 488, Espectroscopia de fluorescência, Fibras Amilóides, Interacção lípido-proteína, Modelo de Membranas

TABLE OF CONTENTS

LIST OF ABBREVIATIONS/ACRONYMS

The acronyms used are expanded on first usage and whenever seemed necessary to improve clarity. Amino acid residues in the text are indicated using the three letter code, but primary sequences are indicated using the one-letter code to simplify.

AFM – Atomic Force Microscopy

Alexa 488 – Alexa Fluor 488

Aβ – Amyloid-β peptide

bCT- Bovine Calcitonin

CD – Circular Dichroism spectroscopy

CR – Congo Red

CT – Calcitonin

DLS - Dynamic Light Scattering

DOPC – 1,2-dioleoyl-sn-glycero-3-phosphocoline

DOPG – 1,2-dioleoyl-sn-glycero-3-phosphoglicerol

DPPC – 1,2-dipalmitoyl-glycero-3-phosphocoline

DPPG – 1,2-dioleoyl-sn-glycero-3-phosphoglycerol

DTT- Ditiotreitol

EDTA - Ethylenediamine-*N,N,N',N'*-tetraacetic acid

hCT – human calcitonin

hCT-HL488 – HL488-Labelled human calcitonin

HEPES – 4-(2-hydroxyyethyl)-1-piperazineethanesulfonic acid

HFIP - 1,1,1,3,3,3-hexafluoro-2-propanol

hIAPP – human islet amyloid polypeptide

HL488 – Hilyte fluor 488 dye

HPLC – High Pressure Liquide Chromatography

IAPP – Islet amyloid polypetide

IDP – intrinsically disordered proteins

IRF – Instrument Response Function

LUVs – Large Unilamellar Vesclies

MS – Mass Spectroscopy

NAYA - N-Acetyl-L-tyrosinamide

NDP – Nucleation Dependent Polymerization

NMR – nuclear magnetic resonance spectroscopy

PC – phosphatidycholine

PET – Photoinduced electron transfer

PG – phosphatigylglycerol

POPC - 1-Palmitoyl-2-oleoyl-*sn*-glycero-3-phosphocholine

POPS - 1-palmitoyl-2-oleoyl-*sn*-glycero-3-phosphoserine

PTH – parathyroid hormone

RT – Room Temperature

sCT – salmon calcitonin

sCT-HL488 - HL488-Labelled salmon calcitonin

TFE - 2,2,2-trifluorehtanol

Tht – Thioflavin T

TRES – Time Resolved Emission Spectra

TABLES LIST

Chapter II – Materials and Methods

Chapter III - Results and Discussion

Chapter I

Introduction

1. INTRODUCTION

The extracellular accumulation of insoluble aggregates of proteins/peptides generically designated as amyloid fibrils is a hallmark of a wide variety of devastating human disorders classified as protein misfolding or amyloid diseases (Chiti & Dobson 2006). These pathologies are widespread and include maladies like Alzheimer's disease, Type II diabetes Mellitus and Parkison disease, as well as other major conditions including Chronic Traumatic Encephalopathy and Huntington's disease (Nath & Rhoades 2013). These diseases represent a major health problem, which most probably will overwhelm the health systems of developed countries in the near future (Quintas 2013). Most of these so-called amyloid diseases are predominantly sporadic and result from defects in the conformational folding of specific proteins that leads to their pathological self-assembly and deposition, producing amyloid fibrils in the brain or in several other tissues (Chiti & Dobson 2006; Quintas 2013). There is therefore a urgent and significant clinical interest in understanding the factors that trigger the pathological self-assembly of amyloid proteins/peptides and in the development of pharmacological tools by which these diseases may be arrested or diminished, being the misfolding and aggregation of these proteins a key step in the development of these disorders.

1.1. PROTEIN FOLDING AND AMYLOIDOGENESIS

After synthesis of their primary sequence in the ribosome, newly synthesized proteins are packed via intramolecular contacts into their native structure acquiring a unique three-dimensional conformation (Figure 1.2). Protein folding is a complex process that does not follow a specific pathway but presents different routes towards the native structure, in which the global free energy progressively decreases with the adoption of a more ordered structure, reaching their energy minimum in the native three-dimensional conformation (Figure 1.1) (Hartl & Hayer-Hartl 2009). Thus, the pathway of protein folding consists of a series of sequential steps between increasingly native-like species, until the final native structure is formed. However, under some conditions proteins tend to expose their hydrophobic amino acid residues and do not fold correctly into their native structure, leading to misfolded states that can cause malfunctions and lead to the early mentioned amyloid diseases (Figure 1.2), This can be seen as a modification in the protein folding pathway according to the free energy landscape theory as illustrated in Figure 1.1.

The possible factors that might modulate the features of the protein free energy landscape are the amino acid sequence, pos-translational modifications, ligands, cofactors and environmental condition. Misfolded proteins are thermodynamically unstable and present a high tendency to aggregate (self-assemble) into amorphous aggregates that can evolve to highly ordered filamentous structures called amyloid fibrils. The term "amyloid" has been historically referred to misfolded proteins that deposit in tissues as filamentous structures (amyloid fibrils) due to their propensity to aggregate. Accumulating evidence leads support to the hypothesis that structural transformation of a polypeptide chain into a partially folded conformation is a critical prerequisite for fibril formation (Kelly 1998; Rochet & Lansbury 2000; Gorbenko & Kinnunen 2006), but this process can also occur from native-like conformations (Chiti & Dobson 2009). Complete protein unfolding does not appear to be necessary, but some structural flexibility is needed in order for aggregation to occur. However, protein aggregation is not promoted by the least ordered regions but by particular aggregation-prone sequences, such as those having a high hydrophobicity (Relini et al. 2013).

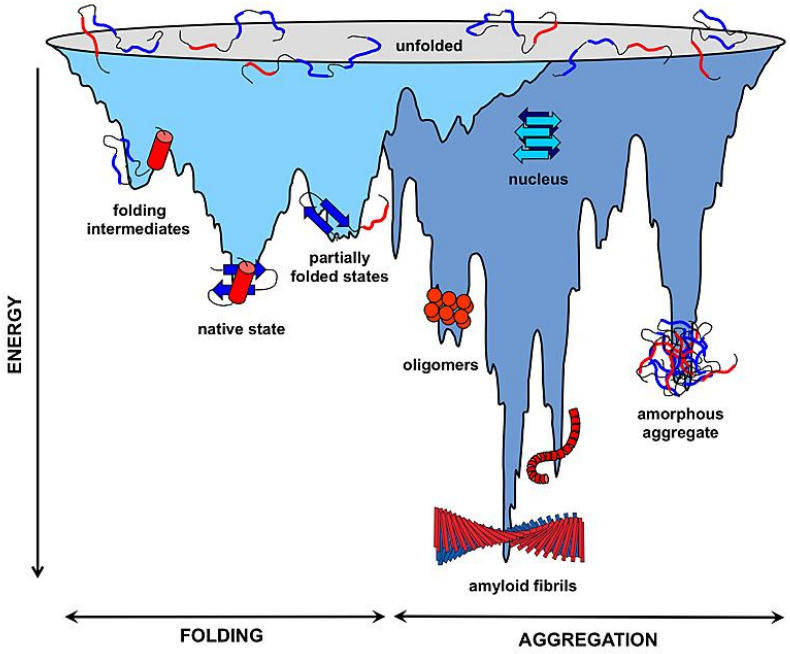

Figure 1.1: A schematic energy landscape for protein folding and aggregation. The surface shows the multitude of conformations 'funnelling' towards the native state via intramolecular contact formation, or towards the formation of amorphous aggregates or more organized amyloid fibrils via intermolecular contacts. [Adapted from (Jahn & Radford 2005)].

Several proteins implicated in amyloid diseases, such as Aβ peptides in Alzheimer's disease, amyloid islet protein (hIAPP) in Type II diabetes, and α-synuclein in Parkinson's disease, are intrinsically disordered proteins (IDPs) (Relini et al. 2013). Unlike globular proteins, the energy landscapes of IDPs do not show one deep local minimum but are much shallower with many minima without intrinsic large energy barriers (Uversky 2013). Thus these proteins can easily sample many conformations. As an example, kinetic studies on prokaryotic hydrogenase maturation factor (HypF-N) have shown that under slightly destabilizing conditions, where the protein is still predominantly in its native state, the population of molecules in a partially folded state increases, and it is this state that is responsible for increased aggregation under these conditions (Marcon et al. 2005). A variety of biophysical methods has provided experimental evidence that this intermediate is much more likely to aggregate than the native state (Rennella et al. 2013). These partially folded intermediates can thus act as links between folding and aggregation landscapes (Figure 1.1)

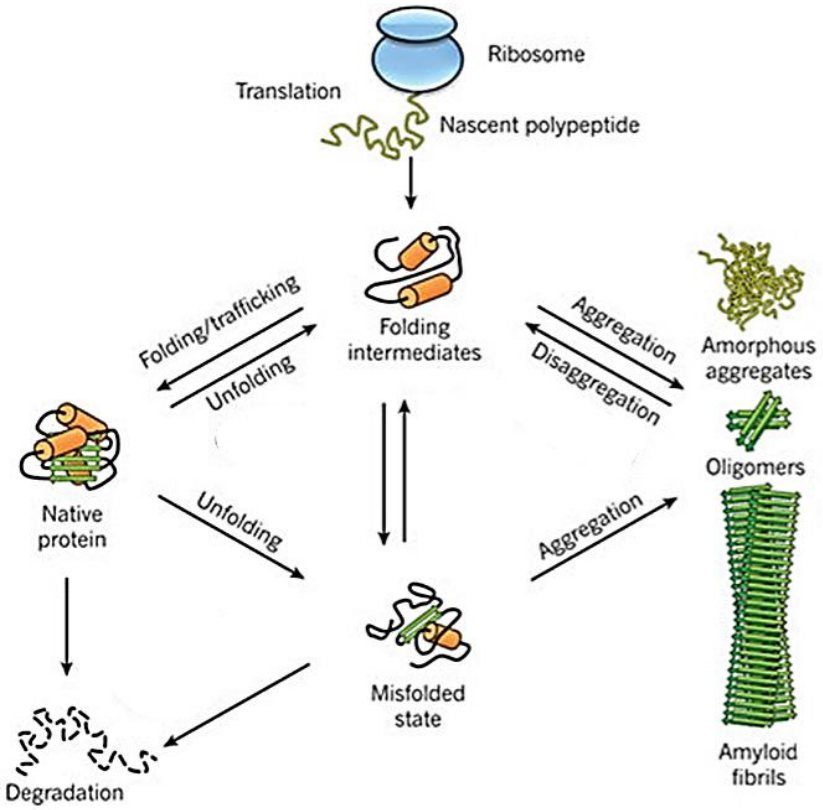

Figure 1.2: Schematic representation of some conformational states that can be adopted by polypeptide chains. Polypeptide chains evolve from an unfolded state to a native or misfolded state, but not all aggregated states should be denoted with an amyloid disease. Recently even functional fibers have been found in living systems. [Adapted from (Hipp et al. 2014)].

1.1.1. AMYLOID FIBRIL STRUCTURE

Until few years ago, there was a general agreement on the idea that only a limited number of proteins could form "amyloids". However it has recently been demonstrated that almost every protein has segments that can assemble into amyloid fibrils, so the ability to form these structures is not limited to proteins associated with conformational diseases (Gorbenko & Kinnunen 2006; Diociaiuti et al. 2011). All complex proteins have segments, with are typically six amino acids long, which can be exposed when a protein partly unfolds and promote its aggregation.

One of the striking characteristics of the amyloid diseases is that the filamentous structures formed are very similar in their overall properties (highly stable and insoluble) and appearance, forming a β-cross structure in which continuous β-sheets are formed with β-strands running perpendicular to the long axis of the fibril (Figure 1.3) (Jahn & Radford 2005; Chiti & Dobson 2006; Bellotti & Chiti 2008). Backbone hydrogen bonds are parallel to the axis and stabilize the overall structure. These structures are resistant to proteases and some molecular probes like Thioflavin T (ThT) and Congo Red (CR) can specifically bind to intermediates and mature amyloid fibrils (Ryan et al. 2008).

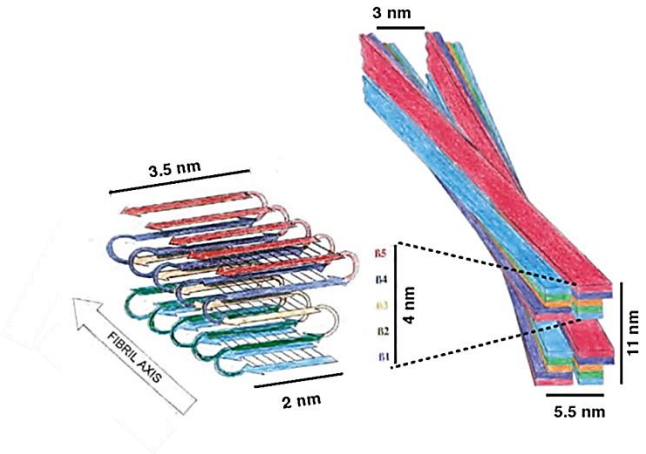

Figure 1.3: Representation of polypeptide chains in amyloid fibrils. Hydrogen bonds are formed between the parallel and anti-parallel polypeptide chain producing perpendicular twisted β-sheet chains along to the axis of the fibril. [Adapted from (Vilar et al. 2008)]

It is now generally agreed that the pathogenic aggregates are not the mature fibrils, but the intermediate soluble oligomers (Gorbenko & Kinnunen 2006; Diociaiuti et al. 2011). It has been proved that oligomers of different amyloid proteins not associated with any disease are also neurotoxic and share a surprising structural and functional similarity, suggesting that a shared structural feature of these is at the basis of their neurotoxicity.

In the case of the fibrils, oligomers often have a β-sheet structure (Relini et al. 2004; Chimon et al. 2007; Ono et al. 2009), but cases in which they are composed of loosely aggregated β-strands have also been reported (Ahmed et al. 2010). The direct cytotoxicity of pre-fibrillar amyloid assemblies has been confirmed for all proteins and peptides associated with amyloid diseases, including Aβ peptides, α-synuclein, IAPP and other (Conway et al. 2000; Poirier et al. 2002; Cleary et al. 2005) and also for many not associated with any disease (Bucciantini et al. 2002; Sirangelo et al. 2004). The use of antibodies in some studies has revealed the existence of distinct families of amyloid oligomers possibly with different cytotoxicity (Glabe 2008).

Mutations that increase hydrophobicity or decrease charge often increase the rate of misfolding to amyloid structures, as well as mutations that increase the likelihood of the sequence to adopt a β-sheet structure (Chiti et al. 2002). Both these situations make it more likely that protein molecules will interact with each other and aggregate. In addition, Kim and Hecht found a strong correlation between aggregation and both hydrophobicity and propensity to adopt a β-sheet structure (Kim & Hecht 2005).

1.1.2. AMYLOID FIBRILATION FORMATION KINETICS

Protein fibrillization is an extremely complex process, commonly involving kinetic competition between formation of amorphous aggregates and fibrillar species, a variety of intermediates, multiple conformational states, and a number of filamentous forms (Figure 1.2). The experimentally observed sigmoidal profile characteristic of a fibrillogenesis kinetics is usually interpreted as a Nucleation Dependent Polymerization (NDP) model, in which protein assembling into fibrillar structures can be divided in three stages: (i) the initial slow nucleation (*lag phase*) where the monomers associate into critical oligomeric nucleus, being the highest energy state and thus the thermodynamically unfavourable species along the polymerization pathway, followed by (ii) an *elongation phase*, where the elongation of the nucleus via the attachment of additional monomers becomes energetically favourable, thereby resulting in exponential fibril growth, leading to a (iii) a *plateau phase*, where mature and large amyloid fibrils take over (Gorbenko & Kinnunen 2006; Butterfield & Lashuel 2010)(Figure1.4). The process is time-dependent and proceeds through the formation of dimers, trimers, tetramers and different kinds of proto-fibrils until reaching the final insoluble fibrillar structure.

Other mechanisms have been suggested to describe fibril formation by amyloidogenic polypeptides such as Diffusion-limited Aggregation model (Tomski & Murphy 1992), in which the monomers spontaneously convert to octamers and later stack into fibrils, the template assembly (TA), monomer-directed conversion (MDC), and nucleated conformational conversion (NCC) models (Kelly, 1998), in which two structurally distinct peptide states are considered, a soluble state that eventually converts into an assembly-competent state by structural transitions.

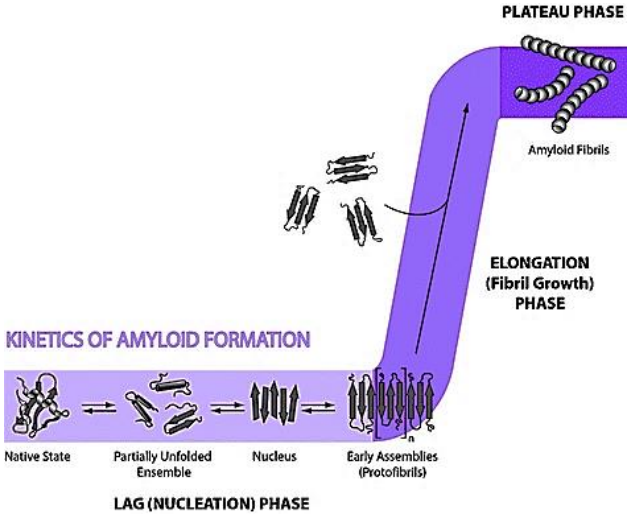

Figure 1.4: Illustration of nucleation-dependent polimerization mechanism for the amyloid fibril formation kinetics. [Adapted from (Butterfield & Lashuel 2010)]

It is still unclear which conformational species is a direct precursor for fibril formation, but the involvement of partially folded structures that successively accumulate to a small amount in solution has been accepted (Lundberg et al. 1997; Raffen et al. 1999; Blackley et al. 2000). The rate of amyloid formation was found to be promoted by the addition of preformed fibrils for several amyloid proteins (seeding experiments) (Hamada & Dobson 2002), a finding indicative of a nucleation-dependent process.

1.2. THE ROLE OF BIOLOGICAL MEMBRANES ON AMYLOIDOGENESIS

Recently, several studies have suggested that biological membranes can promote the pathological conversion of amyloidogenic proteins/peptides into toxic aggregate structures by providing a soft surface (Zhao et al. 2004; Butterfield & Lashuel 2010; Relini et al. 2013). These studies have shown that lipid-protein/peptide interactions can strongly modulate the amyloid fibril formation by decreasing the energy barrier for protein unfolding which leads to the instability of protein/peptide native states, promoting its misfolding and aggregation (Zhao et al. 2004; Gorbenko & Kinnunen 2006).

In fact, *in vitro* studies have demonstrated that surfaces in general have an aggregation-inducing action and a direct role on the kinetics of aggregation. The fibrillation effect appears to correlate directly with the hydrophobicity of the surface (Bellotti & Chiti 2008). Thus, membrane surfaces can act as an effective two-dimensional catalyst of fibrillogenesis, depending on their lipid composition and biophysical features that arise from their chemical characterisitics, such as length of acyl chain, degree of unsaturation, the surface net charge, its phase state, bilayer curvature and the degree of hydration.

1.2.1. LIPID-PROTEIN INTERACTIONS

Cellular membranes are essential components of cells and have both functional and structural roles comprising three mains functions: (i) selective permeable barrier for exchange of matter, (ii) stable and fluid ground for reactions of liphophilic substances and proteins, (iii) exchange of energy and information with extra-cellular environment or with cytosol, in the case of organelles (Muller et al. 1996). So the membrane must be stable enough to maintain a permeability barrier while being sufficiently fluid to accommodate changes in shape or enclosed volume, which allows life to develop.

The composition of the cellular membrane is extremely complex due to diversity of membranes proteins and several hundreds of different lipids species with differing head groups and unsaturation of the acyl chains that can be found in these structures (García-Sáez & Schwille 2010). During the last decade it has become clear that lateral protein and lipid heterogeneities are important for a number of cellular processes. Lipid-protein interactions play a key role in a wide variety of cellular processes, including signal transduction, intracellular transport, enzyme catalysis, energy conversion in the cell, antimicrobial defence and control of membrane fusion.

The chemical nature of the bilayer components and structural characteristics of the proteins/peptides in question is likely to have a significant role in determining the mode and extent of the membrane binding of proteins, as well as in the adoption of aggregation-prone protein conformation. Depending on the membrane composition, groups of specific lipids may aggregate into patches with physical properties distinctly different from those of other membrane domains.

Anionic lipids appear to be especially important in membrane-assisted conformational changes and electrostatic interactions in protein-lipid interactions (Zhao et al. 2004). Anionic surfaces have been shown to promote protein aggregation and fibrillization since the high local concentration of protein on these surfaces overcomes the energy barrier for nucleation (King et al. 1999) showing that an increase in the local concentration of the protein in the membrane is essential for the modulation of fibrillization rate (Gorbenko & Kinnunen 2006).

In general, the interaction of a peptide with the lipid membrane is initiated by the electrostatic attraction to the anionic membranes (Figure 1.5). Depending on the peptide charge and size relatively to the membrane surface, potential electrostatic attraction (or repulsion) will increase (or decrease) significantly the concentration of the peptide near the membrane surface (Seelig 2004). In many cases peptides are in a random coil conformation in solution and an α-helical conformation when associated with the lipid membranes. Depending on the relative peptide-to-lipid concentration, Aβ, IAPP and α-synuclein have all been shown to shift to an α-helical structure upon membrane binding (Butterfield & Lashuel 2010).

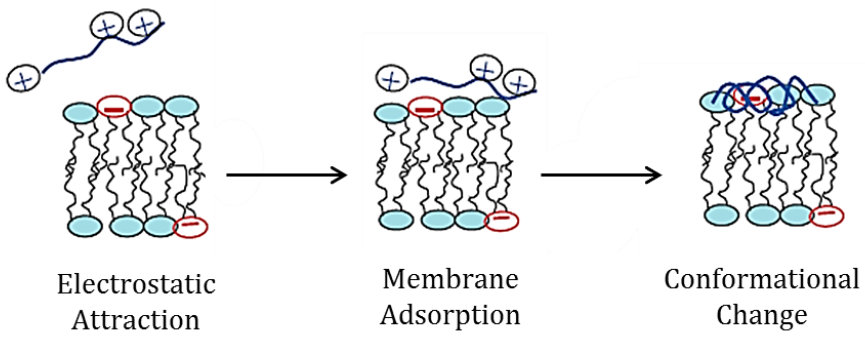

Figure 1.5: Molecular recognition at the membrane surface. The diagram shows different stages of peptide binding: the charged peptide is attracted electrostatically to the membrane surface followed by a conformational change of bound peptide. [Adapted from (Seelig 2004)]

The anchoring of the aggregation-prone peptides to the anionic membrane will enhance the local protein concentration thus favour conformational switching to β-sheet and protein aggregation (Figure 1.6). This shared feature suggests a common mechanism for membrane-mediated misfolding of proteins/peptides and their subsequent self-assembly. *In vitro* conversion of IAPP, α-synuclein and Aβ peptides from a disorder monomeric peptide to highly ordered amyloid fibrils has been extensively studied (Nath & Rhoades 2013) giving significant evidences for the role of anionic lipids in the amyloidogenesis catalysed by cellular membranes.

In the case of IAPP, several studies found that IAPP binding to membranes containing anionic lipids led to its conversion into an α-helical form and to eventual formation of β-sheets and fibrillization (Jayasinghe & Langen 2005; Apostolidou et al. 2008; Knight et al. 2008), leading to a decrease in the lag time and increasing the rate of fibrils growth. Fibrillization studies of IAPP induced by DOPC/DOPG (Knight & Miranker 2004) and in the presence of vesicles composed of zwitterionic (PC) and anionic (PG) phospholipids (Knight et al. 2008) has been demonstrated to exhibit a sigmoidal profile, with an initial lag phase of relatively slow fibril nucleation and a rapid elongation phase, during which the remainder of the soluble peptide was converted into amyloid, showing that the free energy contribution of the lipid bilayer to the transition state of fibril formation is determined by increasing the local peptide concentration.

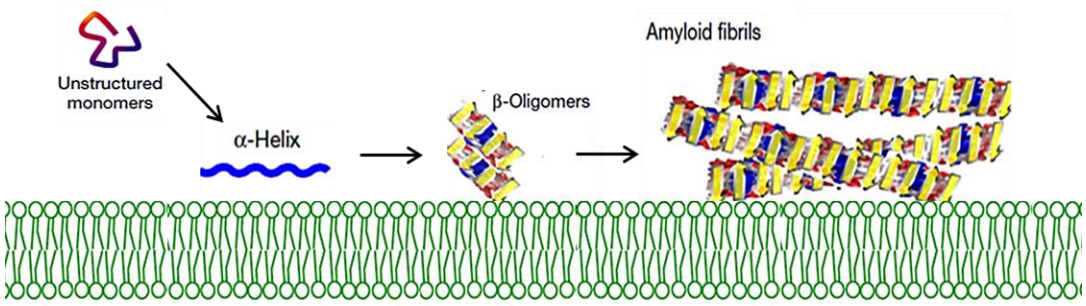

Figure 1.6: Schematic representation of amyloid fibril formation catalysed by an anionic lipid membrane. The binding process causes a conformational change of the membrane-bound peptide to an α-helical form that further shifts to a β-sheet-rich fibril upon increasing the local peptide concentration. [Adapted from (Fantini & Yahi 2010)]

In the case of α-synuclein, interactions with anionic lipids cause both an increase in α-helical content and aggregation (Jo et al. 2000; Davidson et al. 1998). The presence of membranes appears to make the helical conformation more stable. Single molecule studies have also shown that in the presence of lipids, the energy landscape of α-synuclein acquires two local minima corresponding to two α-helical conformations, the favoured one depending on the concentration of the lipid and curvature of the vesicles (Ferreon et al. 2009).

In the case of Alzheimer peptides, binding to negatively charged lipids bilayers leads first to a β-structure (low lipid to protein ratio) and then to a α-helix formation (high lipid to protein ratio) (Seelig 2004). The preference of Aβ peptides to bind to anionic membranes is a recurring observation (Butterfield & Lashuel 2010).

It was demonstrated that Aβ40 inserts spontaneously into anionic DPPG rather than zwitterionic DPPC lipid monolayer (Chi et al. 2008) and PG-containing vesicles induced a β-sheet conformation in Aβ40 as well as peptide oligomerization (Wong et al. 2009).

The changes in composition and physicochemical properties of lipid bilayer associated with aging or other physiological or pathological processes may increase membrane binding of specific proteins thereby triggering amyloidogenesis *in vivo*. Unfortunately, in spite of the significant progress in understanding how proteins attain their native state, we still know very little about the effects of the cellular environment on folding.

1.2.2. MEMBRANES AS A TARGET OF AMYLOID-LIKE STRUCTURES

It is commonly accepted that the interaction between amyloid aggregates and membranes results in disruption of the barrier function of the membrane, followed by intracellular calcium dysregulation and oxidative stress. Recently, it has been raised the possibility that a subpopulation of doughnut-shaped oligomers (amyloid pores) may account for amyloid toxicity. Early aggregates appearing as small annular rings with a central pore have been identify by electron microscopy (EM) and atomic force microscopy (AFM) in the fibrillization pathway of many proteins and peptides (Quist et al. 2005; Diociaiuti et al. 2006). These findings support the channel hypothesis of amyloid toxicity stating that amyloid aggregates form non-specific pore-like structures in the membrane of the exposed cells impairing their selective permeability (Figure 1.7).

This mechanism of toxicity is similar to those described for antibacterial toxins and viral proteins (hydrophobicity-based toxicity). Several models have been proposed to predict Aβ peptide ability to insert in the lipid bilayer and several pore arrangements were identified, all starting from a basic structure composed of a β-hairpin followed by a helix-turn-helix motif (Durell et al. 1994; Mobley et al. 2004; Diociaiuti et al. 2011). Additionally, it has been widely demonstrated that the secondary structure of membrane bound Aβ peptide and its ability to insert into the bilayer are strongly affected by the lipid composition with particularly importance to the presence of "raft-like" lipid domains in the membrane.

Other molecular mechanisms like the Carpeting model and Detergent-like effect were also proposed to explain the cytotoxicity created by amyloidogenic proteins/peptides (Reviewed in Relini et al. 2013 and Butterfield & Lashuel 2010).

The Carpeting model suggests that that the oligomers or other prefibrillar species bind to the outside leaflet of the membrane producing an asymmetric pressure between the two leaflets and finally leading to outflow of small molecules (Hebda & Miranker 2009). Some studies reported membrane thinning and nonspecific membrane permeabilization, supporting this model. In the Detergent-like effect, the amyloid precursor act as a surfactant and can uptake lipids from the membranes, leading to membrane thinning and possible transient holes. It was found that the assembly of IAPP fibrils at the membrane causes disruption by extracting lipids and incorporating them into emerging fibril trough a detergent-like mechanism (Sparr et al. 2004).

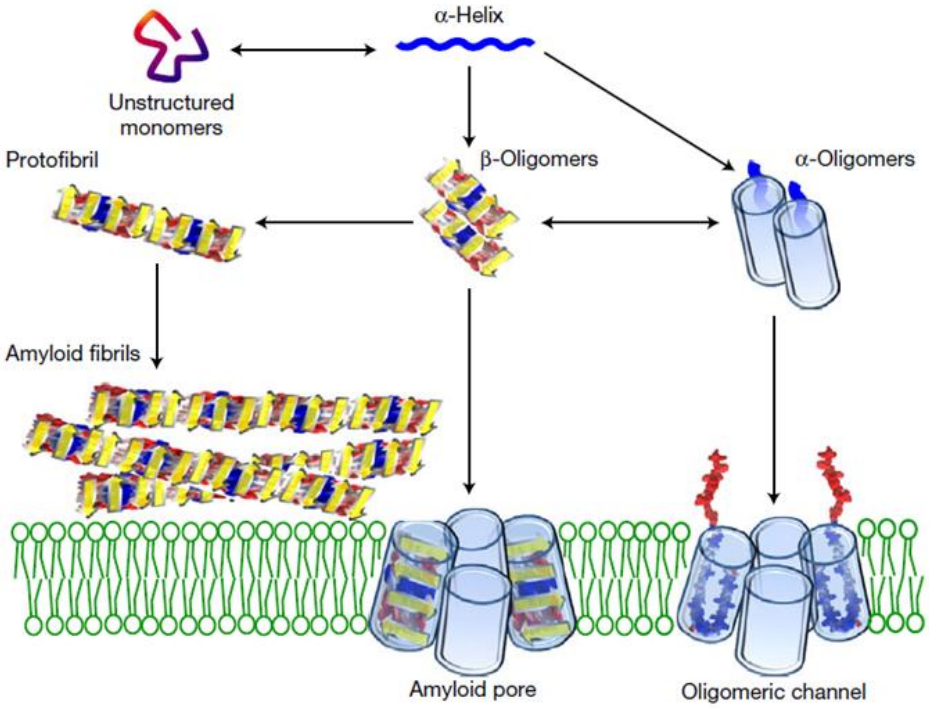

Figure 1.7: Different pathways of amyloidogenic protein oligomerization and fibrillation on membrane surfaces illustrating the channel hypothesis. Upon interaction with anionic membranes, unstructured soluble monomers undergo an α-helix shift of their conformation. Further accumulation of the proteins on the surface of the membrane induces their oligomerization into β-sheet aggregates or α-oligomers. Oligomers can form protofibrils, amyloid fibrils and amyloid pores (annular protofibrils) with ion-channel properties. [Adpated from (Fantini & Yahi 2010)].

So far, the major unsolved problem remains the molecular mechanism whereby the barrier properties of the cells are hampered. Although many models have been proposed in the literature, the molecular mechanisms for toxicity have not been entirely solved. More than one mechanism might be active in increasing the ionic fluxes, which cause interference with ion homeostasis and the toxic cascade of events associated with amyloid diseases.

1.3. CALCITONIN AS A MODEL PEPTIDE

Calcitonin (CT) is a polypeptide hormone released by the C cells in the thyroid gland which plays an important role in calcium metabolism (Figure 1.8) (Arvinte & Drake 1993; Wang et al. 2005; Itoh-Watanabe et al. 2013). The major physiological role of CT is to control the calcium concentration in the body, reducing the amount of calcium in the blood stream. CT reduces the amount of calcium excreted by the bone, inhibiting the osteoclast activity and decrease bone reabsorption. Its production is inhibited when the calcium concentration is decreased beyond normal levels and the parathyroid hormone (PTH) is then secreted, which promotes the opposite reactions to CT in the body. These two hormones act to maintain a normal concentration of calcium in the bloodstream.

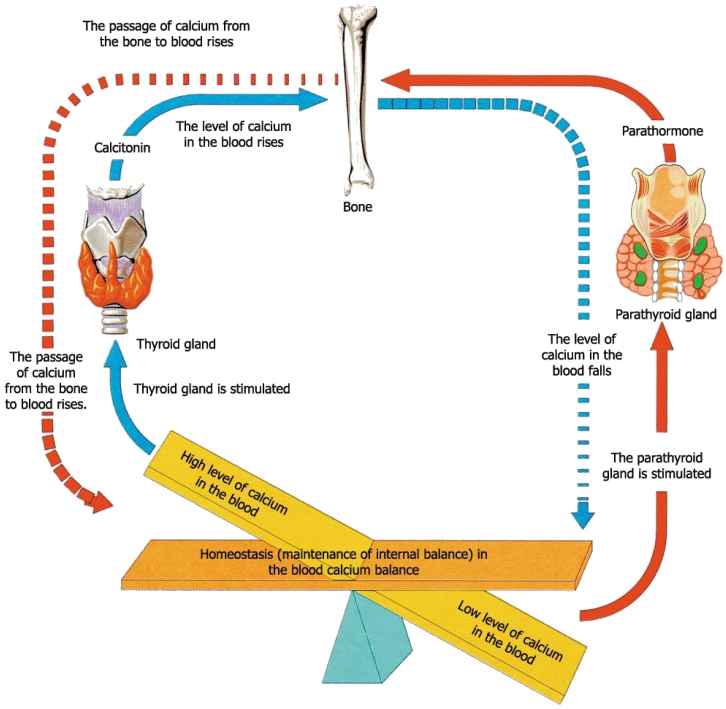

Figure 1.8: Calcium Homeostasis. CT reduces the amount of calcium excreted by the bone, inhibiting the osteoclast activity and decrease bone reabsorption. In response to declines in serum calcium, the parathyroid glands secrete parathyroid hormone (PTH). PTH stimulates the release of Ca^{2+} from bone, increasing bone resorption. Therefore, these two hormones act to maintain a normal concentration of calcium in the bloodstream. [adapted from http://newdrugapprovals.org. Consulted on 2014/09/24].

The primary sequence of the calcitonin has been determined for many species (including human, sheep, rat, pig, salmon and eel calcitonins) and differ mainly in the sequence of amino acids forming the central portions of the polypeptide (Diociaiuti et al. 2011). It has been found that salmon (sCT) and eel (eCT) calcitonins are more potent than the actual human calcitonin (hCT) (Torres-lugo & Peppas 2000).

The reason for this phenomenon is still not fully understood. The basic structure of the CT is characterized by a primary sequence of 32 amino acids and a disulfide bridge between the cysteine residues at positions 1 and 7 (Figure 1.9). CT has been administered in the treatment of bone diseases such as Paget's disease, hypercalcemia, osteoporosis (Torres-lugo & Peppas 2000) and other metabolic bone diseases due to its ability to reduce osteoclast activity. The use of hCT has been limited by its high tendency to self-associate in the form of amyloid fibrils in aqueous solution (Kanaori & Nosaka 1995; Bauer et al. 1994; Itoh-Watanabe et al. 2013) and because it has been associated with medullary carcinoma of the thyroid. The high potency of sCT and lower tendency to self-associate made it a more suitable target for drug development for treatment of osteoporosis as an alternative to hCT.

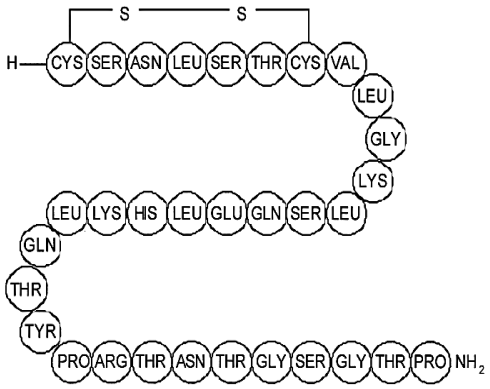

Figure 1.9: Illustration of the primary sequence of 32 amino acids of salmon calcitonin. A disulfide bridge is present linking Cys1 and Cys7. The differences between salmon and human calcitonin are described in the next chapter [Adapted from (Andreassen et al. 2014)].

It has been shown that both hCT and sCT can aggregate in solution over time (Kanaori & Nosaka 1995; Wang et al. 2005; Diociaiuti et al. 2011; Itoh-Watanabe et al. 2013), starting with the formation of oligomers which eventually results in the deposition of fibrils and plaques. hCT tends to aggregate in aqueous solution more rapidly than sCT, and this difference was attributed to the different pK values (8.7 and 10.4 for hCT and sCT, respectively) with one positive charge for hCT and three positive charges to sCT at pH 7.4 (Diociaiuti et al. 2011).

Thus, sCT is characterized by a very slow aggregation rate which makes it a suitable tool to be used in the study of molecular mechanisms of amyloid formation with particular attention to the early stages of aggregation, when the oligomers are produced, and to their possible interaction with cell membranes.

Some studies showed that in aqueous solution sCT and hCT are in a random coil conformation, but in the presence of organic solvents or phospholipids, they easily acquire a α-helix secondary structure (Arvinte & Drake 1993; Diociaiuti et al. 2011). The interaction of sCT (Diociaiuti et al. 2006; Diociaiuti et al. 2011) and hCT (Stipani et al. 2001) with model membranes demonstrates that incorporation in the lipid layer leads to a dramatic conformational change towards β-structure and this change was correlated to the observation of the membrane permeability and pore-like structures that could form ion channels in osteoblast plasma membrane, leading to calcium influx. These observations were completely dependent on the lipid composition of cell membranes, namely the presence of chol/DPPC/GM_1 domains favoured the binding process.

Additional evidence showed that the fibrils of hCT and bovine calcitonin (bCT) were toxic in cell cultures (Rymer & Good 2001) and that bCT conformation is highly affected by the membrane environment (Wang et al. 2005). In the presence of oxidizing agents in solution and in the presence of lipid rafs (liposomes containing cholesterol and GM_1), sCT shows an instant change in the secondary structure to β-rich conformation (Diociaiuti et al. 2011). On the other hand, *N*-terminally truncated derivatives of hCT, lacking hormonal activity, represent a novel class of weakly cationic cell penetrating peptides (CCPs) which have been systematically investigated (Herbig et al. 2005). CPPs have been suggested as vectors for cytoplasmic and nuclear delivery of hydrophilic biomolecules and drugs.

1.4. OBJECTIVES AND EXPERIMENTAL STRATEGY

The ability of anionic lipid membranes to induce the formation of amyloid-like assemblies by non-amyloidogenic proteins under conditions close to physiological has been an important research line over the last couple of years at the host laboratory (Melo et al. 2011; Melo et al. 2013; Melo et al. 2014). This work further extends this topic since it is part of a larger project aimed at elucidating the role that accessory cellular components, like biological membranes and glycosaminoglycans, can play in the modulation of amyloid pathologies.

The major goal of this study was to use CT as a model polypeptide to gain a detailed molecular description about the ability of negatively-charged lipid membranes in modifying the aggregation pathway of this polypeptide in solution, which was being studied in parallel by another lab member. Full-length (residues 1-32) CT peptides prepared with the human and salmon amino acid sequences were both used here.

hCT in an ideal model since it is considered an amyloid polypeptide due to its high tendency to self-associate, which leads to the formation of oligomers, and eventually results in the deposition of fibrils, as described in the last section. On the other hand, sCT has been the clinically preferable alternative to hCT for several years because of its substantially lower propensity to aggregate. Therefore, the salmon sequence of CT is expected to be mechanistically informative about the fibrillogenesis kinetics undergone by the full-length hCT, as it is anticipated to sample intermediate-like states and to form amyloid fibrils in a much longer time scale (Diociaiuti et al. 2011).

Both unlabelled and fluorescently-labelled hCT and sCT polypeptides, which were covalently conjugated to a very bright and photostable fluorophore - HiLyte 488 (HL488) – at their N-terminal, were employed in this study. This labelling position was chosen to minimize the possibility that the dye might interfere with the formation of a β-structure since this is known to involve the *C*-terminus (25-32) of the polypeptide sequence (Jonsson et al. 2008; Jha et al. 2012). In this way, by exploring the intrinsic and extrinsic fluorescence properties of these polypeptides using both steady-state and time-resolved fluorescence measurements, we specifically sought: (i) to characterize the aggregation state of both the unlabelled and HL488-labelled CT variants in aqueous solution; (ii) to study the influence of lipid composition, particularly the anionic lipid content of the liposomes, on both the unlabelled and HL488-labelled CT variants binding to the lipid vesicles; (iii) to evaluate the changes in the oligomerization state of the HL488-labelled CT variants on the membrane surface as a function of the peptide-to-phospholipid (P/L) molar ratio used.

Fluorescence is an extremely versatile spectroscopy as exemplified by the array of fluorescence parameters that can be explored in a single experiment (fluorescence intensity, spectral distribution, lifetime and anisotropy). Each of these parameters can be used as a sensitive reporter of distinct aspects related to the mechanism of action of CTs at the membrane level, like their membrane partition coefficients, location, rotational dynamics and self-assembly (Munishkina & Fink 2007; Nath & Rhoades 2013). Furthermore, due to the high sensitivity and specificity of this technique only trace amounts of the fluorescently-labelled peptides are eventually needed to be used in the experiments which, in turn, will enable the performance of co-mixing assays with unlabelled peptide, minimizing the chances of labelling interference in the process under study.

The model membrane systems used in this work were always large unilamellar vesicles (LUVs) prepared with a variable lipid composition. In fact, from the three main types of phospholipid vesicles (small, large and giant unilammelar vesicles) also referred as liposomes, composed by a single bilayer, LUVs have been a popular scaffold for monitoring peptide-membrane interactions in general due to its suitable diameter (around 100nm) and degree of curvature (Mäler & Gräslund 2009). Given their spherical shape and water filled interior, vesicles are thought to be the most biologically relevant mimic of natural cell membranes (Butterfield & Lashuel 2010). The phospholipids used in this study were 1-palmitoyl-2-oleoyl-*sn*-glycero-3-phosphocholine (POPC) and 1-palmitoyl-2-oleoyl-*sn*-glycero-3-phosphoserine (POPS), which were chosen as representatives of a zwitterionic and an anionic unsaturated phospholipid, respectively.

Both hCT and sCT are intrinsically fluorescent peptides due to their aromatic residues (Tyr12, Phe16, Phe19, Phe22 and Tyr 22 are present in hCT and sCT, respectively) (Figure 2.1). Therefore, the ability of the intrinsic fluorescence properties of both sCT and hCT on reporting their binding to anionic lipid membranes (POPC:POPS 80:20 LUVs) was first evaluated in this work. The results obtained in this section were also a useful control of the possible impact exerted by the extrinsic fluorophore HL488 on the partitioning properties of both CT variants.

In the second part of this study, the extrinsic fluorescence properties resulting from the covalent conjugation of the HL488 fluorophore to the *N*-terminal of both CT variants were then used to study their interaction with POPC LUVs containing a variable anionic lipid content (0, 10, 20 and 30mol% POPS, respectively). Since this fluorophore is only recently available commercially, there is not much information about it in the literature. Therefore, a brief characterization of several spectroscopic properties presented by both the free HL488 dye and the HL488-labeled CT variants was first made in a small set of solvents, namely several alcohols with variable lengths of aliphatic chain (methanol, ethanol, propanol and butanol) and two fluoro alchools (1,1,1,3,3,3-hexafluoro-2-propanol and 2,2,2-trifluorehtanol).

Chapter II

Materials and Methods

2. MATERIALS AND METHODS

2.1. REAGENTS AND STOCK SOLUTIONS

Calcitonin Peptides and Free Dye: Synthetic unlabeled and labeled human and salmon calcitonin (hCT and sCT, respectively) incorporating HiLyte Fluor 488 (sCT-HL488 and hCT-HL488, respectively) were purchased from AnaSpec (Table 2.1) and used without additional purification. Fluorophore attachment to the *N*-terminus position of the calcitonin peptides was performed by the manufacturer. The percentage of singly-labeled calcitonin peptide was measured by the manufacturer using mass spectroscopy (MS) and high-performance liquid chromatography (HPLC), and was reported as ≥95% for all batches used in this work (Table 2.1). All calcitonin peptides contain a disulfide bridge between Cys-1 and Cys-7 in the primary sequence and their *C*-terminal is amidated (Figure 2.1). The free dye HiLyte Fluor 488 acid, succinimidyl ester (HL488) was also obtained from AnaSpec (catalogue #81161). Although its chemical structure has not yet been disclosed by the manufacturer, the overall charge of the dye is known to be +1 (Figure 2.1). The lyophilized peptides and free dye were kept frozen at -20°C.

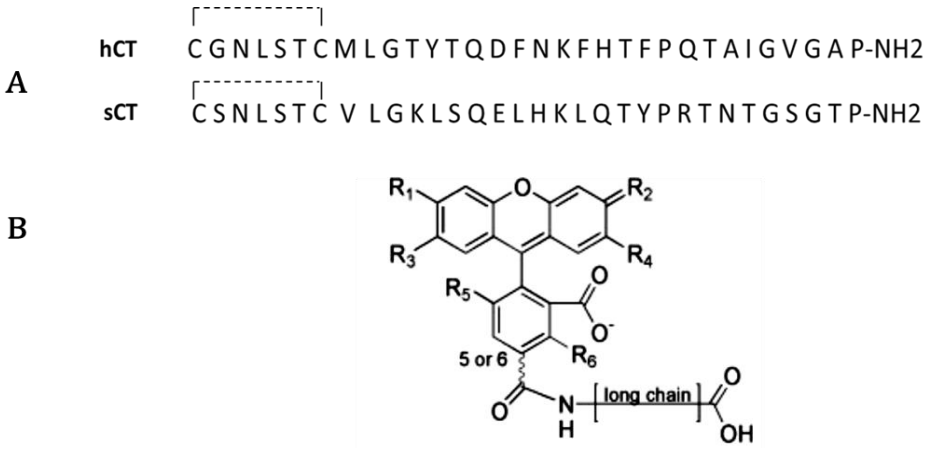

Figure 2.1: (A) Comparison between the primary sequences of human (hCT) and salmon (sCT) calcitonin variants. **(B)** Chemical structure of Hilyte Fluor 488 [adapted from (Jungbauer et al. 2009)].

It is important to start the studies from a monomeric solution of peptides as the presence of preformed aggregates can seed its oligomerization in solution. It has been shown that treatment of peptides with 1,1,1,3,3,3-hexafluoro-2-propanol (HFIP) can remove pre-existing aggregates (seeds) in solution (Andreotti et al. 2011).

Therefore, the stock solutions of unlabeled and fluorescently labeled sCT and hCT were usually prepared by directly dissolving 1 mg of the lyophilized powder in 200µL of pure HFIP to a final concentration of about 1mM. After a brief sonication step in a bath sonicator (Branson) of about 1 minute at room temperature (RT), the peptide stock solutions were stored at -20°C. The HL488 stock solution was prepared by directly dissolving the free dye in ethanol.

Table 2.1: Additional information for the synthetic fluorescently labeled and unlabeled human and salmon calcitonins obtained from AnaSpec. The counter ions were trifluoroacetate for all peptides.

Reagents	[M+H$^+$] (g mol^{-1})		Purity [1]	Net charge	Catalogue number
	Theoretical Mass	Determined by MS			
sCT	3432.9	3431.5	95%	+3	87666
hCT	3418.1	3419.2	98%	+1	76191
sCT-HL488	3788.4	3790.0	98%	+3	Custom Synthesis
hCT-HL488	3774.4	3774.3	96%	+1	Custom Synthesis

[1] determined by % peak area in HPLC analysis

The stock solutions were quantified spectrophotometrically using a molar absorption coefficient of 1615 M^{-1}cm^{-1} at 280 nm for the unlabeled CTs and 70 000 M^{-1}cm^{-1} at 502 nm for both the free dye and the HL488-labeled calcitonins as provided by the manufacturer. The molar absorption coefficient for the unlabeled peptides at 280 nm, $\varepsilon(280)$, was calculated accordingly to Pace et al. (Pace et al. 1995), using the following equation based on the number of tryptophan (#Trp), tyrosine (#Tyr) and disulfide bonds(#cys) present in each peptide sequence:

$$\varepsilon(280)(\mathrm{M^{-1}cm^{-1}}) = (\#Trp)(5{,}500) + (\#Tyr)(1{,}490) + (\#cys)(125) \qquad [2.1]$$

Phospholipids: 1-Palmitoyl-2-oleoyl-*sn*-glycero-3-phosphocholine (POPC) and 1-palmitoyl-2-oleoyl-*sn*-glycero-3-phosphoserine (POPS) (Figure 2.2) were obtained from Avanti Polar Lipids. The lyophilized phospholipids were stored frozen at -20°C. Approximately 20 mM stock solutions of POPC and POPS were prepared in chloroform and stored at -20°C. The exact concentration of each stock solution was determined using phosphate analysis (McClare 1971).

Other reagents: Ethylenediamine-*N,N,N',N'*-tetraacetic acid (EDTA) and potassium hydroxide were obtained from Merck; HEPES (4-(2-hydroxyethyl)-1-piperazineethanesulfonic acid), insulin from bovine pancreas and *N*-acetyl-*L*-tyrosinamide (NAYA) were purchased from Sigma-Aldrich; *L*-tyrosine was obtained from Fluka and fluorescein was purchased from Molecular Probes, Invitrogen. All other chemicals were purchased from Sigma-Aldrich, unless otherwise stated. All reagents had purity grade higher than 95% and were kept at RT.

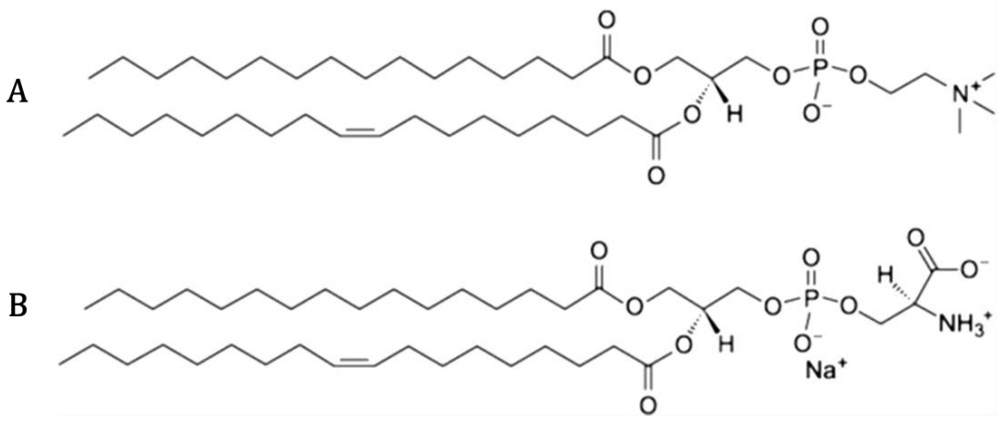

Figure 2.2: Molecular structures of **(A)** 1-palmitoyl-2-oleoyl-*sn*-glycero-3-phosphocholine (POPC) and **(B)** 1-palmitoyl-2-oleoyl-*sn*-glycero-3-phosphoserine (POPS) [Adapted from avantilipids.com accessed August 2014].

Buffers: The main buffer system employed in this work was 20 mM HEPES-KOH, 0.1 mM EDTA, pH 7.4 (HEPES-KOH buffer, pH 7.4). A high ionic strength buffer was also used in some studies (20 mM HEPES-KOH, 0.1 mM EDTA, 150 mM NaCl, pH 7.4). Buffer solutions were prepared using ultrapure water, obtained from a Milli-Q system (>18 MΩ·cm) and stored at 4°C. All buffer solutions were always filtered with 0.22 μm cellulose acetate filters (Millipore) prior to sample preparation.

Solvents: Chloroform, HFIP, ethanol and 2-propanol were obtained from Merck; 2,2,2-trifluorehtanol (TFE) was obtained from Fluka; glycerol and methanol were purchased from Sigma-Aldrich. All solvents were of spectroscopic UVasol grade or purity grade higher than 99%. Table 2.2 summarizes additional information for the solvents used.

Table 2.2: Solvent Properties: Dielectric constant, ε. viscosity, η, and refractive index, *n*, of the solvents used in this work (T= 20°C) (Lakowicz 2006; Haidekker et al. 2005).

Solvent	ε	η (mPa·s)	*n*
Water	80.4	1.00	1.33
Methanol	33.1	0.59	1.33
Ethanol	25.1	1.20	1.36
Propanol	21.7	1.94	1.39
Butanol	17.9	2.54	1.40
Glycerol	47.0	945	1.47
HFIP	57.0	1.65	1.28
TFE	26.1	1.75	1.29

2.2. SPECTROSCOPIC STUDIES IN HOMOGENEOUS MEDIUM

Each peptide- and free dye-containing sample was prepared independently, usually just before the spectroscopic measurements, by evaporation of the organic solvent (HFIP and ethanol, respectively) from the required volume of the stock solution using a nitrogen flow. In each case, the stock solution of the peptide in HFIP and HL488 in ethanol were allowed to thermally stabilize at RT for 10 min. Additionally, the stock solution of the peptide was sonicated for approximately 1 min in a bath sonicator prior to its use. The films were subsequently re-suspended in HEPES-KOH, pH 7.4 buffer or in other solvent to a final concentration of approximately 0.8μM and 1μM (unless otherwise mentioned) for peptide and free dye, respectively. Particularly, for free dye-containing samples prepared in glycerol each sample was incubated at RT overnight with magnetic stirring to ensure a complete homogeneity of the system, due to the high viscosity of the solvent.

2.3. INTERACTION WITH ANIONIC LIPID VESICLES

2.3.1. PREPARATION OF LARGE UNILAMELAR VESICLES

Large unilamellar vesicles (LUVs) were prepared by the extrusion technique (Mayer et al. 1986). The adequate volumes of each phospholipid stock solution were mixed in a round bottom flask in order to prepare lipid mixtures containing POPC and 0, 10, 20 or 30 mol% of POPS, respectively. After submitting the samples to a N_2 flow, they were kept overnight under an oil pump vacuum to remove any residual solvent.

Each lipid mixture was then re-suspended in HEPES-KOH buffer, pH=7.4 and submitted to several vortex cycles for a couple of seconds in order to remove the entire lipid film from the flask wall. The resulting lipid dispersions were equilibrated by 10 freezing and melting cycles using liquid nitrogen and a 50°C water bath. Finally, the lipid suspensions where extruded 21 times through 100 nm pore size polycarbonate membranes (Nucleopore) using a mini extruder device from Avestin and Hamilton syringes. The resulting liposome solutions were stored at 4°C until further use. The lipid vesicles were usually stable for at least one week under these conditions, but they were usually used within 2 days of preparations at most (Melo et al. 2013).

2.3.2. PREPARATION OF CALCITONIN SAMPLES

The interaction of both unlabeled and HL488-labeled calcitonins with POPC LUVs containing a variable mol% of anionic phospholipid, POPS, were studied by taking advantage of their intrinsic or extrinsic fluorescence properties, respectively. Briefly, a fixed amount of peptide was added to an increasing concentration of liposomes (usually within the concentration range 0 - 3mM) in HEPES-KOH buffer, pH 7.4. UV-Vis absorption, steady-state and time-resolved fluorescence measurements were then performed for each sample using the conditions described below.

Each peptide containing sample was prepared independently, usually just before the spectroscopic measurements, using one of two methods: (method A) direct injection of the required volume from a calcitonin stock solution prepared in HFIP to HEPES-KOH buffer, pH 7.4 buffer already containing the anionic lipid vesicles. The final concentration of the solvent was always kept <1% (vol/vol); (method B) Evaporation of the organic solvent (HFIP) from the required volume of the peptide stock solution using a nitrogen flow and subsequent re-suspension of the peptide film in HEPES-KOH buffer, pH 7.4. The lipid vesicles were then added to the peptide solution. In each case, the stock solution of the peptide in HFIP was allowed to thermally stabilize at RT for 10 min and then sonicated for approximately 1 min in a bath sonicator prior to its use.

2.3.3. DETERMINATION OF PARTITION COEFIFICIENTS

The partition coefficient of the peptide under study was determined by monitoring the changes in its steady-state fluorescence anisotropy in both the intrinsic and extrinsic fluorescence partition studies performed with the unlabeled and fluorescently labeled calcitonins, respectively.

On thermodynamic grounds, the membrane bound peptide molar fraction, x_l, can be written as function of its partition coefficient between the lipid and aqueous phases, K_p, where $[L]$ and $[W]$ are the phospholipid and water concentration, respectively (Castanho & Prieto 1992; Poveda et al. 2003; Santos et al. 2003):

$$x_l = \frac{K_p[L]}{[W] + K_p[L]} \qquad [2.2]$$

This function is obtained considering the mass balance of the system and the simplified formulation of the partition coefficient, K_p, given by equation 2.3, where n^w and n^l are the number of moles of water and lipid, respectively, and the n_p^i are the number of moles of the peptide in each phase (i=w for aqueous phase and i=l for lipid phase):

$$K_p = \frac{n_p^l}{n^l} \times \frac{n^w}{n_p^w} \qquad [2.3]$$

In addition, considering that the steady-state fluorescence anisotropy is an additive parameter (Valeur 2002; Lakowicz 2006), the fluorescence anisotropy of a peptide in the presence of liposomes can be written as:

$$< r >= \sum f_i r_i = f_w r_w + f_l r_l = \frac{\varepsilon_w \Phi_w x_w}{\varepsilon_w \Phi_w x_w + \varepsilon_l \Phi_l x_l}\, r_w + \frac{\varepsilon_l \Phi_l x_l}{\varepsilon_w \Phi_w x_w + \varepsilon_l \Phi_l x_l}\, r_l \qquad [2.4]$$

where f_i is the fraction of light emitted by the peptide and x_i is its molar fraction in the aqueous (i= w) and lipid phase (i= l), respectively. ε_i , Φ_i and r_i are the molar absorption coefficient, the fluorescence quantum yield and the steady-state fluorescence anisotropy of the peptide in each phase. Taken together equations 2.2 and 2.4, the fluorescence anisotropy of the peptide can be described as a function of $[L]$ by equation 2.5, where $Q = \varepsilon_l \Phi_l / \varepsilon_w \Phi_w$.

$$< r >= \frac{r_w[w] + K_p[L] r_l Q}{[w] + K_p[L] Q} \qquad [2.5]$$

Further assuming that the molar absorption coefficient of the peptide is invariant with the environment, the Q parameter simplifies to Φ_l / Φ_w. K_p as well as r_l can be retrieved from a non-linear regression fit of equation 2.5 to the experimental steady-state fluorescence anisotropy data obtained for the peptide in the presence of increasing concentrations of phospholipid, $[L]$. This non-linear regression fit was made taken into account the accessible phospholipid concentration, which was considered half of the total lipid concentration (Melo et al. 2013).

Scatter Control in Intrinsic Fluorescence Studies

The increase in phospholipid concentration can cause an artificial decrease in the fluorescence anisotropy of the peptide due to light scattering (turbidity of the lipid suspensions)(Eisinger & Flores 1985), particularly in intrinsic fluorescence measurements when low excitation wavelengths are used (λ_{exc}= 275nm). To control the scatter effect on these samples, an optimization of the steady-state fluorescence anisotropy measurements was performed, which included testing different cuvettes (with variable path length: 1 mm, 2 mm, 4 mm, 5 mm and 10 mm) and geometric arrangements (right angle and front face geometries), in order to decrease the light scattered by the liposome-containing samples (Figure 2.3A).

Briefly, the same experimental design as the one used for the partition studies described above was employed, but now 100mol% POPC vesicles were prepared and a fixed bovine insulin concentration of 25μM was used instead of salmon calcitonin. Both the lipid vesicles and insulin have no net charge at pH=7.4, so the peptide is not expected to interact strongly with these zwitterionic membranes and the observed variations in its steady-state anisotropy can be assumed to be due the scattering effect of the liposome suspensions (Figure 2.3B). The relative decrease in the steady-state fluorescence anisotropy of insulin measured for each phospholipid concentration was therefore added to the respective value measured for the calcitonin-containing sample with an equivalent scattering contribution at the excitation wavelength used.

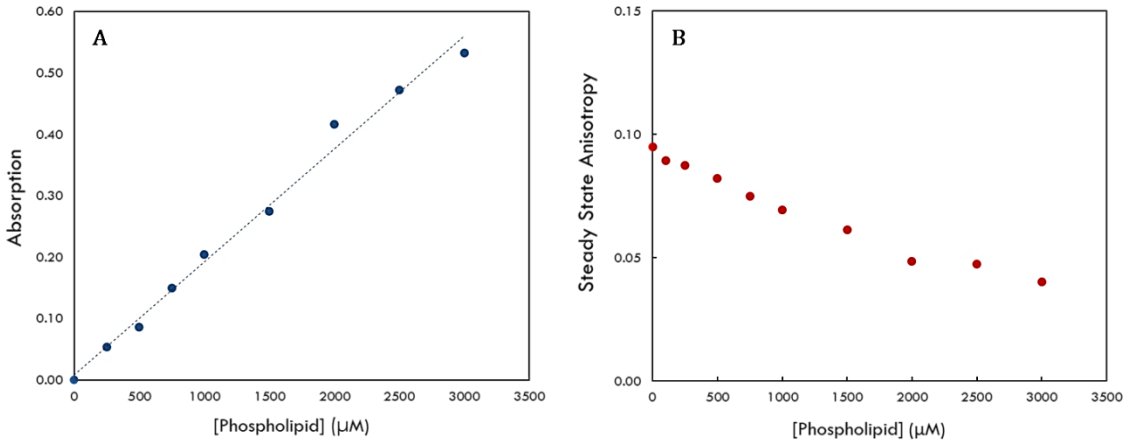

Figure 2.3: Typical results obtained for the variation of **(A)** the pseudo-absorbance at 275 nm and **(B)** the steady-state fluorescence anisotropy of 25μM insulin with the total phospholipid concentration in solution using POPC LUVs. The spectroscopic measurements were performed using 5x5mm quartz cuvettes at RT.

2.3.4. PEPTIDE-INDUCED LIPOSSOME AGGREGATION

The possibility of peptide-induced aggregation of liposomes was evaluated from the changes in 90° light scattering, which putatively follows the increase in turbidity upon addition of the unlabeled or HL488-labeled peptide to the lipid vesicles due to cross-bridging of the liposomes. Right-angle light scattering was evaluated in a spectrofluorometer from a 10s emission time trace with the excitation and emission wavelengths set at 650 nm (2 and 4nm bandwidths for excitation and emission, respectively), a spectral region where there is no HL488 absorption or emission.

2.4. UV-VIS SPECTROSCOPY

UV-Vis absorption spectra were measured at RT using a double-beam V-660 spectrophotometer from Jasco Analytical Instruments. Typically, the absorption spectra of the samples were taken from 250nm to 700nm in 5x5mm path length quartz cuvettes using a bandwidth and a sampling interval of 1 nm, after an air *versus* air baseline. Occasionally, black 10x4mm path length quartz cuvettes were also for determining the peptide concentration in buffer.

2.4.1. BASELINE CORRECTIONS

In a set of measurements performed with a fixed peptide concentration in the presence of increasing phospholipid concentrations (partition studies), it was observed that the control absorption spectrum obtained for each sample (liposomes at a given concentration) did not exactly overlap the spectrum obtained for the respective peptide containing sample (liposomes + peptide), probably due to difficulties in positioning the cuvettes in the spectrophotometer in a reproducible way (Fig.2.4A). For this reason, a "pseudo-background" spectrum was obtained for each sample by performing a non-linear regression fitting of an empirical power law (equation 2.6) to its absorption spectra (liposomes + peptide) in the wavelength range where significant absorption does not occur:

$$Abs = b + \lambda^{-k} \qquad [2.6]$$

The wavelength interval(s) used for the unlabeled calcitonins was 450-800nm and for the HL488-labeled peptides 350-400nm & 550-700nm, respectively.

The empirical fitting parameters obtained, *b* and *k*, were used to extrapolate equation 2.6 to all wavelength values, resulting in an "pseudo-background" baseline that was subtracted from each sample, producing a corrected absorption spectrum that could be inter-compared (Figure 2.4B). This correction allowed the decomposition of each spectrum in its absorption and turbidity spectra (adapted from Castanho et al. 1997).

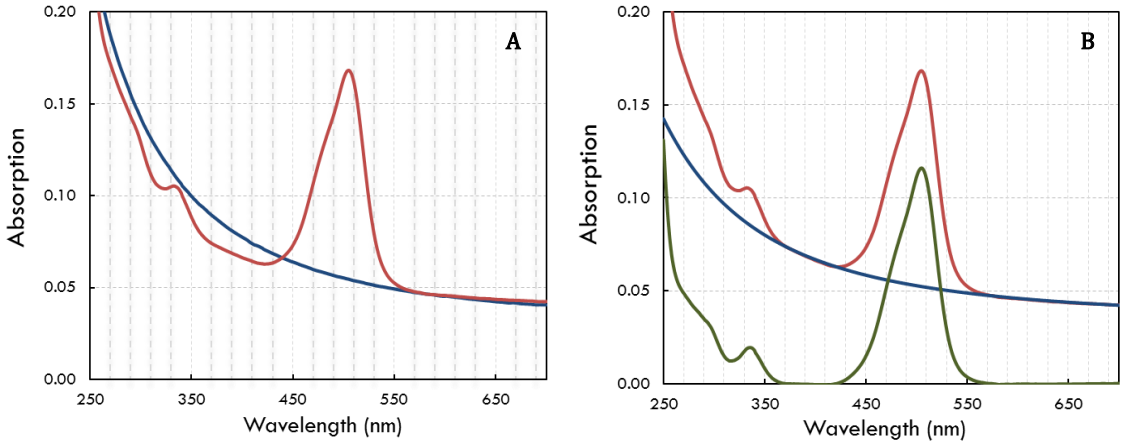

Figure 2.4: (A) Absorption spectra obtained for 250μM POPC LUVs containing 20mol% of POPS in the absence (blue curve) and in the presence of 3.4μM sCT-HL488 (red curve). **(B)** Corrected absorption spectrum (green curve) resulting from subtracting the extrapolated "pseudo-background" baseline (blue curve) from the sample absorption spectrum (red curve). See the text for more details.

The adequacy of this data treatment was evaluated by confirming that the relative absorption at the maximum absorption wavelength, ΔAbs_{max}, obtained for each corrected absorption spectrum was essentially independent of the phospholipid concentration used in each assay (Figure 2.5A) and that the average ΔAbs_{max} calculated for three different peptide concentrations used obeyed the Beer-Lambert law (Figure 2.5B).

2.5. FLUORESCENCE SPECTROSCOPY

2.5.1. STEADY-STATE FLUORESCENCE MEASUREMENTS

Intrinsic fluorescence studies: Intrinsic fluorescence measurements for both unlabeled calcitonin peptides (sCT and hCT) were performed in a HORIBA Jobin Yvon Fluorolog-3-21 spectrofluorometer (New Jersey, USA) since the quantum yield of their tyrosine residues was very low and this was the most sensitive apparatus in the laboratory. This spectrofluorometer has double excitation and single emission monochromators (IHR 320, New Jersey, USA), respectively, and is fitted with automated rotating Glan-Thompson polarizers.

The light source was a 450-Watt Xe lamp and the reference was a silicon diode. This spectrofluorometer contains a R928P photomultiplier tube detector which provides sensitive spectral characterization in the UV through the visible range of wavelengths. In addition, this apparatus is equipped with a FI-3751 thermoelectric temperature controller (Wavelength Electronics) which allows programming the temperature for data acquisition.

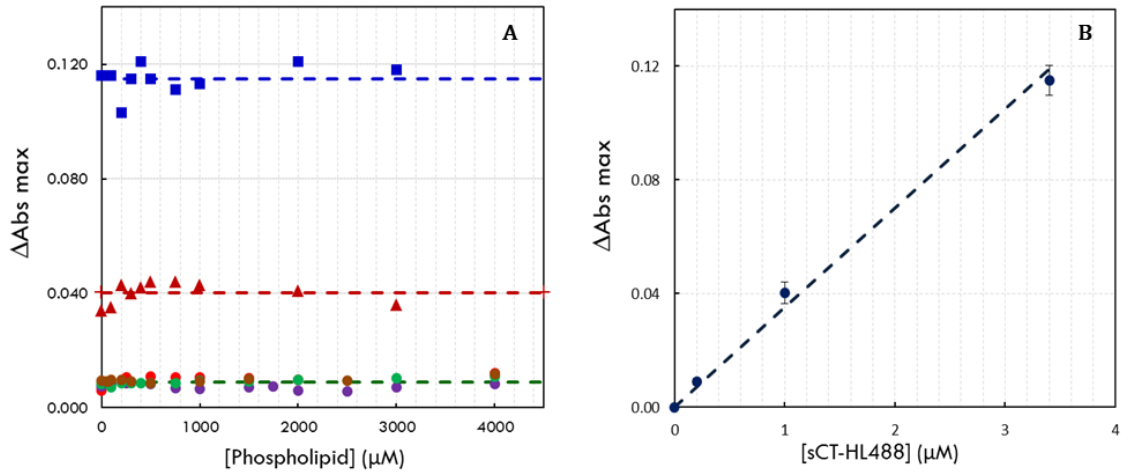

Figure 2.5: (A) Representation of the relative absorption at the maximum absorption wavelength, ΔAbs_{max}, obtained for each peptide corrected absorption spectrum as a function of total phospholipid concentration present in the sample. The sCT-HL488 concentrations used were 0.2 μM (green, purple and orange dots for POPC:POPS 90:10, 80:20 and 70:30 LUVs, respectively), 1.0 μM (red triangles for POPC:POPS 80:20 LUVs) and 3.4 μM (blue squares for POPC:POPS 80:20 LUVs). The dashed lines represent the mean ΔAbs_{max} value obtained for each peptide concentration. **(B)** The average ΔAbs_{max} obtained obeys the Beer-Lambert law. The dashed line represents the predicted value for each peptide concentration assuming that its molar absorption coefficient is independent of the lipid concentration used (ε= 70 000 M^{-1} cm^{-1} and a path length of 5 mm).

Typically, an excitation wavelength of 275 nm as well as an emission of 300 nm was used for tyrosine intrinsic fluorescence measurements, with excitation and emission bandwidths of 3 and 6 nm, respectively. Steady-state fluorescence anisotropy measurements were taken with excitation and emission wavelengths of 275 and 300 nm, respectively, using excitation and emission bandwidths of 7 nm (Table 2.3).

Extrinsic fluorescence studies: Fluorescence measurements for the free dye and both *N*-terminally HL488-labeled calcitonins (sCT-HL488 and hCT-HL488, respectively) were performed on a SLM-AMINCO 8100 spectrofluorometer from SLM Instruments Inc. with double excitation and emission monochromators. This apparatus, which also contains automated rotating Glan-Thompson polarizers, was operated in photon-counting mode. The reference was a Rhodamine B quantum counter solution.

The sample temperature was controlled with a water circulating bath from Julabo (model F25). Typically, the emission and excitation spectra were measured using λ_{exc}=480 nm and λ_{em}=525 nm, respectively, through an excitation and emission bandwidths of 2 and 8 nm, respectively. Steady-state fluorescence anisotropy measurements were taken with excitation and emission wavelengths of 335 nm/525 nm or 480 nm/525 nm, respectively, using excitation and emission bands of 4 and 8 nm (Table 2.3).

For both spectrofluorimeters, the measurements were usually performed using 5x5mm width quartz cuvettes at RT in right-angle geometry (unless mentioned exceptions) and background intensities were always taken into account and subtracted from the measured sample intensities.

Determination of Spectral Shifts

The shift in the fluorescence emission spectra were determined by calculating the intensity average emission wavelength, $< \lambda >$, that is given by the simple calculation of the centre of mass (CM) of the emission spectrum (equation 2.7), where I_i is the intensity value for each wavelength, λ_i (Royer et al. 1993). Mathematically, the CM is the point that divides the area of the spectrum in two parts of equal area. Concerning to the emission energy, the CM is the medium point of the spectrum.

$$< \lambda > = \sum_{i=1}^{N} (I_i \lambda_i) / \sum_{i=1}^{N} (I_i) \qquad [2.7]$$

This method is more reliable than just the maximum peak intensity since is less prone to instrumental noise than is the peak maximum because it is an integral measurement, and also a more sensitive value because it arises from a calculation involving the entire spectrum, and thus it reflects changes in the shape of the spectrum as well as in position.

Steady-State Fluorescence Anisotropy

The steady-state fluorescence anisotropy, $<r>$, was obtained by measuring the vertically (parallel, I_{VV}) and horizontally (perpendicular, I_{VH}) polarized components of the fluorescence emission with the excitation polarized vertically, as defined by:

$$< r >= \frac{I_{VV} - G I_{VH}}{I_{VV} + 2G I_{VH}} \qquad [2.8]$$

The G factor is the ratio of the sensitivities of the detection system for vertically and horizontally polarized light, and is defined as $G=I_{HV}/I_{HH}$. This parameter corrects for the bias in the transmissivity between vertically and horizontally polarized components of the emission introduced by the detection system (Lakowicz 2006). Background intensities were always taken into account and subtracted from the measured samples intensities.

Fluorescence Quantum Yield Measurements

The efficiency of the fluorescence process was evaluated by measuring the fluorescence quantum yield of the fluorophore, Φ_F, using a relative method (Valeur 2002). This parameter is related to that of a standard, Φ_{FS}, by equation 2.9, where Abs_i is the absorption of a diluted solution of each compound at the excitation wavelength, F_i is the area under the corrected emission curve and n_i is the refractive index of the solvent used. The subscripts i= S and i= X refer to the standard and to the unknown species, respectively.

$$\frac{\Phi_F}{\Phi_{FS}} = \left(\frac{1-10^{-Abs_S}}{1-10^{-Abs_X}}\right)\left(\frac{F_X}{F_S}\right)\left(\frac{n_X^2}{n_S^2}\right) \qquad [2.9]$$

It is always advantageous to choose a standard with absorption and emission bands close to those of the unknown and to excite both compounds at the same wavelength (Fery-Forgues & Lavabre 1999). For this reason *N*-acetyl-*L*-tyrosinamide (NAYA) was chosen as a standard in the determination of the fluorescence quantum yield of the unlabeled peptides ($\Phi_{FS} = 0.049$ in (Noronha et al. 2007)) and fluorescein was used as a standard for the fluorescently labeled peptides ($\Phi_{FS} = 0.95 \pm 0.03$ in NaOH (Lakowicz 2006)). The measurements were performed at 25°C.

2.5.2. TIME-RESOLVED FLUORESCENCE MEASUREMENTS

Time-resolved fluorescence intensity measurements were performed by the time-correlated single-photon timing technique (TCSPT). Briefly, the time between each laser excitation pulse and the detected photon is measured in this technique, producing a photon distribution histogram that represents the number of photons detected within the time interval, describing the fluorescence intensity decay (Lakowicz 2006). The experimental conditions used were adjusted so that less than one photon was detected per laser pulse. The samples were excited by frequency doubling of a rhodamine 6G or DCM dye laser for intrinsic fluorescence measurements (λ_{exc}=280 nm) and extrinsic fluorescence measurements (λ_{exc}=335 nm), respectively.

Fluorescence intensity decays, $I(t)$, were measured with an emission polarizer set at the magic angle (54.7^{o}) relative to the vertically polarized excitation beam with excitation wavelength of 280 nm or 335 nm for the unlabeled and fluorescently labeled peptides, respectively. This condition was used to avoid the effects of rotational diffusion and/or anisotropy on the intensity decay (Lakowicz 2006). The fluorescence was detected at 300 nm (for the unlabeled peptides) or 525 nm (for the labeled peptide) using a Jobin-Yvon HR320 monochromator in combination with a cutoff filter to avoid interference from Rayleigh-scattered light and a Hamamatsu R-2809U microchannel plate photomultiplier (Table 2.3) The instrument response function, *IRF(t),* was recorded as excitation light scattered by a Ludox solution (silica, colloidal water solution from Aldrich).

The data were collected in a multichannel analyzer with a time window of 1024 channels, at typically 19.5 picoseconds per channel, for intrinsic fluorescence decays, and 24.4 picoseconds per channel for extrinsic fluorescence decays. Generally up to 50 000 and 20 000 counts in the peak channel of the IRF and decay curves, respectively, were collected. In some cases, the two components of the fluorescence, polarized parallel, $I_{VV}(t)$ and perpendicular, $I_{VH}(t)$ to the plane of polarization of the excitation beam, were recorded sequentially by automatically alternating the orientation of the emission polarizer every 30 or 60 s.

Table 2.3: Summary of the excitation and emission wavelengths typically used in the steady-state and time-resolved fluorescence measurements performed with the free dye (HL488), unlabeled peptides (sCT and hCT) and fluorescently labeled peptides (sCT-HL488 and hCT-HL488), respectively.

Samples	Steady-State Fluorescence Emission Spectra		Steady-State Fluorescence Anisotropy		Time-resolved measurements	
	λ_{exc} (nm)	λ_{em} (nm)	λ_{exc} (nm)	λ_{em} (nm)	λ_{exc} (nm)	λ_{em} (nm)
sCT	275	275-380	275	300	280	300
hCT	275	275-380	275	300	280	300
HL488	480	485-680	480	525	335	525
sCT-HL488	480	485-680	480	525	335	525
hCT-HL488	480	485-680	480	525	335	525

Data Analysis for Intensity Decays

The fluorescence intensity decay curves, $I(t)$, were described by a sum of discrete exponential terms, as defined by equation 2.10, where α_i and τ_i are, respectively, the normalized amplitude and the decay time of the ith decay component of the fluorescence:

$$I(t) = \sum_{i=1}^{n} \alpha_i \exp(-t/\tau_i) \qquad [2.10]$$

The decay parameters were obtained by an iterative convolution of the empirical function above with the instrumental response function, $IRF(t)$:

$$I_{calc}(t) = I(t) \otimes IRF(t) \qquad [2.11]$$

and fitting $I_{calc}(t)$ to the experimental data $I(t)$ using a non-linear least squares regression method. It was helpful to calculate the amplitude-weighted lifetime of the decay, $<\tau>_1$, which is proportional to the area under the decay curve and consequently to the fluorescence quantum yield of the fluorophore in the absence of static quenching (equation 2.12):

$$<\tau>_1 = \sum_{i}^{n} \alpha_i \tau_i \qquad [2.12]$$

and the intensity-weighted mean fluorescence lifetime, $<\tau>_2$:

$$<\tau>_2 = \int_0^{\infty} I(t)dt = \frac{\sum \alpha_i \tau_i^2}{\sum \alpha_i \tau_i} = \sum_{i}^{n} f_i \tau_i \qquad [2.13]$$

The values obtained for α_i and τ_i can also be used to calculate the fractional contribution, f_i, of each decay time to the steady state Intensity (equation 2.13).

Data Analysis for Anisotropy Decays

The fluorescence anisotropy decay curves, $r(t)$, were also described by a sum of discrete exponential terms (equation 2.14), where β_i and φ_i are the normalized amplitude and the rotational correlation time of the ith decay component of the anisotropy, and r_∞ is the residual anisotropy, respectively:

$$r(t) = \sum_{i=1}^{n} \beta_i \exp(-t/\varphi_i) + r_\infty \qquad [2.14]$$

When the anisotropy value does not decay to zero at long times, it means that the angular range of the rotational motion is limited, caused by a barrier that prevents rotational diffusion of the fluorophore beyond a certain angle. The r_∞ parameter corresponds to the residual anisotropy, containing information about that restriction of the depolarizing process. Rotational correlation times, φ_i, are determined by the size, shape and flexibility of the macromolecules, resulting in anisotropies that are sensitive to the micro environment and interactions with other molecules.

The time-resolved anisotropy decays were globally analyzed using a two-step procedure. When a fluorophore is excited, the total intensity decay at the magic angle can be calculated using equation 2.15, which eliminates the contribution of $r(t)$ to the total decay:

$$I(t) = I_{VV}(t) + 2I_{VH}(t) \qquad [2.15]$$

Therefore, the fluorescence intensity decay parameters were first obtained by iterative convolution of equation 2.10 with the $IRF(t)$ and fitting to the experimental data, as calculated above using a nonlinear least-squares regression method. Then, simultaneous iterative convolution of $I_{VV}(t)$ (equation 2.16) and $I_{VH}(t)$ (equation 2.17) with the $IRF(t)$ and globally fitting to the experimental parallel and perpendicular polarized components of the fluorescence intensity were performed in order to obtain the anisotropy decay parameters:

$$I_{VV}(t) = \frac{1}{3} I(t)[1 + 2\, r(t)] \qquad [2.16]$$

$$I_{VH}(t) = \frac{1}{3} I(t)[1 - r(t)] \qquad [2.17]$$

These polarized intensity decays were then used to calculate the time-dependent anisotropy as given by equation 2.18, after fixing in this analysis the fluorescence intensity decay parameters obtained in the first step:

$$r(t) = \frac{I_{VV}(t) - I_{VH}(t)}{I_{VV}(t) + 2I_{VH}(t)} \qquad [2.18]$$

The experimental steady-state fluorescence anisotropy, *<r>,* was sometimes used as a constraint in the global analysis of the data, by introducing a *G* factor in this analysis that is related to the experimental data according to equation 2.19.

This parameter accounts for experimental artifacts such as photobleaching and laser fluctuations during the time-resolved fluorescence measurements. The instrumental G factor for our setup system is expected to be one because the polarized fluorescence light components were depolarized before the entrance slit of the monochromator. Accordingly, and as expected, this factor varied only slightly between 0.95 and 1.05.

$$G = \frac{1 - < r >}{1 + 2 < r >} \cdot \frac{\int_0^\infty I_{VV}(t)dt}{\int_0^\infty I_{VH}(t)dt} \qquad [2.19]$$

To further confirm the adequacy of the time-resolved anisotropy fit, the expected steady-state fluorescence anisotropy was calculated using the parameters obtained from the time-resolved analyses using equation 2.20, which relates the average of the anisotropy decay with the steady state value, yielding highly consistent results (data not shown trough the work).

$$< r >_{calc} = \frac{\int_0^\infty I(t)r(t)dt}{\int_0^\infty I(t)dt} \qquad [2.20]$$

The fluorescence intensity and anisotropy decays obtained were analyzed using the TRFA Data Processing Package Version 1.4 of the Scientific Software Technologies Center (Belarusian State University). To evaluate the goodness of the fits, the reduced χ^2 parameter was used. We assumed that the empirical fitting models used were adequate when the reduced χ^2 was lower than 1.3 and a random distribution of weighted residuals and autocorrelation plots were obtained (Lakowicz 2006).

Time-Resolved Emission Spectra

Evolution of fluorescence spectra during the lifetime of the excited state can provide interesting information about the microenvironment around a fluorophore. A typical example is the solvent relaxation around an excited-state compound whose dipole moment is higher in the excited state than in the ground state (Valeur 2002; Lakowicz 2006). When a fluorophore is excited to an unrelaxed state, the solvent reorients around the excited-state dipole moment and it will relax to a new equilibrium with the surrounding molecules since the excited molecules have a higher dipole moment than those in the ground-state. At the moment of excitation all the molecules are assumed to be in the unrelaxed state and no molecules are in the totally relaxed state until some relaxation has occurred. The fluorescence intensity decays will therefore depend on the observation wavelength because of the time needed for the unrelaxed state to become totally relaxed or reach some intermediate state (Figure 2.6).

The solvent relaxation results in a gradual red-shift of the fluorescence spectrum. The fluorescence intensity decay measured on the short-wavelength side of the total emission shows a more rapid decay than the decay of the total emission because the short-wavelength emission of the fluorophore is decaying by both emission and relaxation

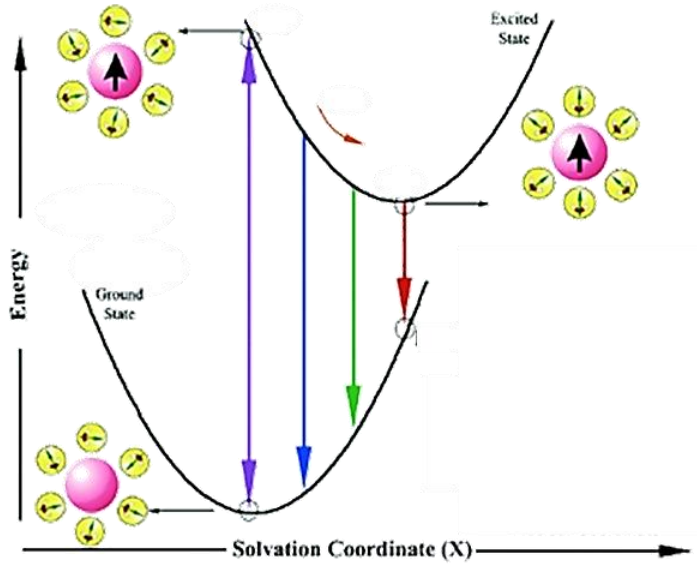

Figure 2.6: Schematic illustration of the solvation dynamics showing the orientational motions along the solvation coordinate. As the solvation relaxation proceeds the energy of the solute decreases giving rise to a red-shift of the fluorescence spectrum until the completely relaxed state is reached. (Adpated from (Pal et al. 2002).

On the long-wavelength side of the emission, the emission is essentially occurring from the relaxed species in solution and a rise in the intensity at long wavelengths was observed, representing the formation of the relaxed state. This rise is associated with the negative amplitudes obtained in the intensity decay analysis. In the course of time the fluorophore will relax due to solvent reorientation and the excited state energy slides towards the equilibrium state of the relaxed species, then the emission occurs at all positions along the reaction coordinate (Lakowicz, 2008).

The time-resolved emission spectra (TRES) are basically the emission spectra of the compound at a given time after the excitation pulse. In order to determine TRES, fluorescence intensity decays at several emission wavelengths, $I(\lambda,t)$, are measured, together with the corrected steady-state fluorescence emission spectra, $F(\lambda)$.

$$I(\lambda, t) = \sum_{i=1}^{n} \alpha_i(\lambda)\, exp[-t/\tau_i(\lambda)\,] \qquad [2.21]$$

This enables the calculation of the TRES given by $F(\lambda,t)$ using equation 2.22 (Easter et al. 1976; Berberan-Santos et al. 1991).

$$F(\lambda,t) = \frac{F(\lambda,t)I(\lambda,t)}{\int_0^\infty I(\lambda,t)dt} \quad [2.22]$$

The intensity decays were analysed in terms of a multi-exponential model (equation 2.10) and no molecular significance is assigned to the intensity decay parameters for each emission wavelength.

2.5.3. FLUORESCENCE TIME COURSE MEASUREMENTS

The kinetics of interaction between the HL488-labeled peptides and the lipid vesicles prepared with variable lipid composition were measured using a POLARstar OPTIMA micro plate reader. Peptide containing samples were prepared independently in Eppendorf tubes according to methods (A) or (B) described above (section 2.3.2) and applied to a 96-well Greiner Bio-One non-binding black microplate. Both the time course of the steady-state fluorescence intensity and anisotropy were measured for each sample using excitation and emission filters centred at 485 nm and 520nm, respectively, with a 10 nm bandwidth. Each kinetics was monitored during 16 hours at 25°C, with measurements taken at every 4 min with a 30 seconds shaking cycle before each point.

2.6. DYNAMIC LIGHT SCATTERING AND ZETA POTENTIAL

Dynamic Light Scattering

The Dynamic Light Scattering (DLS) technique measures the Brownian motion of the particles and relates it to their size/shape (Figure 2.7B). For monodisperse spherical particles in solution, the fluctuations in intensity of scattered light at a single angle are detected and analyzed with an autocorrelation function (equation 2.23) according to the Doppler effect (Murphy 1997; Domingues et al. 2008) where D is translational diffusion coefficient of the particle, τ is the decay time and q is the scattering vector, which is a function of the solvent refractive index, the scatter angle and the wavelength of the incident beam.

$$g(\tau) = \exp(-Dq^2\tau) \quad [2.23]$$

Thus, as the frequency shift through variations on the scatter pattern, the diffusion coefficient of the particle is obtained from the decay rate of the intensity.

The measured quantity is then the translational diffusion coefficient of the particle which is used to calculate the hydrodynamic radius, R_h using the Stokes-Einstein equation (equation 2.24) where k_B is the Boltzmann's constant and η the viscosity of the medium at the absolute temperature T.

$$D = \frac{k_B T}{6\pi\eta R_h} \quad [2.24]$$

Electric Zeta potential

The electric potential Zeta, ζ, gives an indication of the potential stability of the colloidal system (Figure 2.7A). If all the particles in suspension have a large negative or positive zeta potential they will tend to repel each other and there will be no tendency for the particles to come together. Otherwise (low zeta potential values) they will tend to generate an unstable suspension and the particles will likely aggregate (Freire et al. 2011; Domingues et al. 2008; Faustino et al. 2014) (see Figure 2.7A for details).

ζ-potential is calculated by measuring the electrophoretic mobility of the particles in solution, when an oscillating electric field is applied. The electrophoretic mobility can be calculated by laser Doppler velocimetry in Zeta-sizer devices, in which particle velocity is related to the frequency measured by intensity fluctuation of the scattered light. The electrophoresis mobility, *U*, is related to the ζ-potential by Henry's equation 2.25 where ε is the dielectric constant and *f(κa)* is the Henry's function, which is related with the "thickness" of the electrical double layer:

$$U = \frac{2\varepsilon\zeta f(\mathrm{ka})}{3\eta} \quad [2.25]$$

Henry's function is equal to 1.5 when working in an aqueous medium with moderate ionic strength (Smoluchowski approximation).

Using DLS and Zeta-Potential to characterize LUVs

Large unilamellar vesicles were extruded through 100 nm pore polycarbonate filters as previously described and typically used immediately after preparation. The average size of POPC:POPS vesicles was investigated as a function of mol%POPS. In order to characterize the phospholipid vesicles, both ζ-potential and DLS measurements were performed using a Malvern Zetasizer Nano ZS Apparatus (Malvern,UK) with a backscattering detection at a constant 173° scattering angle. The apparatus was equipped with a He–Ne laser (λ = 632.8 nm). Aliquots of 400 μM POPC LUVs containing 0, 10, 20 or 30 mol% POPS were prepared in triplicate in Eppendorf tubes using filtered HEPES-KOH buffer.

For DLS measurements, each sample was filtered into a DLS cuvette and the instrument performed 3 scans with 10 runs each, with an initial equilibration time of 2 min at 25°C. The scattering intensity data were processed using the software of the instrument to obtain the size distribution of each sample. Malvern's software analyses the acquired correlogram and the hydrodynamic diameters of the particles were estimated from the autocorrelation function using the method of cumulants (Frisken 2001).

For ζ-potential measurements, each sample was filtered into a zetasizer folded capillary cells DTS 1060 (Malvern,UK) and the instrument performed 10 scans with a maximum of 100 runs (the scan stopped when the measurement had enough statistical significance) with an initial equilibration time of 2 min at 25°C. Values of the viscosity and refractive index values were set at 0.8872 cP and 1.330, respectively. Data analysis was processed using the instrumental Malvern's DTS software to obtain the mean zeta-potential value.

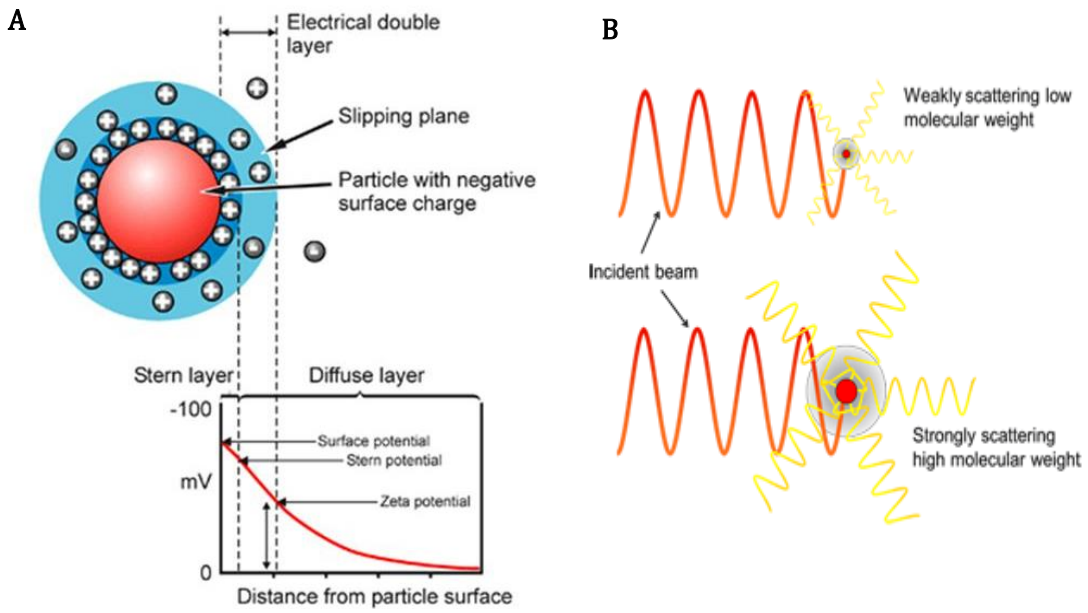

Figure 2.7: (A) Charge particles in solution attract ions to their surface, forming two layers: an internal layer called Stern Layer, where the counter ions are strongly attached to the particle, and an outside layer, where the attachment to the particle is weak and ions diffuse more freely. In the presence of an electrical field, the particle moves and the ions within the double layer move with it, but the ions on the diffuse boundary do not move concomitantly to the scattering particle. The electric potential that exists at this boundary is called the ζ-potential. **(B)** The speed at which the particles are diffusing due the Brownian motion is measured by quantification of the fluctuations in the scattered light by an incident laser as a function of time. In a solution with millions of particles the detected signal has a pattern that varies over time due to Brownian motion of the particles. The information about the particle size is obtained by a correlation function that measures the degree of similarity of intensity patterns over time. [Adapted from Malvern's Zetasizer User Manual consulted in July 2014]

Table 2.4: Results obtained for the zeta potential, ζ, and liposome diameter (from intensity peak distribution) for POPC LUVs prepared with a variable mol% of POPS by extrusion in Hepes-KOH 20mM, pH 7.4 buffer. The values are presented as mean ± standard deviation for *n*=3 independent sample measurements.

mol% POPS	ζ-potential (mV)	Diameter (nm)
0	- 6.1 ± 2.7	110.5 ± 0.6
10	- 13.1 ± 0.9	107.9 ± 0.8
20	- 24.4 ± 1.7	103.7 ± 2.1
30	- 43.9 ± 1.9	106.6 ± 0.45

As expected, the average lipid vesicle diameter, ϕ, was found to be essentially independent of the mol% of POPS used to prepare the liposomes (ϕ= (107 ± 3) nm, *n*= 4), whereas the ζ-potential progressively decreased upon augmenting the anionic phospholipid content of the lipid mixtures used to prepare the liposomes, reflecting an increase in their anionic net surface charge density (Table 2.4).

Chapter III

Results and Discussion

3. RESULTS AND DISCUSSION

3.1. INTRINSIC FLUORESCENCE STUDIES

In the first part of this work, the intrinsic fluorescence properties of both salmon (sCT) and human (hCT) calcitonin were evaluated as a possible tool to gain insights on the interaction and insertion of these peptides into the anionic lipid membranes. In fact, both CT variants used in this work are intrinsically fluorescent due to the presence of a single tyrosine and no tryptophan residues in each sequence (Y22 and Y12 in sCT and hCT, respectively, see Figure 2.1 in Chapter II). Typically, the intrinsic fluorescence of tyrosine has been less used than that of tryptophan residues to explore the interaction of peptides and proteins with lipid membranes, mainly because of the low quantum yield, low extinction coefficient and short absorption wavelength, as well as its low sensitivity to changes in the surrounding environment (Poveda et al. 2003). However, despite these apparent disadvantages, tyrosine shows a high intrinsic anisotropy and fluorescence lifetime optimal to characterize nanosecond and subnanosecond motions in peptides and proteins and therefore, it could be a useful probe to study structural and dynamics changes in both CT variants in solution and upon their interaction with membranes (Rolinski et al. 2010; Amaro et al. 2011). Moreover, this methodology offers the additional advantage that no extrinsic fluorophores are covalently linked to the polypeptide sequences, which have the potential to perturb their native structure in solution and affect the aggregation kinetics

3.1.1. HUMAN AND SALMON CALCITONINS IN AQUEOUS SOLUTION

The photophysical and dynamic proprieties of both CT variants were first analysed in buffer solution. For this, each sample was freshly prepared independently by direct injection of the required volume from a calcitonin stock solution in HFIP into the aqueous buffer solution (Method A) and characterized using both steady-state and time-resolved fluorescence measurements. Both the wavelengths of maxima excitation and emission fluorescence intensity of sCT and hCT were similar to the ones obtained for free NAYA in solution as expected (Figure 3.1A and Table 3.1), since NAYA mimics a tyrosine residue establishing two peptide bonds. However, the fluorescence quantum yields measured for sCT and hCT were $\Phi = 0.012 \pm 0.009$ and $\Phi = 0.013 \pm 0.010$, respectively, much lower than the characteristic value presented by NAYA in aqueous solution (Table 3.1).

Table 3.1: Maximum absorption, excitation and emission wavelengths (λ_{abs}^{max}, λ_{exc}^{max} and λ_{em}^{max}, respectively), Quantum yield (Φ) and steady-state fluorescence anisotropy, $<r>$ (λ_{exc}=275 nm; λ_{em}=300 nm) of NAYA, sCT and hCT in HEPES-KOH, pH 7.4 buffer. The anisotropy values are presented as mean ± standard deviation for a set of ten measurements. Concentrations of 10μM were used for all samples.

Sample	λ_{abs}^{max} (nm)	λ_{exc}^{max} (nm)	λ_{em}^{max} (nm)	Φ	$<r>$
NAYA	275	276	303	0.049 ± 0.007	0.005 ± 0.005
sCT	274	275	304	0.012 ± 0.009	0.060 ± 0.004
hCT	275	275	305	0.013 ± 0.010	0.070 ± 0.003

The steady-state fluorescence anisotropies of sCT and hCT were $<r>$= 0.060±0.04 and $<r>$= 0.070±0.03, respectively (Table 3.1). The time-resolved decays of both peptides in aqueous solution were best fitted to three exponential functions (Table 3.2). The three exponential decay reflects the existence of ground-state rotamers sensing different chemical environments (Poveda et al. 2003; Amaro et al. 2011). The slightly different fluorescence decays obtained for the two peptides must reflect differences in local interactions sensed by the rotamers due to the changes in their polypeptide chain sequences and position of the tyrosine residue in the primary structure (see Figure 3.1B).

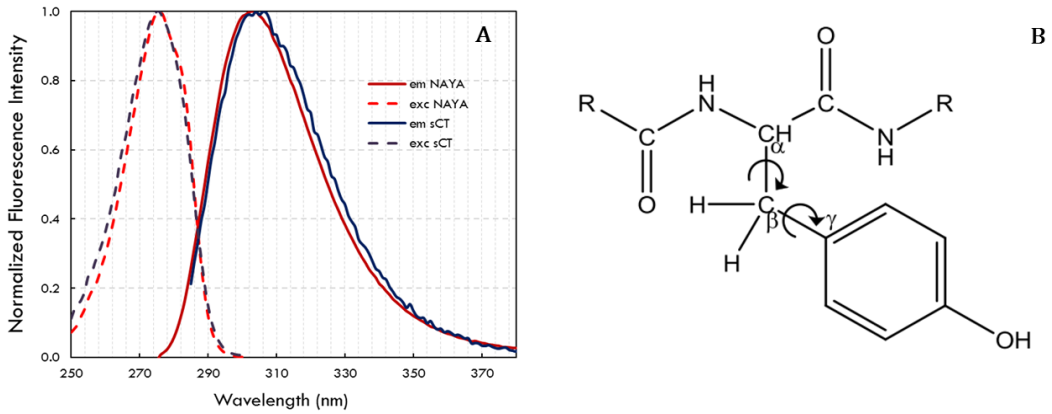

Figure 3.1: (A) Fluorescence excitation (dashed lines, λ_{em}=300 nm) and emission spectra (solid lines, λ_{exc}=275 nm,) for 10μM NAYA (red) and sCT (blue) in HEPES-KOH (pH 7.4) buffer **(B)** Ilustration of the tyrosine residue structure showing the possible rotation aound Cα-Cβ and the possible positions of the phenol group. [Adapted from (Amaro et al. 2011)]

According to literature, tyrosine and NAYA display a bi-exponential decay and proteins/peptides with a single tyrosine residue typical display two or more decay times (Lakowicz 2006; Rolinski et al. 2010; Amaro et al. 2011) in agreement with our results. When the side chain (the phenol group) of NAYA is exposed to different environments can adopt various conformational states (rotational isomers) which interchange slowly on the nanosecond scale, producing a multi-exponential decay (Figure 3.1B), since each of the excited state of the rotamers has its own decay with its specific lifetime. In agreement with this, the changes in the tyrosine surroundings created by the polipeptidic chain dynamics result in different environments for each rotameric conformation of tyrosine side chain, producing different types of rotamers and creating a more complex decay (Chamberlain & Bowie 2004; Amaro et al. 2011).

Table 3.2: Fluorescence intensity decay parameters obtained for 10 μM NAYA, sCT and hCT in HEPES-KOH (pH 7.4) buffer. The pre-exponential factors obtained for each lifetime component, τ_i, were normalized so that $\sum\alpha_i=1$. $<\tau>_1$ and $<\tau>_2$ are the amplitude-weighted and intensity-weighted mean fluorescence lifetimes (Equation 2.12 and 2.13), respectively. The decays were performed using λ_{exc}=280 nm and λ_{em}=300 nm.

Sample	α_1	τ_1 (ns)	α_2	τ_2 (ns)	α_3	τ_3 (ns)	$<\tau>_1$ (ns)	$<\tau>_2$ (ns)	χ^2
NAYA	0.14	0.47	0.86	1.54			1.39	1.49	0.99
sCT	0.20	0.28	0.70	1.34	0.10	2.70	1.24	1.55	1.08
hCT	0.31	0.28	0.53	1.08	0.16	2.28	1.03	1.44	1.27

3.1.2. INTERACTION OF CALCITONIN WITH ANIONIC LIPID VESICLES

The interaction of 10μM sCT with POPC:POPS 80:20 LUVs was first studied using steady-state fluorescence measurements. Each sample was prepared independently and freshly before the assay by direct injection of the required volume from a calcitonin stock solution into the liposome suspension prepared with a variable total phospholipid concentration (within the range 0 to 3mM) (Method A).

Both UV-VIS absorption and fluorescence emission spectra of sCT remained invariant upon addition of anionic vesicles (data not shown). On the other hand, the steady-state fluorescence anisotropy (Figure 3.2B) was observed to increase with the increasing phospholipid concentration, reflecting an adsorption of sCT on the lipid surface. The membrane-bound peptide was found to present a fluorescence quantum yield 1.3 times higer than the one obtained for the free sCT in aqueous solution (Figure 3.2A).

After correcting the experimental steady-state anisotropy data for the scattering effects as described in section 2.3.3, equation 2.5 was fitted to the corrected data using a non-linear regression method and a $K_p = (5.5 \pm 0.3)\text{x}10^5$ of and $r_l = 0.11 \pm 0.03$ were obtained (using $Q = 1.3$). A similar study was performed with hCT. However, in this case, the corrected steady-state anisotropy values where essentially independent of the total phospholipid concentration used (<*r*>= 0.062±0.009 (*n*=8)), indicating that no interaction was established with the 20mol% POPS-containing POPC membranes in this case (Figure 3.2B).

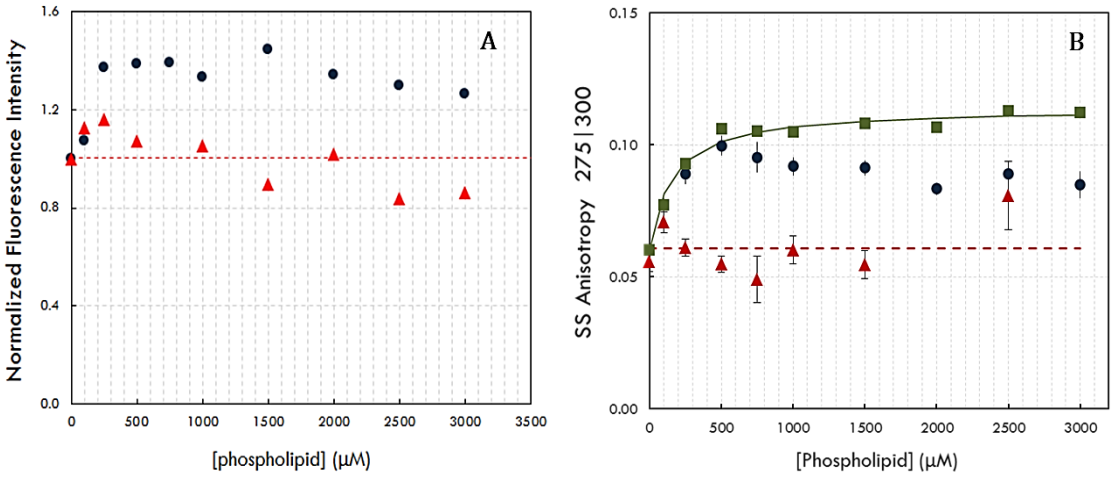

Figure 3.2: (A) Integrated fluorescence emission intensity and **(B)** steady-state anisotropy values for 10 μM sCT (blue circles) and hCT (red triangles) as a function of phospholipid concentration (POPC:POPS 80:20 LUVs), with (green squares and red triangles) and without (blue circles) correction for the scatter effect (section 2.3.3). The green solid line represents the non-linear fit of equation 2.5 for *K*p estimation. The red dash line represents the mean anisotropy value obtained for hCT: <*r*>=0.062±0.009 (n=8).

3.2. EXTRINSIC FLUORESCENCE STUDIES

Both CT variants used in this work are intrinsically fluorescent due to the presence of a tyrosine residue in each peptide (Figure 2.1) as mentioned before. However, both peptides present low molar absorption coefficients and fluorescence quantum yields in aqueous solution, as discussed above in section 3.1, which renders their application in biological fluorescence studies problematic, particularly in the presence of highly scattering suspensions like liposomes.

Therefore, full-length (residues 1-32) CT peptides prepared with both the human and salmon amino acid sequences were conjugated to HL488 (Figure 2.1) at their *N*-terminus. This fluorescent extrinsic probe was chosen due to its spectroscopic properties, namely high water solubility and insensitivity to pH from 4 to 10, together with its high photostability and fluorescence quantum yield (catalogue from Anaspec). In the first part of this section (section 3.2.1) the spectroscopic proprieties of free HL488 dye as well as of both HL488-labelled calcitonin variants were first characterized in homogeneous media using UV-Vis absorption, steady-state and time-resolved fluorescence techniques. The solvents used to explore the environmental effects on HL488 photophysics were HEPES-KOH buffers and a number of alcohols with different lengths of aliphatic chain (methanol, ethanol, propanol and butanol) and fluoro alchools (TFE and HFIP). These studies were important to provide an interpretation framework for the spectroscopic data obtained later when studying the interaction of both HL488-labelled calcitonin variants with liposomes prepared with a variable lipid composition, which are presented in the second part of this section (section 3.2.2).

3.2.1. SPECTROSCOPY STUDIES IN HOMOGENEOUS MEDIUM

3.2.1.1. Free HL488 Dye

Absorption and Steady-State Fluorescence Properties

Free HL488 dye presents maximum absorption and emission wavelengths of 500 and 523 nm in both low and high ionic strength HEPES-KOH, pH 7.4 buffers, respectively (Figure 3.3A and Table 3.3). The fluorescence quantum yield obtained for the free HL488 dye in HEPES-KOH (pH 7.4) buffer using fluorescein as reference standard was $\Phi=0.74 \pm 0.05$, slightly less than the one described by the manufacturer for the dye in dimethylsulfoxide (DMSO) or dimethylformamide (DMF) ($\Phi=0.91$), possibly due to the different solvent used.

Upon reducing the dielectric constant of the medium from ε = 80.4 (water) to ε = 47.0 (glycerol) (Table 3.3), there was a bathochromic shift of 12 and 6 nm in its absorption and fluorescence emission spectra, respectively, while the shape of both spectra remained essentially invariant (Figure 3.3A). In contrast, when the free dye was solubilized in both fluoroalchools TFE and HFIP, both spectra presented a pronounced hypsochromatic shift of 10 – 12 nm relatively to the ones obtained in aqueous solution (Table 3.3).

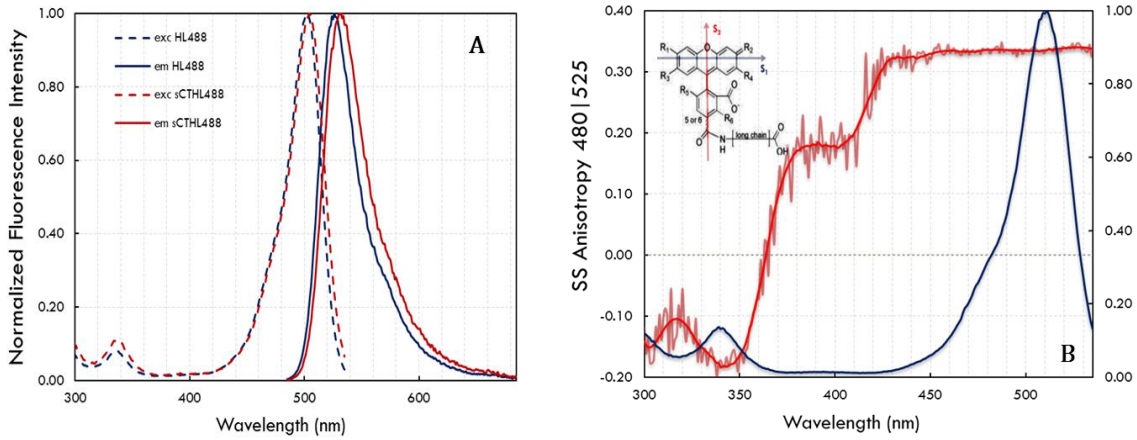

Figure 3.3: (A) Fluorescence excitation (dashed lines, λ_{em}=525 nm) and emission spectra (solid lines, λ_{exc}=480 nm,) for 1μM free HL488 dye in HEPES-KOH (pH 7.4) buffer (red) and glycerol (blue). **(B)** Excitation anisotropy and fluorescence excitation spectra (red/left and blue/right curves/scales, respectively) of 1μM free HL488 dye in glycerol. The solid red line represents the experimental anisotropy data after a smoothing operation. **Inset:** Illustration of the putative electronic absorption dipole moments for the $S_1 \leftarrow S_0$ and $S_2 \leftarrow S_0$ transitions in HL488 dye (red and blue vectors, respectively). The chemical structure of Alexa Fluor 488 was used as a reference (Rusinova et al. 2002; Schröder et al. 2005) due to its similar structure.

Specific solvents effects such as hydrogen bonding, acid-base chemistry or charge transfer interactions can be produced due to specific chemical properties of both the fluorophore and solvent and result in substantial spectral shifts compared to simple polarity effects (Lakowicz 2006). Both these alcohols are substituted with fluorine, and exhibit distinct effects, more than the ones expected from the decreased solvent polarity (Yamaguchi et al. 2006). Possibly the HL488 dye can establish specific interactions with both TFE and HFIP, due to the high hydrogen-bonding ability of both fluroalcohols (Sekhar & Udgaonkar 2011; Natalello et al. 2011).

Table 3.3: Spectroscopic properties of HL488 free dye and HL488-labelled calcitonins in different solvents. Maximum absorption, excitation and emission wavelengths (λ_{abs}^{max}, λ_{exc}^{max} and λ_{em}^{max}, respectively) and steady-state fluorescence anisotropy, $\langle r \rangle_{S1}$ (λ_{exc}=480 nm; λ_{em}=525 nm). The anisotropy values are presented as mean ± standard deviation for a set of ten measurements. The concentrations used were 0.8 µM and 1 µM for the free dye and HL488-labelled peptides, respectively.

Sample	Solvent	λ_{abs}^{max} (nm)	λ_{exc}^{max} (nm)	λ_{em}^{max} (nm)	$\langle r \rangle_{S1}$
HL488	Buffer [1]	500	500	523	0.014 ± 0.013
	+ NaCl [2]	500	500	523	0.017 ± 0.013
	Methanol	502	503	523	0.026 ± 0.006
	Ethanol	505	505	526	0.026 ± 0.004
	Propanol	504	504	524	0.088 ± 0.008
	Butanol	506	507	523	0.099 ± 0.011
	Glycerol	512	513	529	0.362 ± 0.005
	HFIP	488	489	505	0.036 ± 0.010
	TFE	490	493	513	0.045 ± 0.015
sCT-HL488	Buffer [1]	504	504	527	0.069 ± 0.009
	+ NaCl [2]	505	504	527	0.066 ±0.009
	DTT[3]	504	504	527	0.080 ± 0.005
	Methanol	504	505	527	0.048 ± 0.005
	Ethanol	508	507	528	0.232 ± 0.023
	Propanol	508	506	527	0.115 ± 0.007
	Butanol	n.d. [4]	509	528	0.228 ± 0.015
	HFIP	489	489	506	0.083 ± 0.007
	TFE	493	493	515	0.088 ± 0.004
hCT-HL488	Buffer [1]	504	503	529	0.079 ± 0.003
	+ NaCl [2]	504	505	528	0.081 ± 0.005
	DTT[3]	504	504	528	0.080 ± 0.005
	Methanol	504	504	528	0.046 ± 0.003
	Ethanol	506	506	529	0.095 ± 0.005
	Propanol	508	507	527	0.196 ± 0.003
	Butanol	509	510	528	0.231 ± 0.011
	HFIP	488	491	512	0.083 ± 0.007
	TFE	492	492	516	0.081 ± 0.011

[1] 20 mM HEPES-KOH, 0.1 mM EDTA, pH 7.4

[2] 20 mM HEPES-KOH, 0.1 mM EDTA, 150 mM NaCl, pH 7.4

[3] 20 mM HEPES-KOH, 0.1 mM EDTA, pH 7.4 + 100mM DTT

[4] not determined

Fluorescence emission decay kinetics

The fluorescence intensity decays measured for free HL488 dye in several solvents were well described by a mono exponential function, presenting a lifetime of ~ 3.9 – 4.0 ns in HEPES-KOH, pH 7.4 buffer (Figure 3.4A and Table 3.4), which is close to the one described by the manufacturer (τ=4.1ns) and reported in the literature (τ=4.10±0.15 ns (Schauerte et al. 2010). The only exception was the solvent glycerol since a complex three exponential function was now necessary to describe the kinetics of free HL488 fluorescence emission in this solvent (Figure 3.4A).

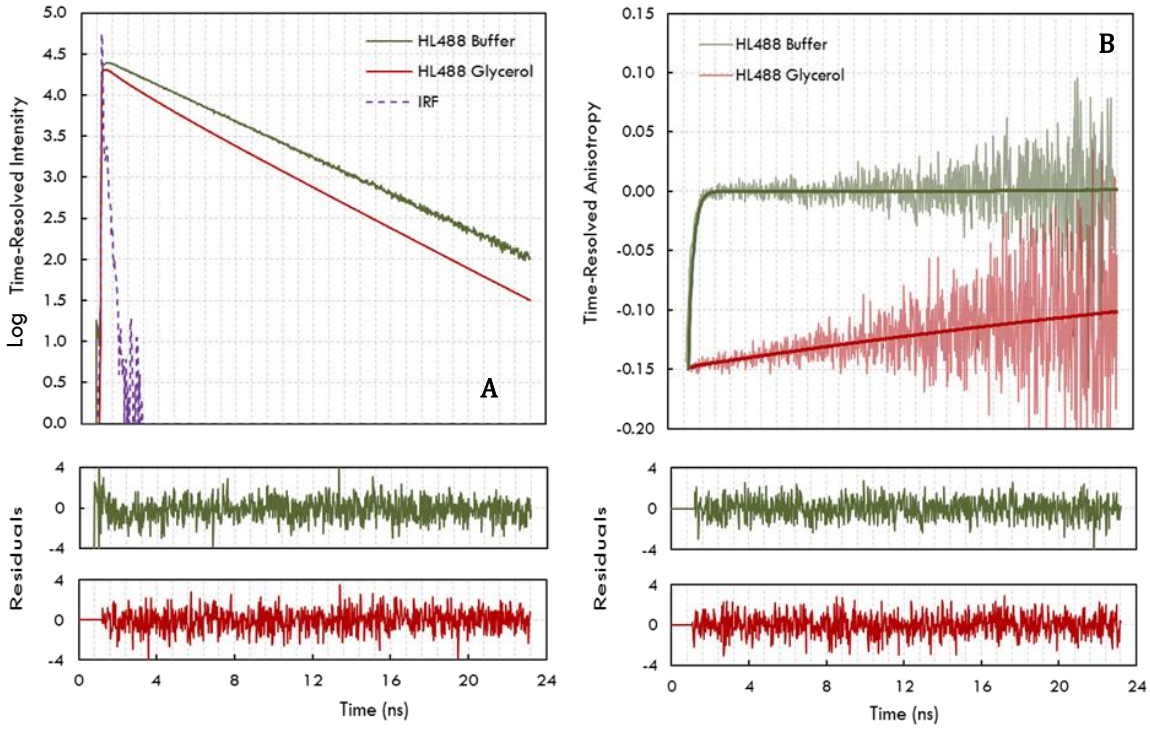

Figure 3.4: **(A)** Fluorescence intensity and **(B)** anisotropy decays for the free HL488 dye in HEPES-KOH (pH 7.4) buffer (green) and glycerol (red) (λ_{exc}= 335 nm; λ_{em}= 525 nm). The high viscosity of glycerol at RT greatly reduces the rotational diffusion of the probe resulting in a slow depolarization of its fluorescence emission.

Glycerol characteristically presents a high viscosity at RT and therefore the previous result could be due to a slower relaxation rate of the solvent molecules around the excited state of this fluorophore. In order to study the dynamics of solvent relaxation, time-resolved emission spectra (TRES) were calculated for the free HL488 dye in glycerol accordingly to the method described in chapter II (section 2.5.2). The fluorescence intensity decay parameters obtained for 0.8μM HL488 free dye in glycerol at different emission wavelengths are presented in Table 3.5.

Table 3.4: Fluorescence intensity decay parameters obtained for 0.8 µM HL488 free dye and 1 µM HL488-labelled calcitonins in different solvents. The pre-exponential factors obtained for each lifetime component, τ_i, were normalized so that $\sum\alpha_i=1$. $<\tau>_1$ and $<\tau>_2$ are the amplitude-weighted and intensity-weighted mean fluorescence lifetimes (Equation 2.12 and 2.13), respectively. The decays were performed using λ_{exc}=335 nm and λ_{em}=525 nm.

Sample	Solvents	α_1	τ_1 (ns)	α_2	τ_2 (ns)	α_3	τ_3 (ns)	$<\tau>_1$ (ns)	$<\tau>_2$ (ns)	χ^2
HL488	Buffer [1]					1.00	3.94	3.94	3.94	1.14
	+ NaCl [2]					1.00	3.93	3.93	3.93	1.08
	Methanol					1.00	4.06	4.06	4.06	1.12
	Ethanol					1.00	3.88	3.88	3.88	0.98
	Propanol					1.00	3.75	3.75	3.75	1.14
	Butanol					1.00	4.39	4.39	4.39	1.16
	Glycerol	0.11	0.77	0.22	1.49	0.66	3.52	2.75	3.49	1.01
	HFIP					1.00	4.01	4.01	4.01	1.07
	TFE					1.00	4.01	4.01	4.01	1.06
sCT-HL488	Buffer [1]	0.13	0.09	0.10	1.38	0.77	3.95	3.19	3.83	0.91
	+ NaCl [2]	0.09	0.26	0.10	1.98	0.80	4.01	3.44	3.86	1.02
	+ DTT [3]	0.05	0.28	0.05	1.54	0.89	3.95	3.62	3.89	1.04
	Methanol					1.00	4.17	4.17	4.17	1.02
	Ethanol	0.07	0.29			0.93	3.98	3.71	3.91	1.02
	Propanol	0.22	0.23	0.32	2.18	0.46	4.26	2.71	3.64	1.29
	Butanol	0.21	0.13	0.15	2.02	0.64	3.89	2.83	3.65	1.13
	HFIP					1.00	4.63	4.63	4.62	1.13
	TFE					1.00	4.45	4.45	4.45	1.11
hCT-HL488	Buffer [1]	0.13	0.25	0.18	1.86	0.70	3.96	3.13	3.70	1.05
	+NaCl [2]	0.13	0.31	0.19	1.98	0.68	4.00	3.12	3.70	1.07
	+ DTT [3]	0.14	0.25	0.14	1.48	0.72	3.74	2.94	3.54	1.06
	Methanol					1.00	4.26	4.26	4.26	1.10
	Ethanol	0.07	0.29			0.93	3.98	3.71	3.96	1.09
	Propanol	0.07	0.90			0.93	3.94	3.73	3.89	1.07
	Butanol	0.15	0.27	0.60	3.24	0.26	4.79	3.23	3.80	0.98
	HFIP					1.00	4.65	4.65	4.65	1.11
	TFE					1.00	4.58	4.58	4.58	1.04

[1] 20 mM HEPES-KOH, 0.1 mM EDTA, pH 7.4

[2] 20 mM HEPES-KOH, 0.1 mM EDTA, 150 mM NaCl, pH 7.4

[3] 20 mM HEPES-KOH, 0.1 mM EDTA, pH 7.4 + 100mM DTT

As expected, the amplitude-weighted mean fluorescence lifetime obtained for the free dye progressively increased from $<\tau>_1 \sim$ 1.6 ns at λ_{em}=500 nm to $<\tau>_1 \sim$ 3.9 ns at $\lambda_{em} \geq$ 540 nm. Concomitantly, a negative pre-exponential was required to describe the intensity decays for $\lambda_{em} \geq$ 540 nm, i.e. a rise in the intensity was observed at long wavelengths, revealing the formation of a new species: the solvent relaxed state of HL488 in glycerol, with a characteristic fluorescence time of 3.6 ns (Figure 3.5A and Table 3.5).

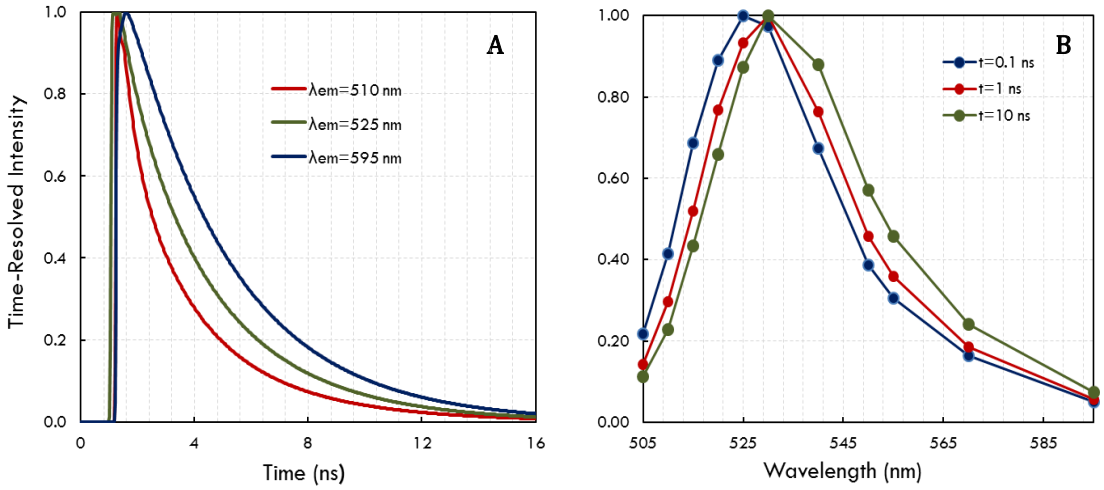

Figure 3.5: (A) Fluorescence intensity decays for free HL488 dye in glycerol at RT with λ_{em}=510 nm (red), 525 nm (green) and 595 nm (blue), respectively (λ_{exc}= 335 nm). At longer wavelengths (blue), a rise in fluorescence intensity can be detected at short times reflecting the formation of the relaxed excited state. This characteristic result is associated with negative amplitude obtained during the analysis of the fluorescence decays obtained using $\lambda_{em} \geq$ 540 nm (Table 3.5). **(B)** Time-Resolved Emission Spectra of HL488 in glycerol at 0.1, 1.0 and 10 ns after the excitation pulse calculated from the decay data presented in Table 3.5.

Figure 3.5B displays the emission spectra calculated for the free dye in glycerol at 0.1, 1.0 and 10 ns after the excitation of the sample, respectively. There was a clear time-dependent red shift while the spectral shape remained essentially invariant with time reinforcing the conclusion that the complex decay detected in glycerol was due to the slow rotational dynamics of the glycerol molecules around the excited state of the fluorophore at RT. If the sample displayed only ground-state heterogeneity, the decays would be dependent upon the emission wavelength but no rise in intensity would be observed because all the pre-exponential factors would be positive (Berberan-Santos et al. 1991).

Table 3.5: Fluorescence intensity decay parameters obtained for 0.8 μM HL488 free dye in glycerol at different emission wavelengths. The pre-exponential factors obtained for each lifetime component, τ_i, were normalized so that $\sum\alpha_i=1$. $<\tau>_1$ and $<\tau>_2$ are the amplitude-weighted and intensity-weighted mean fluorescence lifetimes (equation 2.12 and 2.13, respectively), respectively. The decays were performed using λ_{exc}=335 nm.

λ_{em} (nm)	α_1	τ_1 (ns)	α_2	τ_2 (ns)	α_3	τ_3 (ns)	$<\tau>_1$ (ns)	$<\tau>_2$ (ns)	χ^2
505	0.42	0.34	0.39	1.97	0.19	4.34	1.73	3.16	1.23
510	0.34	0.37	0.36	1.84	0.30	3.81	1.92	2.94	1.05
515	0.31	0.35	0.37	2.01	0.31	3.88	2.08	2.90	1.20
520	0.20	0.42	0.27	1.82	0.53	3.53	2.45	3.02	1.01
525	0.13	0.45	0.28	2.09	0.59	3.58	2.76	3.07	1.22
530			0.19	1.66	0.81	3.48	3.14	3.20	1.02
540	-0.11	0.14			1.11	3.48	3.84	3.30	1.10
550	-0.14	0.53			1.14	3.55	3.98	3.49	1.09
555	-0.13	0.48			1.13	3.59	4.00	3.61	1.05
570	-0.08	0.54			1.08	3.61	3.86	3.64	1.01
595	-0.08	0.54			1.08	3.61	3.86	3.65	1.01

Fundamental Anisotropy

Due to the breakdown of the Titanium-Sapphire laser available in the laboratory, it was necessary to use an excitation wavelength of 335 nm instead of the usual 480 nm in both types of time-resolved fluorescence measurements performed in this work. This implies that the HL488 fluorophore was excited at its $S_2 \leftarrow S_0$ instead of $S_1 \leftarrow S_0$ absorption band (Figure 3.3). These experimental conditions should bear no influence on its fluorescence intensity decay kinetics measured at the magic angle due to the extremely fast internal conversion from the S_2 to the S_1 excited state. This was already confirmed by comparing the fluorescence lifetimes of the free dye in homogeneous media with the values reported in the literature. However, the fundamental anisotropy of the molecule, r_0, *i.e.* its fluorescence anisotropy value in the absence of any motion, is known to critically depend on the choice of the excitation wavelength used to perform the measurements due to the photoselection effect. This occurs when the excitation brings the fluorophore to an excited state other than the first singlet state from which fluorescence is emitted. It can be shown that for any fluorophore randomly distributed in an homogeneous solution, the value of its fundamental anisotropy, r_0, must be within the range from -0.2 (the absorption and emission transition moments are perpendicular) to 0.4 (the absorption and emission transition moments are collinear) (Lakowicz 2006).

In effect, when the emission transition moment of the fluorophore is displaced by an angle θ relative to the transition moment of the absorption, its fundamental anisotropy, r_0, can be calculated using:

$$r_0 = \frac{2}{5}\left(\frac{3cos^2\Theta - 1}{2}\right) \quad [3.1]$$

The dependence of the steady-state fluorescence anisotropy of free HL488 in glycerol with its excitation wavelength is displayed in Figure 3.1B. This solvent was chosen due to its high viscosity at RT (η=945 mPa S (Table 2.2)), allowing to minimize fluorescence depolarization due to Brownian motions. Figure 3.3B shows that the HL488 fluorescence anisotropy presents a maximum of approximately 0.37 at excitation wavelengths from 450 to 650 nm, decreasing to a minimum around -0.18 at 335 nm. As explained above, this behavior is due to the presence of two electronic transitions, excitation from the singlet ground state, S_0, to the S_1 and S_2 excited states, respectively, whose transition dipole moments must be close to perpendicular to each other (inset of Figure 3.3B).

Steady-state and Time-resolved Fluorescence Anisotropy Properties

The steady-state fluorescence anisotropy measured for the free HL488 dye in its S_1 absorption band is rather low in the majority of the solvents used (Table 3.6), as expected for a small fluorophore. Only in the more viscous solvents, a progressive increase in its value was observed due to the slower rotational depolarization of its fluorescence emission, reaching $<r>_{S1}$ = 0.362±0.005 in glycerol (Table 3.6 and Figure 3.3B) in agreement with the predictions from the Perrin equation for a rigid hydrated sphere:

$$< r > = \frac{r_0}{1 + \tau/\varphi} \quad [3.2]$$

where:

$$\varphi = \frac{\eta V}{RT} \quad [3.3]$$

The rotational correlation time, φ, depends on the the viscosity of the medium, η , and the volume of the hydrated sphere containing the fluorophore, V, at a given temperature, T. R is the ideal gas constant (R=8.314 J K^{-1} mol^{-1}). The use of an excitation wavelength of 335 nm implies that the dynamic range for the time-resolved anisotropy measurements is approximately half of the one available when λ_{exc}=480 nm (Figure 3.3.B). However, information about the rotational diffusion of the fluorophores during its excited state lifetime can still be retrieved from the anisotropy decays, as it is exemplified in Figure 3.4B.

The fluorescence anisotropy decay for the free dye in HEPES-KOH (pH 7.4) buffer was very fast, presenting a fast rotational correlation time of φ~ 0.2 ns, in agreement with the low molecular weight of HL488 (698.4 g mol^{-1}). The depolarization of HL488 fluorescence in the more viscous solvent glycerol was much slower, as expected (φ=55 ns (Table 3.6)). It should be noted that in both cases, $r(0)= \beta_1 + \beta_2$ is approximately -0.14 or -0.15, which is very close to the fundamental anisotropy measured for HL488 at this excitation wavelength (Figure 3.3B). The small differences in this value are due the ultrafast motions that cannot be observed within the time resolution of our instrumental step-up.

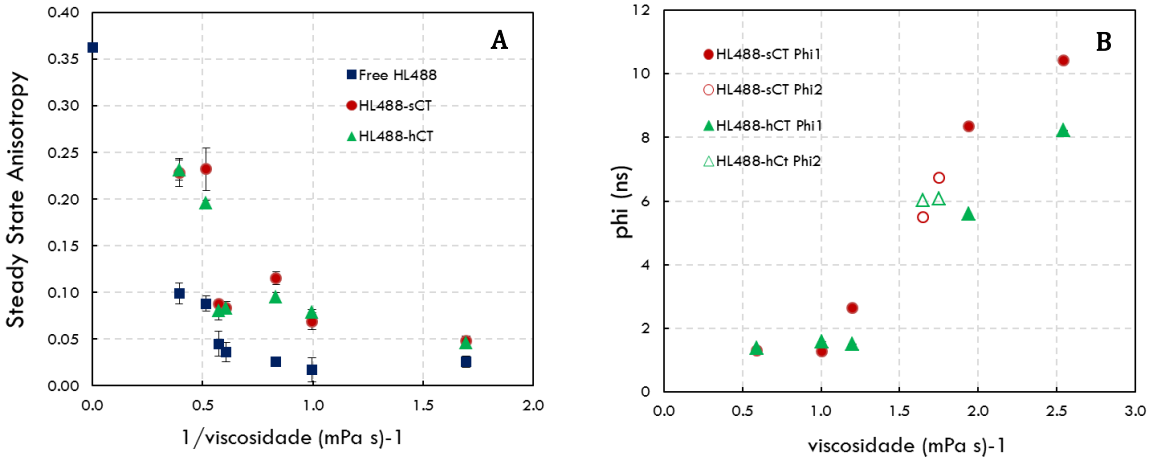

Figure 3.6: (A) Variation of the steady-state fluorescence anisotropy, $\langle r \rangle_{S1}$ (λ_{exc}=480 nm and λ_{em}=525 nm) measured for the free HL488 dye (blue squares), sCT-HL488 (red circles) and hCT-HL488 (green triangles) with the inverse of the viscosity of the solvent. **(B)** Dependence of the rotational correlation time of sCT-HL488 (red circles) and hCT-HL488 (green circles) with the viscosity of the solvent (closed symbols - φ_1 and open symbols - φ_2) (T= 20 °C).

3.2.1.2. HL488-Labelled Calcitonin Variants

Absorption and Steady-State Fluorescence Proprieties

The covalent conjugation of the HL488 fluorophore to both calcitonin variants resulted in a ~4 nm red-shift in both their absorption and fluorescence emission spectra relatively to the free dye, a common feature of organic dyes (Figure 3.7A and Table 3.3).The chemical conjugation of HL488 to the *N*-terminus of both calcitonin variants also decreased its fluorescence quantum yield from Φ=0.74±0.05 (free dye) to Φ=0.60±0.05 and Φ=0.50±0.05 for sCT-HL488 and hCT-HL488 in HEPES-KOH, pH 7.4 buffer, respectively.

Otherwise, the environmental effects produced by the different solvents used on the absorption properties and photophysics of HL488-labelled peptides were very similar to the ones previously described for the free fluorophore in solution: there was a progressive red-shift, mainly in their absorption spectra, upon decreasing the dielectric constant of the medium from water to butanol, and a blue-shift occurred in their absorption and emission spectra when the HL488-labelled peptides were solubilized in HFIP and TFE, as compared to the buffer solution (Table 3.3).

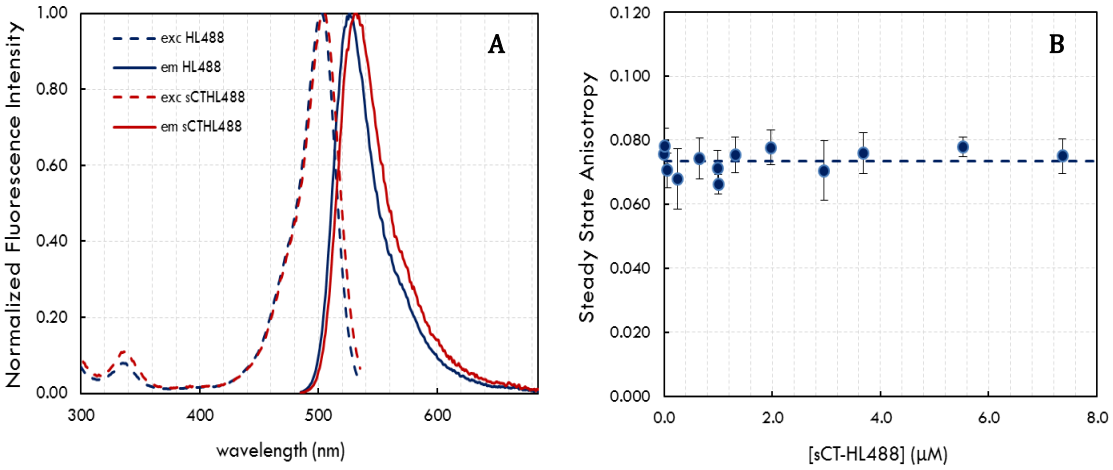

Figure 3.7: (A) Fluorescence excitation (dashed lines, λ_{em}=525 nm) and emission spectra (solid lines, λ_{exc}=480 nm) for 1μM HL488 (blue) and sCT-HL488 (red) in HEPES-KOH (pH 7.4) buffer. **(B)** The steady-state fluorescence anisotropy, $\langle r \rangle_{S1}$ (λ_{exc}=480 nm ; λ_{em}=525 nm) is independent of sCT-HL488 concentration in aqueous solution within a large concentration range (the smallest concentration used in the assay was is 1 nM) $\langle r \rangle_{S1}=0.074 \pm 0.03$ (n=15) . hCT-HL488 displays the same behaviour.

Fluorescence Emission Decay Kinetics

In contrast to the well described mono-exponential functions measured for free HL488 in HEPES-KOH, pH 7.4 buffer, the fluorescence intensity decays of both sCT-HL488 and hCT-HL488 were now well described by a sum of three exponential terms. However, the longer lifetime component of $\tau_3 \sim$ 4.0ns was always dominant, contributing with more than 90% to the total fluorescence intensity of the sample (Table 3.4 and Figure 3.8).

The use of a high ionic strength buffer did not affect significantly the emission kinetics of either HL488-labelled polypeptide. On the other hand, the reduction of their disulfide bond with either 0.1 or 1 mM DTT, a strong reducing agent that forms a stable six-membered ring with an internal disulfide bond (Cleland 1964), produced opposite effects on sCT-HL488 and hCT-HL488.

In the first case, the amplitude-weighted mean fluorescence lifetime increased from $<\tau>_1$= 3.2 to $<\tau>_1$= 3.6 ns, mainly due to a change in f_3 from 0.95 to 0.98, while τ_3 remained essentially invariant. In contrast, for hCT-HL488, there was a decrease in τ_3 from 4.0 to 3.7 ns, which caused $<\tau>_1$ to decrease from 3.1 to 2.9 ns (Table 3.4). In HFIP and TFE, both HL488-conjugated calcitonin variants presented a mono-exponential fluorescence intensity decay, with a long fluorescence lifetime of $\tau\sim$ 4.6 ns. On the other hand, the increase in the chain length of the aliphatic alcohols used to solubilize the conjugated peptides progressively augmented the complexity of their fluorescence decays.

Table 3.6: Fluorescence anisotropy decay parameters obtained for 0.8 µM HL488 free dye and 1 µM HL488-labelled calcitonin variants in several solvents. $r(0)= \beta_1 + \beta_2$. The decays were obtained using λ_{exc}=335 nm and λ_{em}=525 nm.

Sample	Solvents	β_1	φ_1 (ns)	β_2	φ_2 (ns)	$r(0)$	χ^2
HL488	Buffer [1]	-0.14	0.21				1.02
	Glycerol	-0.15	55				1.01
sCT-HL488	Buffer [1]	-0.13	1.28			-0.13	1.26
	+ NaCl [2]	-0.080	0.56	-0.066	2.68	-0.15	1.18
	+ DTT [3]	-0.13	0.89			-0.13	1.09
	Methanol	-0.12	1.31			-0.12	1.09
	Ethanol	-0.13	2.63			-0.13	1.27
	Propanol	-0.11	8.35			-0.11	1.10
	Butanol	-0.13	10.4			-0.13	1.08
	HFIP	-0.04	0.75	-0.10	5.50	-0.14	1.06
	TFE	-0.07	0.75	-0.08	6.73	-0.15	1.18
hCT-HL488	Buffer [1]	-0.13	1.57			-0.13	1.05
	+ NaCl [2]	-0.12	1.47			-0.12	1.15
	+ DTT [3]	-0.13	0.95			-0.13	1.10
	Methanol	-0.12	1.37			-0.12	1.10
	Ethanol	-0.13	1.51			-0.13	1.20
	Propanol	-0.14	5.59			-0.14	1.08
	Butanol	-0.14	8.21			-0.14	1.20
	HFIP	-0.03	0.57	-0.11	6.03	-0.14	1.11
	TFE	-0.04	0.52	-0.11	6.08	-0.15	1.05

[1] 20 mM HEPES-KOH, 0.1 mM EDTA, pH 7.4

[2] 20 mM HEPES-KOH, 0.1 mM EDTA, 150 mM NaCl, pH 7.4

[3] 20 mM HEPES-KOH, 0.1 mM EDTA, pH 7.4 + 100mM DTT

For instance, only a mono-exponential function was necessary to describe the fluorescence intensity decay of sCT-HL488 in methanol, a two-exponential function was used to describe the decay in ethanol, and a three-exponential function was required for sCT-HL488 in propanol and butanol (Table 3.4). The origin of the complex fluorescence decays obtained for the conjugated peptides compared to the free dye in solution must result from dynamic fluctuations of the calcitonin structure which are sensed by the HL488 dye (Vaiana et al. 2009).

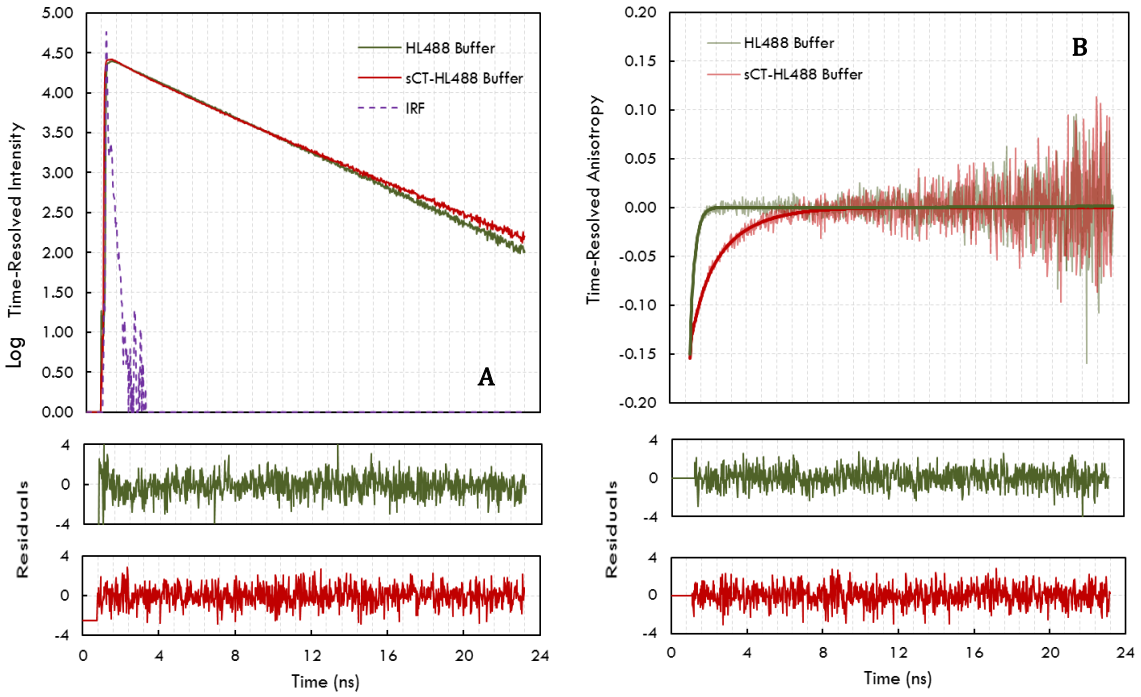

Figure 3.8: (A) Fluorescence intensity and **(B)** anisotropy decays for the free HL488 dye (green) and sCT-HL488 (red) in HEPES-KOH (pH 7.4) buffer) (λ_{exc}= 335 nm; λ_{em}= 525 nm).

Although it is often assumed that fluorophores do not interact with amino acids in the proteins that they label, the flexibility of the short saturated carbon chains (linker) allows for contact with the side chains of nearby amino acids residues, which can result in intramolecular fluorescence quenching (Chen et al. 2010; Doose et al. 2005; Vaiana et al. 2003). These effects can be rationalized in terms of a photoninduced electron transfer (PET) mechanism from an electron donor present in several possible adjacent amino acid residues to the covalently-conjugated dye HL488 when they are in close Van der Waals contact (Chen et al. 2010; Doose et al. 2005), resulting in a non-radiative dissipation of the excited-state energy (Figure 3.9).

In fact, it has been shown that the side chains of several amino acids can act as quenchers of fluorescent organic dyes such as Alexa Fluor (Chen et al. 2010), being Trp and Tyr strong quenchers and His and Met weak quenchers. PET-quenching can occur through dynamic or static quenching (Doose et al. 2009) and is able to report the intramolecular dynamics or conformational changes undergone by the fluorescently-labeled polypeptide chains in solution (Vaiana et al. 2003; Doose et al. 2009). Each of the solvents studied, or the reduction of the polypeptide disulphide bond, can induce different conformations/dynamic fluctuations on sCT-HL488 and hCT-HL488, depending on the type of specific interactions that they are able to make with the HL488 structure and the polypeptide chain, indirectly modulating their fluorescence emission decay kinetics. Alcohols have been used extensively in aggregation studies as they are able to perturb the native state of proteins by weakening hydrophobic interactions (Yamaguchi et al. 2006; Sekhar & Udgaonkar 2011).

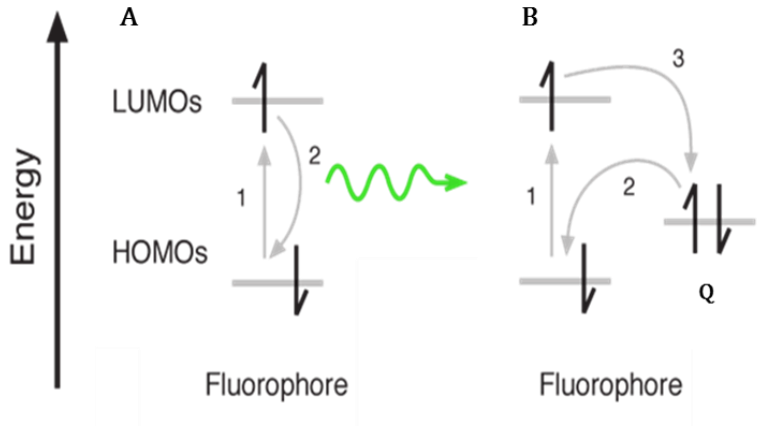

Figure 3.9: (A) When a fluorophore is excited (1) an electron goes from the ground state to the S1. When it returns to the ground-state some energy is released via radiactive process (fluorescence-green arrow). **(B)** In PET the fluorophore is excited (1) and the electron goes to the first excited state (S1). A nearby quencher (Q) donates one of its electrons (2) to the ground state of the fluorophore preventing the excited electron to return to ground state (non-radiactive process). [Adapted from http://labrigger.com/blog/2012/02/29/tsiens-voltagefluors. Consulted on 2014/9/25].

The effectiveness of an alcohol in its ability to perturb protein structure and stability is related to its dielectric constant and viscosity. The reduction of solvent dielectric constant enhances charge-charge interactions and diminishes the advantage of sequestering hydrophobic components away from solvent (Tanizaki et al. 2008). Fluoroalcohols are more effective than ordinary alcohols in disrupting tertiary interactions on folded proteins as they lower the solvent polarity by a more drastic extent and favour the formation of helical structures by promoting intramolecular hydrogen bonding (Sekhar & Udgaonkar 2011).

Steady-State and Time-Resolved Fluorescence Anisotropy Properties

The rotational dynamics of both HL488-labeled calcitonin variants was also studied in different solvents by performing both steady-state and time-resolved fluorescence measurements. Except for the two fluoro alchools used (HFIP and TFE), a single rotational correlation lifetime successfully described the anisotropy decays of both these conjugated peptides (Table 3.6 and Figure 3.8B). As it is displayed in Figure 3.6B, φ_1 (and φ_2 for HFIP and TFE) progressively increased with the viscosity of the solvent used as expected from the Perrin equation (equation 3.2), clearly demonstrating that this (and not the peptide conformation, nor its aggregation state) must be the dominant factor controlling the depolarization of the fluorescence from the HL488-labelled peptides in homogenous solution. On the other hand, the variation of the steady-state fluorescence anisotropy of both sCT-HL488 and hCT-HL488 with $1/\eta$ presents two significant outliers for HFIP and TFE from the general trend obtained with the other solvents (Figure 3.6A), which must be related to the longer mean fluorescence lifetime displayed by these two fluorescent polypeptides in both fluoro alchoools.

For HFIP and TFE, an additional fast rotational correlation time was needed to describe the anisotropy decays of both HL488-labelled peptides (φ_1~0.7 ns and 0.5 ns for sCT-HL488 and hCT-HL488, respectively (Table 3.6)). Since the dye is covalently-attached to the protein, one can assume that the depolarization of the fluorescence is now reflecting two molecular motions: (*i*) the local segmental freedom of the dye, which must somehow be less restricted in these two solvents, and (*ii*) the global tumbling of the derivatized peptide in solution.

A common model used to interpret this behaviour is the "wobbling-in-cone" model (Poveda et al. 2003; Pastor et al. 2007). Considering that the long rotational correlation time (φ_2) was significantly longer than the short one (φ_1), the total anisotropy can be interpreted as the product of two independent processes described above, the first one due to fast movements of the peptide segment containing the HL488 dye, $r_1(t)$, and a second one related to the global rotational motion of the derivatized peptide, $r_2(t)$:

$$r(t) = r_1(t) \cdot r_2(t) = r_1(t) \cdot \exp\left(-t/\varphi_{\text{global}}\right) \qquad [3.4]$$

$$r_1(t) = r(0)\left[\left(1 - S^2_{\text{seg}}\right) \cdot \exp\left(-t/\varphi_{\text{seg}}\right) + S^2_{\text{seg}}\right] \qquad [3.5]$$

S_{seg} is the order parameter describing the restricted range of internal angular fluctuations of the HL488 dye. Considering that an empirical exponential function given by equation 3.6 best fitted the experimental anisotropy decay:

$$r(t) = \beta_1 \exp(-t/\varphi_1) + \beta_2 \exp(-t/\varphi_2) \quad [3.6]$$

the fractional anisotropies, β_i, and the decay correlation times, φ_i, can be related with equations 3.4 and 3.5 above. The order parameters S_{seg} can then be written as:

$$S_{seg}^2 = \frac{\beta_2}{\beta_1 + \beta_2} \quad [3.7]$$

and the long and short rotational correlation times obtained from the fit are respectively related to φ_{global} and φ_{seg} by:

$$\varphi_2 = \varphi_{global} \quad [3.8]$$

$$\varphi_1 = \left(\frac{1}{\varphi_{seg}} + \frac{1}{\varphi_{global}}\right)^{-1} \quad [3.9]$$

Since the fast localized motions derived from the covalently bound dye are restricted, the total light depolarization should not be completed, and the anisotropy should not decay to zero. Nevertheless, the overall rotation of the peptide is responsible for the anisotropy decay to zero at long times (Figure 3.8B). Assuming that the transition dipole moment of the dye is moving freely within a cone with a fixed half-angle, θ_{seg}, the range of angular displacement of these motions can be derived from S_{seg} (Poveda et al. 2003; Pastor et al. 2007):

$$\cos\theta_{seg} = \frac{1}{2}\left[\sqrt{(8S_{seg} + 1)} - 1\right] \quad [3.10]$$

An angle of θ_{seg} ~32° and ~24° were obtained for sCT-HL488 and hCT-HL488 in both solvents, respectively (Table 3.7), suggesting that the angular displacements of the dye are relatively small when compared to the derivatized peptide as a whole during the depolarization process. These constraints on the local motions of the dye are due to the short covalent linkage between the dye and the peptide *N*-terminal. Beyond the probable electrostatic interactions with the peptide surface, HL488 is flanked by a disulfide bond between amino acid residues 1-7, which must help to limit the local rotational freedom of the probe.

Table 3.7: Values obtained for the order parameter S_{seg} and the correspondent half-angle θ_{seg}, which describes the range of angular motions within a cone available to the HL488 fluorophore covalently attached to the two CT variants in homogeneous medium.

Solvents	sCT-HL488		hCT-HL488	
	S_{seg}	θ_{seg}	S_{seg}	θ_{seg}
HFIP	0.83	27.8°	0.88	23.5°
TFE	0.74	35.6°	0.87	24.4°

Finally, an important question regarding the behaviour of sCT-Hl488 and hCT-HL488 is establishing its aggregation state in aqueous solution. As it is exemplified in Figure 3.7B for sCT-HL488, its steady-state fluorescence anisotropy, $<r>_{S1}$, was found to be independent of sCT-HL488 concentration within a large concentration range (1nM ~ 7.5μM): $<r>_{S1}$=0.074±0.03 (n=14). The same behaviour was displayed by hCT-HL488 with $<r>_{S1}$=0.078±0.04 (n=6). Moreover, it was also found that within the range of peptide concentrations used, the steady-state fluorescence anisotropy of sCT-HL488 and hCT-HL488 were also independent of the method used in preparing the samples (Method A or B, section 2.3.2).

Finally, if HL488-labelled calcitonin is assumed to behave like a rigid hydrated sphere with a partial specific volume, $\bar{v}$, and hydration degree, h, the value obtained for φ_{global} can be compared with the theoretical prediction from the Perrin equation (Lakowicz 2006):

$$\varphi = \frac{\eta M_r}{RT}(\bar{v} + h) \qquad [3.11]$$

Here, Mr is the relative molecular mass of sCT-HL488 (3 790 Da) and R the ideal gas constant. Assuming a typically value of $\bar{v} = 0.73 cm^3/g$ for proteins and a hydration of 0.3 g H_2O/g protein at room temperature (T= 293 K), φ_{global} is predicted to be 1.4ns for sCT-HL488 and 1.6ns for hCT-HL488, which is in close agreement to the experimental values (φ_1 = 1.3ns and 1.6ns for sCT-HL488 and hCT-HL488, respectively (Table 3.6). Altogether, these results suggest that both sCT-HL488 and hCT-HL488 behave close to compact monomers in HEPES-KOH, pH 7.4 buffer within a large concentration range.

Curiously, although the disulfide bond present at the *N*-terminal segment of both conjugated polypeptides must help to restrain the local dynamics of the covalently-linked fluorophore, this is not an absolute requirement for both sCT-HL488 and hCT-HL488 to display a monoexponential anisotropy decay in buffer solution (Table 3.6).

In fact, the reduction of the disulfide bond of both HL488-labelled peptides with 1mM DTT only slightly reduced their rotational correlation time, implying that this treatment does not have a pronounced effect on the polypeptide conformational dynamics in buffer solution.

3.2.2. Interaction of HL488-Labelled Calcitonin Variants with Lipid Vesicles

The next step of this work was to study the interaction of both HL488-labelled calcitonin variants with POPC liposomes prepared with variable anionic phospholipid (POPS) content. Since one of the main goals of this investigation was to detect the formation of putatively oligomeric intermediates triggered by the interaction of either HL488-labeled calcitonin variants with negatively charged lipid membranes, these studies were first carried out with relatively high concentrations of the conjugated salmon CT variant, namely 1μM and 3.4μM of sCT-HL488.

3.2.2.1. Influence of sCT-HL488 concentration

In this first set of experiments, a fixed sCT-HL488 concentration (either 1μM or 3.4μM) was added to an increasingly concentration of POPC liposomes containing 20mol% of POPS, within the concentration range 0 – 3 mM of total phospholipid. The method used to prepare the peptide-containing solutions was method A described in section 2.3.2 above. Briefly, the required volume from a concentrated sCT-HL488 stock solution prepared in HFIP was directly injected to the liposome suspension in HEPES-KOH buffer, pH 7.4 buffer. The final concentration of the solvent was always kept low (<1% vol/vol). Each peptide-containing sample was prepared independently and UV-Vis absorption, steady-state and time-resolved fluorescence measurements were performed to detect and characterize in detail the possible intermediate species produced during the interaction of sCT-HL488 with the anionic lipid membranes within a wide range of peptide/lipid (P/L) molar ratios.

UV-Vis Absorption Properties

The absorption spectra of both 1μM and 3.4μM sCT-HL488 revealed a significant red-shift with the addition of increasing concentrations of phospholipid, relatively to the spectra obtained in aqueous solution, reporting the progressive binding of sCT-HL488 to the membrane surface of the negatively-charged lipid vesicles. The maximum absorption wavelength of the HL488-fluorescently labeled salmon CT variant changed from 504 nm to ~508/509 nm for total phospholipid concentrations higher than 2 mM (Figure 3.10A).

Simultaneously, there was a change in the shape of the absorption spectra of sCT-HL488, particularly at low lipid concentrations. As it is exemplified in Figure 3.10B for 3.4μM sCT-HL488 in interaction with 0.1 mM POPC:POPS 80:20 LUVs, a "shoulder" appeared in the blue region of its absorption spectrum, which was gradually lost upon increasing the lipid concentration in solution.

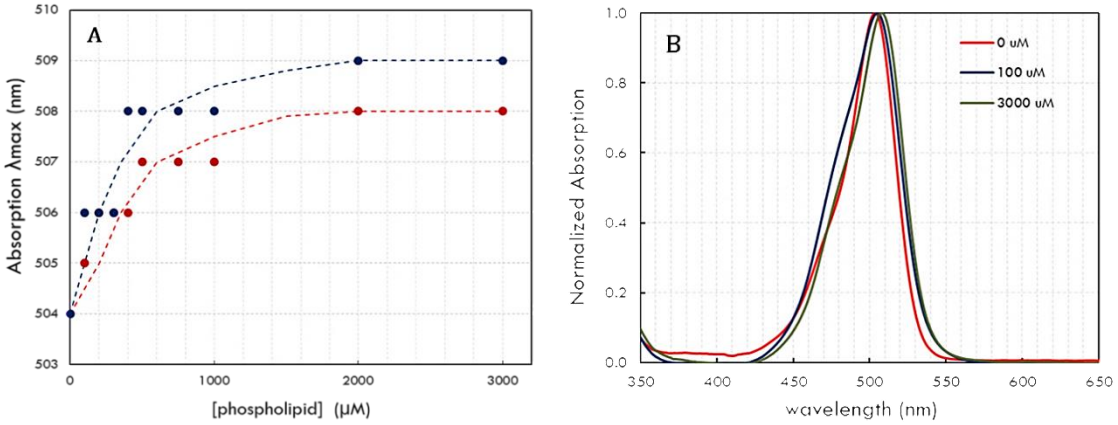

Figure 3.10: (A) Normalized absorption spectra obtained for 3.4μM sCT-HL488 in interaction with increasing concentrations of liposomes: sCT-HL488 in buffer (red), and in the presence of 0.1 mM (blue) and 3mM (green) POPC:POPS 80:20 LUVs. **(B)** Upon increasing the total phospholipid concentration, the maximum absorption wavelength obtained for both 1.0 (blue dots) and 3.4μM (red dots) sCT-HL488 gradually red-shifted from 504 nm to ~508 – 509 nm.

These spectral alterations are characteristic of excitonic interactions between the chromophores due to their dimerization (Green et al. 1989; Castro et al. 2012). Additive interactions like van der Waals or hydrogen bonding have been suggested to explain the forces holding the dye ions together in solution. The self-association between organic dyes exhibit distinct changes in the absorption spectrum as compared to the monomeric species, and can be used to track the aggregation of the labelled peptides/phospholipids in solution/liposomes (Bergström et al. 2002).

The spectroscopic characteristics in systems with interacting chromophores can be explained by the exciton theory, based on a resonance dipole-dipole interaction mechanism (Green et al. 1989). According to this, a system of two non-interacting monomers splits its excited-state level into two new levels through the interaction of the transition dipoles upon dimerization. The interaction energy between the chromophores is a function of the transition moment of the monomer.

Changes in the absorption spectrum depend on the geometry of the dimer: (*a*) for parallel dimers (H-type) the spectrum consists of a single band blue-shifted with respect to the monomer, (*b*) for head-to-tail dimers (J-type) the spectrum shows a single band red-shifted with respect to the monomer, and (*c*) in dimers having intermediate geometries a band splitting is observed and the absorption spectrum shows two bands of similar bandwidth.

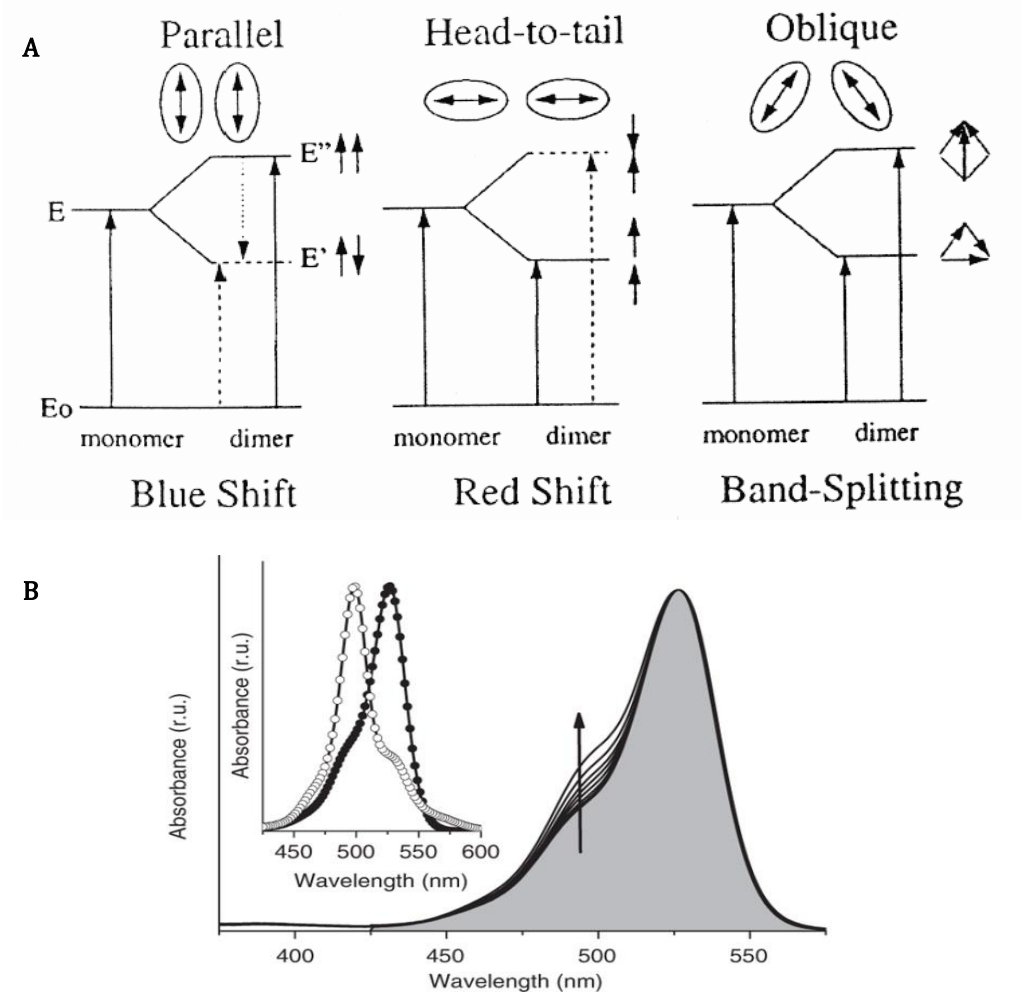

Figure 3.11: (A) When two dipoles are brought to close proximity side by side the energy of the individual molecules, *E*, will split into two new states with the energies *E*'' and *E*': parallel dipoles repel each other and get the higher energy state, while the antiparallel dipoles attract each other, which lowers the energy of that state. Parallel dipoles make up an overall higher dipole moment, i.e. stronger absorption, while antiparallel dipoles cancel each other to make a weak absorption. The net result is a blue shift of absorption. Similarly for head-to-tail arrangement, the lower energy state has a larger transition dipole moment and the net effect is a red shift of absorption. The intermediate, oblique, orientation results in band split - two bands appearing at lower and higher energy. **(B)** Illustrative representation of the theoretical prediction for the impact of progressive H-type dimer formation on the absorption spectra of the chromophore upon increasing its concentration in solution. **Inset:** The normalized absorption spectra of the monomeric and dimeric species (H-type dimer) are depicted by closed and open symbols, respectively. [Adapted from(Kasha et al. 1965)].

This behaviour is related with the forbidden transitions for each excited state as described in more detail in Figure 3.11. Accordingly, the spectral alterations detected in the absorption spectra of sCT-HL488 at a high P/L molar ratio (low phospholipid concentration) reveal the formation of parallel dimers (H-type) between the HL488 chromophores covalently linked to sCT.

As expected, the intensity of the excitonic band was greater for the 3.4μM than for the 1.0μM sCT-HL488 partition study. This result indicates that upon reaching a high local concentration, the fluorescently-labeled peptides must be aligned in parallel on the membrane surface, in order for the chromophores to be able to interact with each other. Upon increasing the liposome concentration in solution, the surface concentration of membrane-bound peptides becomes progressively diluted, effectively preventing their dimerization (Figure 3.12).

Steady-State and Time-Resolved Fluorescence Properties

Concomitantly, the changes undergone by the fluorescence emission properties of both 1.0 and 3.4μM sCT-HL488 upon interacting with POPC:POPS 80:20 liposomes were also characterized. As it is shown in Fig. 3.13A , the intensity-weighted emission wavelength, $<\lambda>$, of both concentrations of sCT-HL488 progressively red-shifted from 540.6 – 541.1 nm to 544.3 nm, upon increasing the total phospholipid concentration in solution, while their fluorescence emission spectra remained essentially invariant (data not shown).

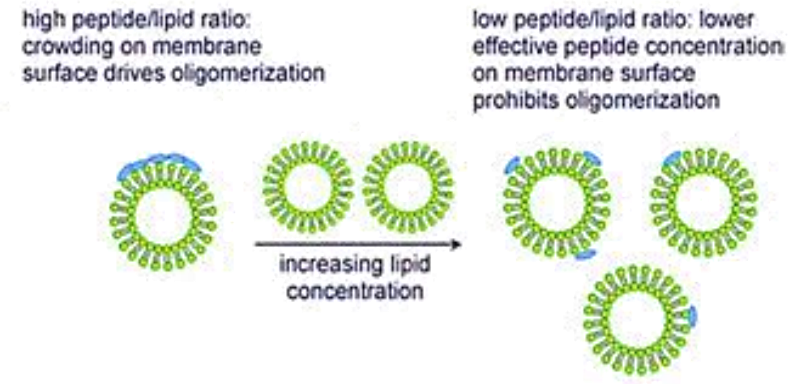

Figure 3.12: Influence of the peptide/lipid molar ratio on oligomer formation and fibrillation rates, as proposed by Wong et al. Upon increasing the phospholipid concentration the surface concentration of membrane bound-peptide becomes more diluted preventing oligomerization on the membrane surface[Adapted from (Wong et al. 2009)].

Simultaneously, the integrated areas calculated for the emission spectra obtained for both concentrations of fluorescently-labeled sCT, normalized to its initial value in aqueous solution, presented a biphasic behaviour (Figure 3.13B). For 1.0 and 3.4μM sCT-HL488, this parameter sharply decreased to a minimum value of ~80 and ~60% of its initial value in buffer solution , respectively, when low concentrations of phospholipid were added to the solution (~ 0.1 and 0.2 mM total phospholipid, respectively). Upon further increase of the phospholipid concentration, there was a progressive recovery of the integrated emission areas which, however, did not reach its initial value when 3.4μM sCT-HL488 was used (Figure 3.13B).

The fluorescence emission decay kinetics of both 1.0 and 3.4μM sCT-HL488 in the presence of increasing concentrations of POPC:POPS 80:20 liposomes were always well described by a tri-exponential function. Typically, the short, intermediate and long lifetimes increased from τ_1~0.2 – 0.3ns to ~0.5ns, τ_2~1.5ns to ~2.0ns and τ_3~4.0ns to 4.2 ns, respectively, upon sCT-HL488 binding to the liposomes (Figure 3.13F). The longest lifetime, τ_3, was always the dominant component of the fluorescence intensity decay, contributing ca. 90% to the fluorescence emission from the conjugated peptide.

At variance with the changes displayed by the steady-state fluorescence intensity of sCT-HL488 (Figure 3.13B), the amplitude-weighted mean lifetime, $<\tau>_1$, for both concentrations of sCT-HL488 was almost independent of the phospholipid concentration used in the assay (Figure 3.13D), slightly increasing from ca. 3.3 ns in buffer solution to ~3.7 ns upon binding to the negatively-charged lipid vesicles. In the presence of low phospholipid concentrations, $<\tau>_1$ marginally decreased from ca. 3.3 ns to ~3.0 ns (Figure 3.13D).

Altogether, the steady-state and time-resolved fluorescence data described so far for sCT-HL488 indicate that the HL488-fluorescently labeled peptide undergoes static fluorescence quenching in the samples prepared with a high P/L ratio. Since the presence of an excitonic band in the absorption spectra of the conjugated peptide is also more easily detected under the same experimental conditions, our results provide evidence for the formation of non-fluorescent dimers (dark states) when sCT-HL488 reaches a high membrane surface concentration at a high P/L molar ratio. Moreover, control experiments revealed that either concentration of the conjugated peptide was not able to induce the aggregation of the liposomes used because the light scattered by the liposomes showed an identical linear profile with the increasing lipid concentration, in the absence and in the presence of the conjugated peptide (data not shown).

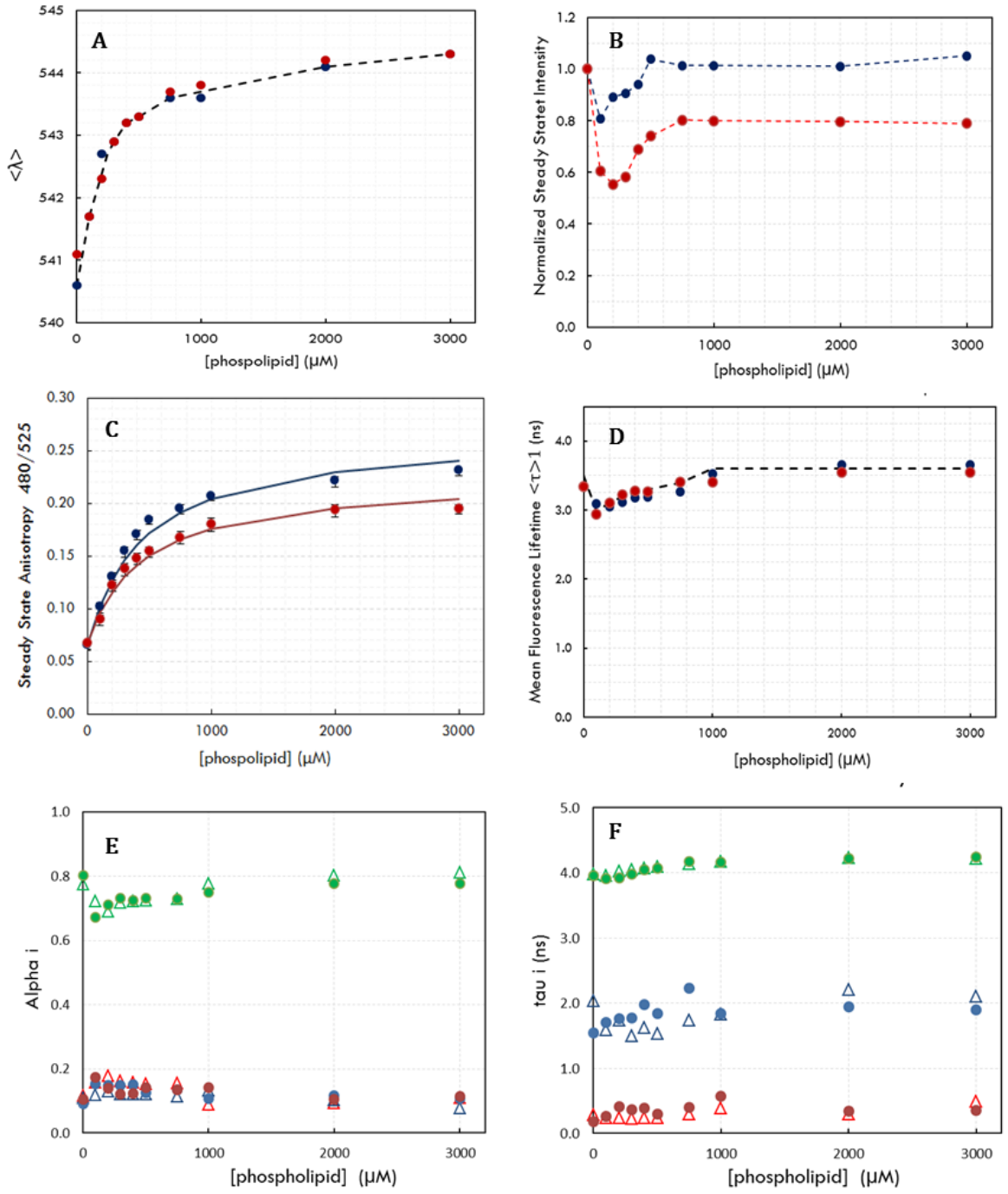

Figure 3.13: Changes in the steady-state and time-resolved fluorescence emission properties of sCT-HL488 upon interaction with POPC:POPS 80:20 LUVs. Variation of the **(A)** intensity-averaged emission wavelength, <λ>, **(B)** integrated emission area, normalized to its value in aqueous solution, **(C)** steady-state fluorescence anisotropy, <r>S1, and **(D)** amplitude-weighted mean fluorescence lifetime, $<\tau>_1$, of 1.0 (blue circles) and 3.4μM (red circles) sCT-HL488 with the total phospholipid concentration in solution. The solid curves in C are the best fit of equation 2.5 to the data (see the text for more details). **(E)** Normalized amplitudes, α_i, associated with **(F)** each lifetime component, τ_i, obtained from the analysis of fluorescence emission decay kinetics of 1μM (circles) and 3.4 μM (triangles) sCT-HL488 in the presence of increasing total phospholipid concentrations: i= 1 (red symbols), i= 2 (blue symbols) and i= 3 (green symbols), respectively.

Steady-state and Time-resolved Fluorescence Anisotropy Properties

Finally, both steady-state and time-resolved fluorescence anisotropy measurements confirmed that sCT-HL488 partitions to POPC liposomes containing 20mol% POPS, corroborating the conclusions retrieved from the spectral alterations described above. Figure 3.13C shows that the steady-state anisotropy of both 1.0 and 3.4μM sCT-HL488 increased hyperbolically from $<r>_{S1}$~0.067 to ~0.23 and ~0.20, respectively, upon increasing the total phospholipid concentration in solution. Upon binding to the anionic lipid vesicles, the rotational mobility of the conjugated peptides was much more limited (see below) (Figure 3.13A), causing an increase in its steady-state anisotropy since the intensity-weighted mean fluorescence lifetime, $<\tau>_2$, of sCT-H488 remained essentially invariant. Interestingly, despite the biphasic changes described earlier for the steady-state fluorescence intensity (integrated emission area) of sCT-HL488 with the lipid concentration, $<r>_{S1}$ varied monotonically with the phospholipid concentration in solution for both peptide concentrations used, further supporting the conclusion about the formation of non-fluorescent dimers of sCT-HL488 at high P/L molar ratios.

Assuming that the only fluorescent molecules in solution are the monomeric conjugated peptides, either free in solution or membrane-bound, and that there is no homo-FRET between the membrane-bound molecules, the large variation observed for the fluorescence anisotropy of sCT-HL488 upon its binding to the lipid membrane allows to retrieve its partition coefficient. By performing a non-linear regression fit of equation 2.5 to the experimental steady-state anisotropy data, a K_p=(3.1 ± 0.2)x10^5 and r_l =0.251±0.004 and $K_p = (2.9 \pm 0.3)$x10^5 and r_l = 0.214±0.005 were obtained for 1μM and 3.4μM sCT-HL488 (Figure 3.13C), respectively, using Q=1.1. As a control, the partition of free HL488 towards liposomes prepared with the same composition was also studied. The dye did not bind to these lipid membranes since there were no spectral alterations, nor changes in its steady-state anisotropy value, upon increasing the total phospholipid concentration in solution (data not shown).

More detailed information about the rotational dynamics of sCT-HL488 upon its binding to the anionic liposomes was obtained from the analysis of its fluorescence anisotropy decays in the presence of increasing phospholipid concentrations (Figure 3.14A). Two correlation times were now used to describe the anisotropy decay curves obtained for sCT-HL488 in the presence of liposomes. Moreover, a residual anisotropy value, r_∞, was also included in these analyses since the fluorescence anisotropy decays of sCT-HL488 did not converge to zero at long times (Figure 3.14A e C).

This value reflects a restricted rotational motion of the fluorescently-labeled peptide upon binding to the anionic membrane. The depolarization of fluorescence due to rotation of the conjugated peptides bound to the liposomes comes now from the local movement of the molecule or a segment of the molecule to which the fluorophore is covalently linked (fast local motions), subjected to the restrictions imposed by the lipid arrangement (intermediate timescale local motions), combined with the rotation of the vesicle as a whole (slow global motion), which is in fact too slow to be significant during the time window defined by the excited-state lifetime of sCT-HL488 (Figure 3.15) (Zanin et al. 2013).

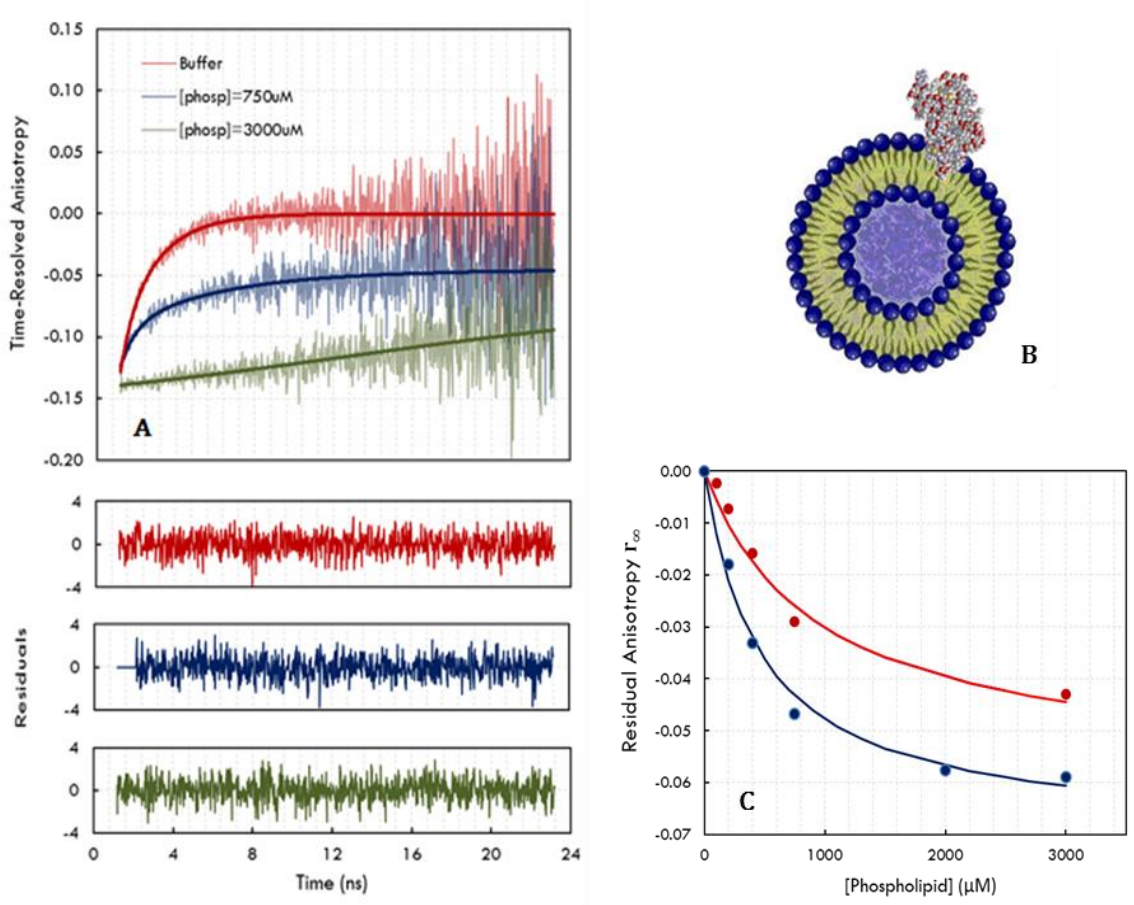

Figure 3.14: (A) Fluorescence anisotropy decays obtained from 1μM sCT-HL488 free in solution and in the presence of POPC:POPS 80:20 LUVs (λ_{exc}= 335 nm; λ_{em}= 525 nm). The red, blue and green solid lines are the best fitting curves of equation 2.14 to the anisotropy decays obtained for sCT-HL488 in the presence of 0, 0.75mM and 3mM POPC:POPS 80:20 LUVs, respectively. The residuals of each fit are also shown below. **(B)** Illustration of sCT-HL488 binding to the anionic lipid vesicles which leads to the restricted rotational motion of the conjugated peptide (not drawn to scale). **(C)** The residual anisotropy value, r_∞, obtained for both 1μM (blue dots) and 3.4μM (red dots) sCT-HL488 progressively decreased upon increasing phospholipid concentration, as expected. The solid curves in C are the best fit of equation 2.5 to the data (see the text for more details).

Table 3.8: Fluorescence anisotropy decay parameters obtained for 1μM sCT-HL488 in the presence of increasing concentrations of phospholipid (POPC:POPS 80:20 LUVs). The decays were obatined using λ_{exc}=335 nm and λ_{em}=525 nm and $r(0)= \beta_1 + \beta_2 + r_\infty$.

[LUVs] (mM)	β_1	φ_1 (ns)	β_2	φ_2 (ns)	r_∞	$r(0)$	χ^2
0.0	-0.13	1.42			0.00	-0.14	1.16
0.2	-0.06	0.89	-0.05	3.9	-0.02	-0.13	1.10
0.4	-0.04	0.54	-0.06	3.9	-0.03	-0.14	1.14
0.75	-0.04	0.74	-0.05	5.1	-0.05	-0.13	0.99
2.0	-0.03	1.10	-0.04	10.7	-0.06	-0.13	1.08

Following the model previously used on the interpretation of the fluorescence anisotropy decays obtained for sCT-HL488 free in solution, the total anisotropy of the conjugated peptide was described by a product of two independent depolarization processes, since the two rotational correlations times obtained for the membrane-bound sCT-HL488 differed by more than an order of magnitude (Table 3.8). In this case, the partition of the peptide to the membrane leads to a restriction in its motion, so it can no longer rotate freely in solution, and this new situation can be described as a "cone-in-a-cone model" (Schröder et al. 2005) or "woobling-in-two-cones" (Melo et al. 2014). The first cone describes the local probe motion covalently attached to the peptide (φ_{seg}), and the second one the restricted motion of the peptide in the membrane (φ_{ads}) (Figure 3.14B). Accordingly, the anisotropy decay can be described as:

$$r(t) = r(0)\left[\left(1\text{-}S_{seg}^2\right)\cdot\exp\left(-t/\varphi_{seg}\right) + S_{seg}^2\right]\left[\left(1\text{-}S_{ads}^2\right)\cdot\exp\left(-t/\varphi_{ads}\right) + S_{ads}^2\right] \qquad [3.12]$$

where $S_{seg}$and S_{ads} are the order parameters characterizing the internal and the whole fluctuations of the membrane-bound HL488-labeled sCT. Since $\varphi_{ads} >> \varphi_{seg}$ the above expression can be simplified to the sum of two exponentials functions and a constant term:

$$r(t) = r(0)\left(1 - S_{seg}^2\right)\cdot\exp\left(-t/\varphi_{seg}\right) + r(0)(1 - S_{ads}^2)S_{seg}^2\cdot\exp\left(-t/\varphi_{ads}\right) + r(0)S_{seg}^2S_{ads}^2 \qquad [3.13]$$

By directly comparing this new equation to the two exponential function used to empirically describe the fluorescence anisotropy decays:

$$r(t) = \beta_1\exp\left(-t/\varphi_1\right) + \beta_2\exp\left(-t/\varphi_2\right) + r_\infty \qquad [3.14]$$

the $S_{\text{seg}}$and S_{ads} parameters can be written as:

$$S^2_{\text{seg}} = \frac{\beta_2 + r_\infty}{r(0)} \quad [3.15]$$

$$S^2_{\text{ads}} = \frac{r_\infty}{\beta_2 + r_\infty} \quad [3.16]$$

By performing a non-linear regression fit of equation 2.5 to the experimental r_∞ data (considering $r^w_\infty = 0$), a K_{p}= $(2.2 \pm 0.3)\text{x}10^5$ and $r^l_\infty = -0.070 \pm 0.003$ and K_{p}=$(1.1 \pm 0.3)\text{x}10^5$ and r^l_∞ = - 0.058 ± 0.007 were obtained for the partition studies carried out with 1.0 and 3.4μM sCT-HL488, respectively, in agreement with the values previously calculated with the steady-state anisotropy values. r^l_∞ is the limiting value that would be obtained for the residual anisotropy when 100% of the fluorescently-labelled peptide is bound to the lipid membranes.

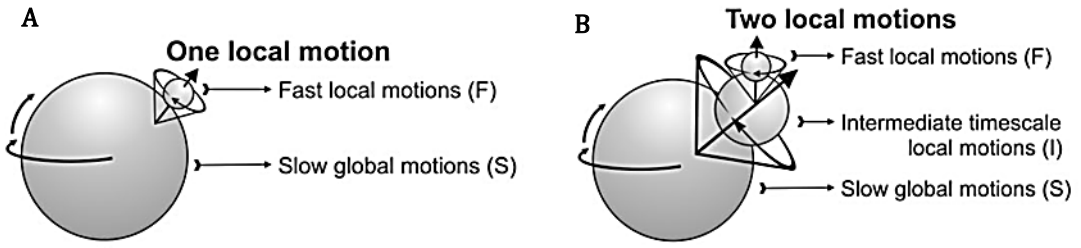

Figure 3.15: (A) Schematic representation of the global peptide rotation (large sphere) and spatially confined local dynamics of the probe (small sphere) covalently bound to the calcitonin peptide free in solution. **(B)** Schematic representation of the fast (probe covalently bound to the peptide – the smallest sphere) and intermediate (peptide bound to the membrane – intermediate sphere) motions which can be analysed according to the wobbling-in-cone model. Slow global motions (anionic lipid vesicles – the largest sphere) could not be measured in the experiments of fluorescence anisotropy decay because typical rotation times are in the domain of microseconds. A and B are not drawn to scale [Adapted from (Ellis et al. 2009)]

It was then possible to calculate the angles θ_{ads} and θ_{seg} using equation 3.10 as previously described, after calculating the respective S parameters accordingly to equations 3.15 and 3.16 above. An angle of $\theta_{\text{seg}} = 18.1^0$ and $\theta_{\text{ads}} = 31.1^0$ and $\theta_{\text{seg}} = 19.7^0$ and $\theta_{\text{ads}} = 35.2^0$ were obtained for the partition studies performed with 1μM and 3.4μM sCT-HL488, respectively (Table 3.9) using the limiting anisotropy value where 100% of the fluorescently-labelled is membrane-bound. These results indicate that the amplitude of the local segmental motions of the fluorophore covalently linked to the sCT variant became to some extent more pronounced upon its binding to the anionic lipid vesicles.

Table 3.9: Partition coefficients, K_p, limiting anisotropy, r_l, order parameters S_{seg} and S_{ads}, and the correspondent half-angles θ_{seg} and θ_{ads} obtained for sCT-HL488 in interaction with POPC:POPS 80:20 LUVs from the analysis of the steady-state and time-resolved fluorescence anisotropy data. r_∞^l is the limiting value that would be obtained when 100% of the fluorescently-labelled peptide is membrane-bound. Q=1.1 in all calculations.

[sCT-HL488] (μM)	Steady-state measurements		Time-resolved measurements					
	K_p (x10^5)	r_l	K_p (x10^5)	r_∞^l	S_{seg}	θ_{seg}	S_{ads}	θ_{ads}
1.0	3.1±0.2	0.251±0.004	2.2±0.3	-0.07±0.003	0.92	18.1º	0.79	31.1º
3.4	2.9±0.2	0.214±0.005	1.1±0.3	-0.058±0.007	0.91	19.7º	0.74	35.2º

In summary, the changes undergone by the spectroscopic properties of 1.0 and 3.4μM sCT-HL488 upon the addition of POPC lipid vesicles containing 20mol% of POPS can be described by two coupled equilibria, as illustrated in Figure 3.16. At low total phospholipid concentrations (high P/L molar ratio), the majority of the HL488-labeled sCT is free in solution; however, due to the low number of liposomes in each sample, the membrane surface is very crowded with membrane-bound sCT-HL488, promoting peptide-peptide interactions (Wong et al. 2009; Melo et al. 2013) (Figure 3.12). This drives the establishment of excitonic interactions between the *N*-terminally covalently linked chromophores and formation of non-fluorescent sCT-HL488 oligomers (possible dimers) on the anionic lipid vesicles.

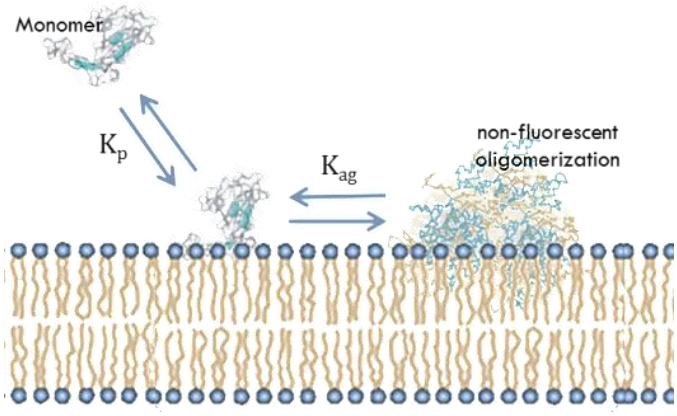

Figure 3.16: sCT-HL488 interaction with POPCPOPS 80:20 LUVs can be described according to a two-coupled equilibria model: briefly, monomeric sCT-HL488 is distributed between the aqueous solution and anionic membrane phases according to a simple partitioning equilibrium, where K_p is the mole fraction partition coefficient defined previously. Upon reaching a high peptide concentration on the membrane surface, sCTHL488 assembles into membrane-bound non-fluorescent oligomers (dark complexes), described by a surface aggregation constant, K_{ag}.

According to this model, and as expected, the use of a higher concentration of sCT-HL488 (3.4μM compared to 1μM) produced a larger static quenching effect, since the oligomerization process of sCT-HL488 is concentration-dependent. Upon progressively raising the lipid concentration (decreasing the P/L molar ratio), most of sCT-HL488 becomes membrane-bound but very surface-diluted among the lipid vesicles, which effectively prevents peptide-peptide interactions and the subsequent membrane-driven peptide oligomerization. The membrane-bound monomeric HL488-labeled sCT is no longer undergoing static quenching, and therefore the steady-state fluorescence intensity of the samples almost recovers its initial value measured for 1.0μM sCT-HL488 free in buffer solution.

3.2.2.2. Influence of lipid composition

After establishing the importance of sCT-HL488 concentration on its interaction with anionic lipid vesicles, we next sought to characterize the influence of the anionic lipid content of the liposomes on the partition coefficient of the fluorescently-labeled CT variant. According to the interaction model presented above, a lower concentration of HL488-labeled peptide was now used in order to shift the coupled equilibria of the system towards the membrane-bound monomeric sCT-HL488 species. Following the same experimental design used earlier, 0.2μM of sCT-HL488 was independently added to 0-4mM POPC liposomes containing 0, 10, 20 or 30mol% of POPS.

There was no spectroscopic evidence for sCT-HL488 binding to 100%mol POPC LUVs. Both its absorption (Figure 3.17A) and fluorescence emission spectra (Figure 3.17C), in addition to its steady-state fluorescence anisotropy (Figure 3.17B), were found to be independent of the total phospholipid concentration added to the solution.

For POPC LUVs containing 10, 20 and 30mol% POPS, a progressive red-shift in the maximum absorption wavelength of each sample was detected upon increasing the phospholipid concentration, as described earlier (Figure 3.17A), providing evidence for sCTHL488 partition to the lipid membranes. Furthermore, no alterations characteristic of excitonic interactions were no longer detected in the absorption spectra due to the lower concentration of the conjugated peptide used in these experiments, as expected (data not shown). The spectral shifts were more pronounced and required a lower concentration of total phospholipid to occur as the anionic phospholipid content of the liposomes increased from 10 to 30mol%, as it is exemplified in Figure 3.17A for $\lambda_{\max}^{\mathrm{Abs}}$.

Surprisingly, in the presence of increasing concentrations of phospholipid up to ~ 2 – 3 mM, the integrated emission areas of 0.2μM sCT-HL488 progressively decreased to nearly 20% of its initial value measured in aqueous solution (Figure 3.17C), contrasting with the previously results. For POPC liposomes containing 30mol% POPS, this parameter almost recovered its initial value upon further increasing the phospholipid concentration used in the assay (Figure 3.17C – orange triangles). In addition, it should be noted that the integrated areas presented a more erratic behaviour than the one obtained earlier with 1.0 and 3.4μM sCT-HL488, which might be related to the lower concentration of peptide used in these experiments and/or with the incubation time of each sample before the measurements (see below).

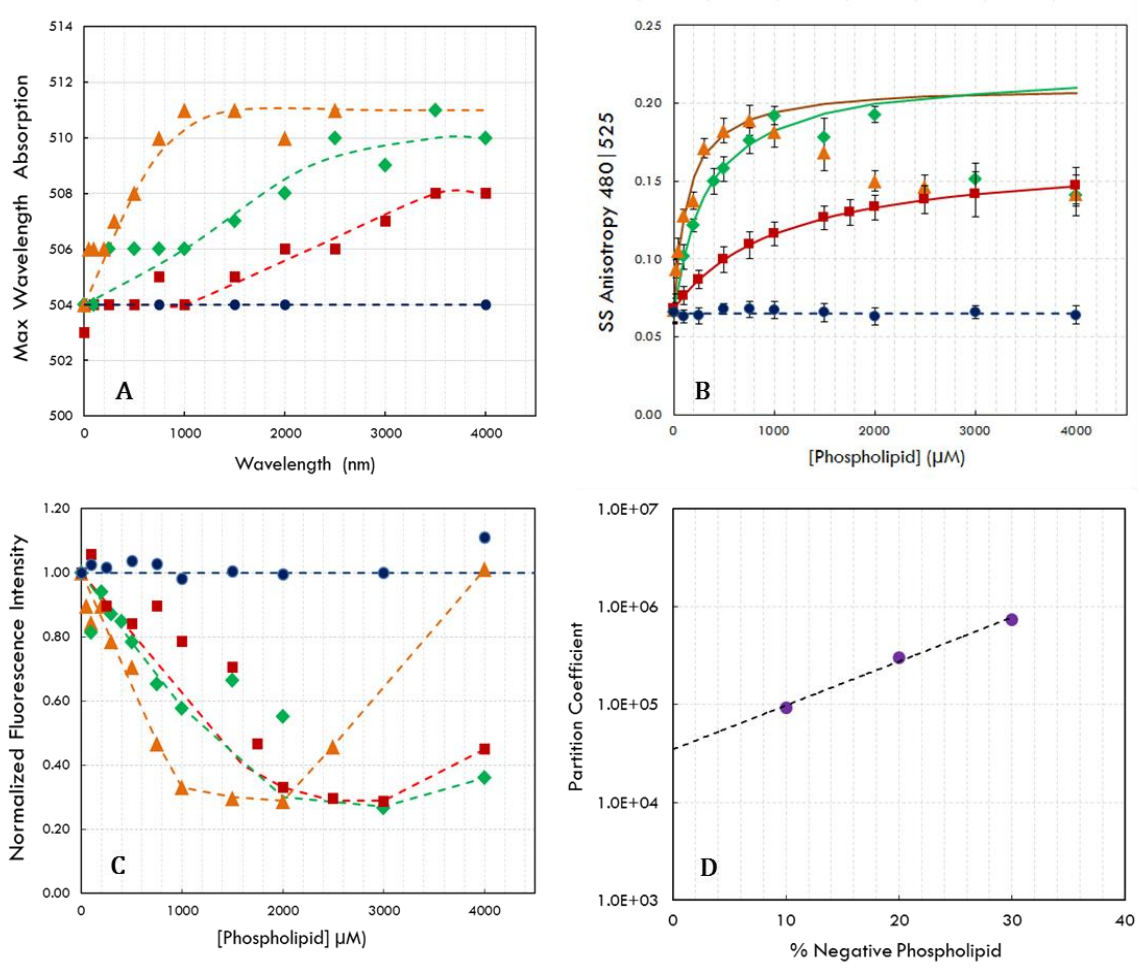

Figure 3.17: Variation of the **(A)** maximum absorption wavelength, **(B)** steady-state fluorescence anisotropy, $\langle r \rangle_{S1}$ and **(C)** integrated emission area, normalized to its value in aqueous solution, with the total phospholipid concentration when 0.2μM sCT-HL488 was added to POPC LUVs constaining 0mol% (blue circles), 10 mol% (red squares), 20mol% (green diamonds) and 30mol% of POPS (orange triangles). The solid lines in (B) are the best fit of equation 2.5 to the initial anisotropy data (see the text for more details). **(D)** Dependence of the apparent or approximate sCT-HL488 mole fraction partition coefficient with the mol% of POPS included in the POPC LUVs.

Concomitantly, the steady-state fluorescence anisotropy of sCT-HL488 gradually increased from $<r>_{S1}$~0.07 to $<r>_{S1}$~0.15 with the total phospholipid concentration when 10mol% POPS-containing POPC liposomes were employed (Figure 3.17C – red squares), confirming that this parameter is an extremely sensitive reporter of HL488-labeled sCT binding to the lipid vesicles. Interestingly, for liposomes containing 20% and 30%mol POPS (green diamonds and orange triangles in Figure 3.17C, respectively), the anisotropy curves after reaching $<r>_{S1}$~0.20 progressively declined to $<r>_{S1}$~0.15 for total phospholipid concentrations higher than approximately 2mM and 0.5mM, respectively. In order to obtain an approximate value for the partition coefficients presented by 0.2μM sCT-HL488 as a function of the anionic lipid content of the liposomes, equation 2.5 was again fitted to the experimental steady-state anisotropy data obtained up to 1mM total phospholipid, as described in the previous section (Table 3.10). The approximate partition coefficients obtained for HL488-labelled calcitonin presented an exponential dependence on the molar fraction of POPS incorporated in the anionic lipid vesicles, confirming the importance of electrostatic interactions in salmon calcitonin binding to the lipid membranes (Melo et al. 2011), as expected due to its net charge of +3.

Table 3.10: Dependence of the apparent or approximate mole fraction partition coefficient, $\boldsymbol{K_p^{app}}$, obtained for 0.2μM sCT-HL488 with the mol% of POPS included in the POPC LUVs. The progressive decline in the steady-state anisotropy data detected in some cases for phospholipid concentrations higher than 0.2 or 1mM was excluded from the fitting equation 2.5 to the experimental steady-state anisotropy data (Q=1.1).

mol% POPS	K_p (x10^5)	r_l
10	(0.9 ± 1.3)	0.168 ± 0.01
20	(3.0 ± 0.4)	0.222 ± 0.01
30	(7.4 ± 1.5)	0.212 ± 0.01

Altogether, the results obtained in this set of experiments were surprising, particularly the biphasic changes presented by the integrated areas and steady-state fluorescence anisotropies measured for 0.2μM of sCT-HL488 in the presence POPC LUVs containing 20 and 30 mol% of POPS. Focusing on the steady-state anisotropy data, which is a less concentration-dependent parameter than the fluorescence intensity, several hypotheses were considered as feasible justifications for the results obtained:

(i) the possibility that light scattering produced by the liposomes at the highest phospholipid concentrations used was affecting these measurements was discarded by two considerations: First, a constant $<r>_{S1}$= 0.065±0.002 was obtained for sCT-HL488 for all POPC concentrations used (Figure 3.17A – blue circles), and secondly the diameter (Table 2.4 in Chapter II), as well as the light scattered by the lipid suspensions, was found to be essentially independent of the anionic lipid content of the LUVs. Furthermore, in either case there was no evidence for peptide-induced aggregation of the liposomes, irrespective of its anionic lipid content, as the light scattered by the liposomes was also found to be independent of the presence of 0.2μM sCT-HL488 in solution (data not shown).

(ii) the possible occurrence of homo-FRET between the membrane-bound sCT-HL488 peptides was also ruled out because this effect only becomes important when membrane surface crowding occurs, i.e. at high P/L molar ratios (Melo et al. 2014), at variance with the experimental data obtained (Figure 3.17B).

(iii) eventually, the final drop in the steady-state anisotropy might be an indirect effect due to a concomitant increase in the intensity-weighted mean lifetime, $<\tau>_2$, of the membrane-bound sCT-HL488. However, this hypothesis is not consistent with the parallel decrease measured in its integrated emission area; unfortunately, no time-resolved measurements were made in this set of experiments which would allow us to rule out this hypothesis.

(iv) finally, it was considered that kinetic effects, eventually related to the method used in the preparation of the samples, might be the major factor responsible for these results. In fact, in order to obtain a lower concentration of the fluorescently-labeled peptide in each sample (0.2μM), the stock I solution of the fluorescently-labeled peptide (sCT-HL488 dissolved in 200μL of HFIP) was diluted by a factor of eight to obtain stock II (still using HFIP as solvent), before its direct injection to the aqueous medium. This procedure might influence the final conformation/aggregation state of the fluorescently-labeled peptide in the aqueous solution and its subsequent interaction with the liposomes. This scenario will be explored in the next section.

3.2.2.3. Influence of the method used to prepare the peptide containing solutions

To evaluate the potential impact of the change made in the method used to prepare the samples, the time evolution of the fluorescence properties of both 0.2 and 1.0μM sCT-HL488 in interaction with variable concentrations of POPC:POPS 80:20 and 70:30 LUVs was monitored at RT using a micro plate reader (exemplified in Figure 3.18 for POPC LUVs containing 20mol% POPS). The time course of the steady-state fluorescence intensity and anisotropy presented a clear dependence on the final concentration of the fluorescently-labeled peptide used.

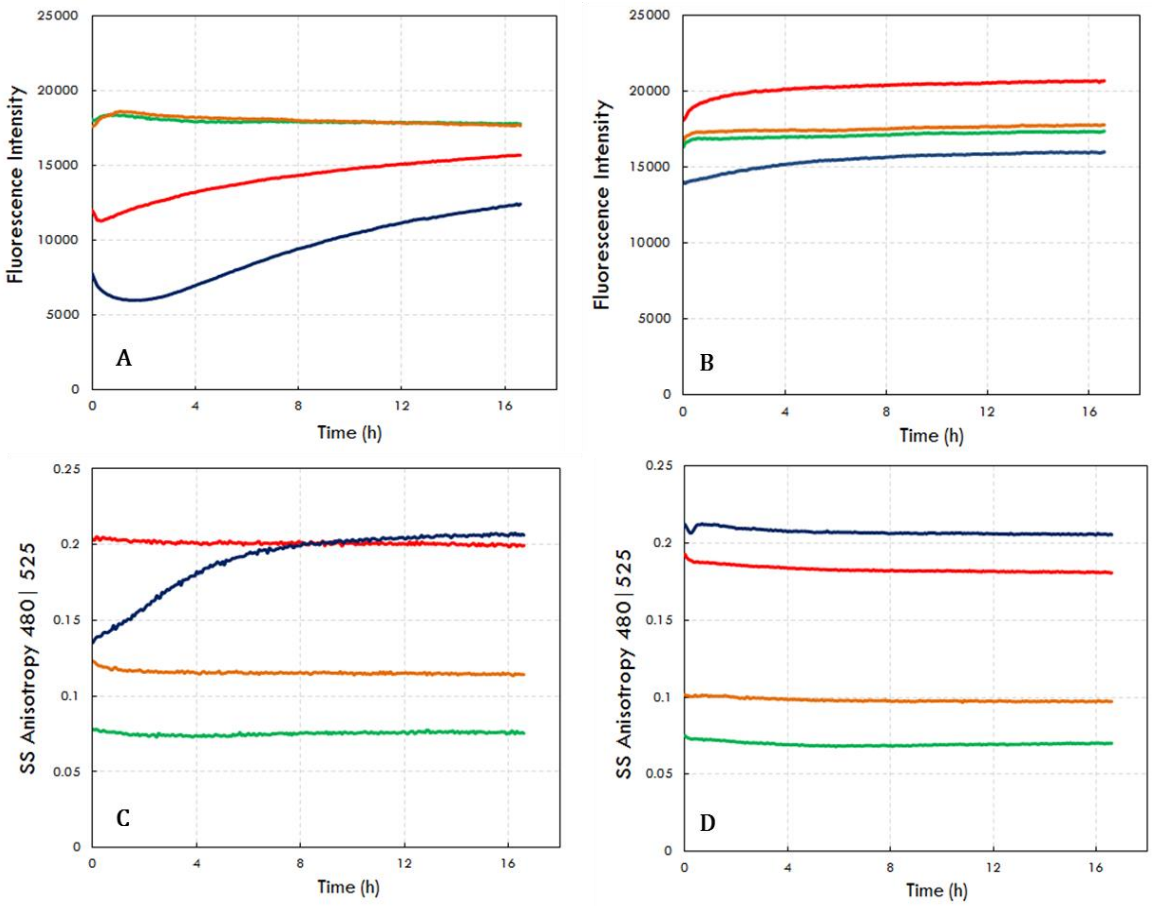

Figure 3.18: Changes in the steady-state **(A and B)** fluorescence intensity and **(C and D)** anisotropy of sCT-HL488 in interaction with 0 (green curve), 0.1mM (orange curve), 1.0mM (red curve) and 3mM (blue curve) POPC:POPS 80:20 LUVs over time. The sCT-HL488 concentrations used were **(A and C)** 0.2μM and **(B and D)** 1.0μM sCT-HL488, which were obtained from directly injecting the stock I and II solutions of the fluorescently-labeled peptide to the liposome suspensions, respectively. Similar data was obtained with POPC:POPS 70:30 LUVs over time.

For 1μM sCT-HL488-containing samples, there were no significant variations of the fluorescence intensity (Figure 3.18A) and anisotropy (Figure 3.18B) of the conjugated peptide with time. In addition, the final steady-state anisotropies of sCT-HL488 measured after ~16h of sample incubation at RT increased with the total phospholipid concentration added to the solution (Figure 3.21), in agreement with the equilibrium study performed earlier (Figure 3.13C). On the other hand, the fluorescence intensity of the 0.2μM sCT-HL488-containing samples significantly augmented over time, still not reaching a constant value even after ~16h of incubation (Figure 3.18C). The initial drop registered for this parameter from the value measured for the fluorescently-labeled peptide in aqueous solution became more pronounced upon increasing the total phospholipid concentration added to the solution, suggesting that this effect is somehow liposome-mediated.

Interestingly, only the 3.0mM phospholipid-containing sample changed its steady-state fluorescence anisotropy over time, rising from $<r>_{S1}$~0.13 until reaching the expected plateau value of $<r>_{S1}$~0.21 after incubating the sample for ≥8h (Figure 3.18D). Overall, these results confirmed that there were significant kinetic effects at play on the data presented above (Figure 3.17); it seems that the final HFIP/sCT-HL488 ratio affects in some way the time necessary for the samples to reach equilibrium fluorescence values. In order to gain more information about the complex behavior of this system, the kinetics of the interaction of 0.2μM sCT-HL488 with 3mM of either 20 or 30 mol% POPS-containing POPC LUVs was also monitored over an incubation time of 6h at RT using time-resolved fluorescence measurements (exemplified in Figure 3.19 for POPC LUVs containing 20mol% POPS). Briefly, the mean fluorescence lifetime of sCT-HL488 was constant over time (Figure 3.19A) but its value was much lower than the usual ($<\tau>_1$ ~(2.4 ± 0.1)ns versus $<\tau>_1$ ~3.5 ns obtained earlier). This result was mainly due to a decrease in the contribution of the longest lifetime component, τ_3, to the fluorescence decay of sCT-HL488, from f_3~90% to f_3~75-80%, showing that the peptide conformation/dynamics was now different in the presence of the anionic lipid vesicles. During the same period of time, the limiting anisotropy of sCT-HL488 (measured in S_2) progressively decreased (Figure 3.19B), which explains the concomitant increase in its steady-state anisotropy value (measured in S_1).

Finally, to overcome the kinetic effects described above a different methodology of sample preparation was tried. This involved re-suspending the HL488-labeled polypeptides using a liposome suspension after obtaining a peptide film due to complete evaporation of the solvent HFIP, as described in 2.3.2 for method B.

Control experiments showed that ~90% of the peptide was recovered after evaporation and ressuspension in buffer (data not shown) making this method a promising alternative to be used in the preparation of the samples. The influence of the three different methodologies used in the preparation of the conjugated peptide-containing samples on the kinetics of sCT-HL488/liposome interaction was then tested in parallel by employing both 20 and 30 mol% POPS-containing POPC LUVs. Briefly, 0.2μM sCT-HL488 samples were prepared by using method A, by either direct injection of the stock solution I or II of the derivatized peptide in HFIP to the liposome suspension, or by employing Method B, i.e. after an evaporation step of the organic solvent. Illustrative kinetic traces obtained for the steady-state fluorescence intensity and anisotropy of the samples are presented in Figure 3.20.

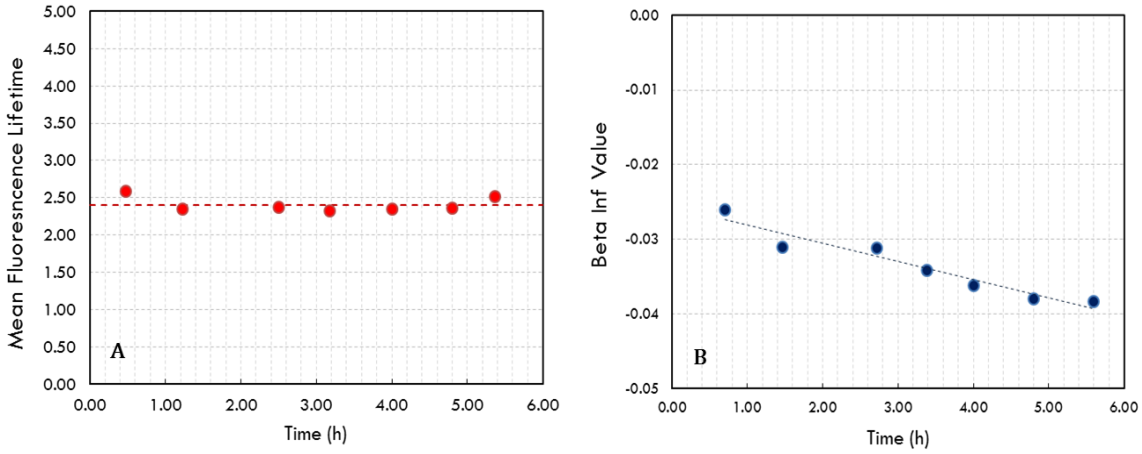

Figure 3.19: Changes in the **(A)** mean fluorescence lifetime and **(B)** limiting anisotropy value for 0.2μM sCT-HL488 in interaction with 3mM POPC:POPS 80:20 LUVs over time, using direct injection from the diluted stock - method A. Similar results were obtained for 0.2μM sCT-HL488 in interaction with 3mM POPC:POPS 70:30 LUVs over time.

The results obtained confirmed that the fluorescence signals from the samples presented a significant time evolution only when Method A/stock II solution was used (Figure 3.20A and B), since after the HFIP evaporation both fluorescence intensity and steady-state anisotropy for 0.2μM kinetics proved to be constant over time (Figure 3.20C and D). Moreover, it was found that the equilibrium values measured for the steady-state anisotropy of sCT-HL488 after an incubation period of approximately 40h varied hyperbolically with the total phospholipid concentration (Figure 3.21). By fitting equation 2.5 to the experimental data by non-linear regression, $K_p = (1.4 \pm 0.1) \times 10^5$ and $r_l = 0.249 \pm 0.005$ were obtained, which are in agreement with the previously data on Table 3.9.

In conclusion, it was established that the method used to prepare the sCT-HL488-containing samples critically affects the kinetics of its interaction with POPC liposomes prepared with a variable content of POPS, a negatively-charged phospholipid. To overcome these effects, the method used to prepare the samples was therefore switched to method B.

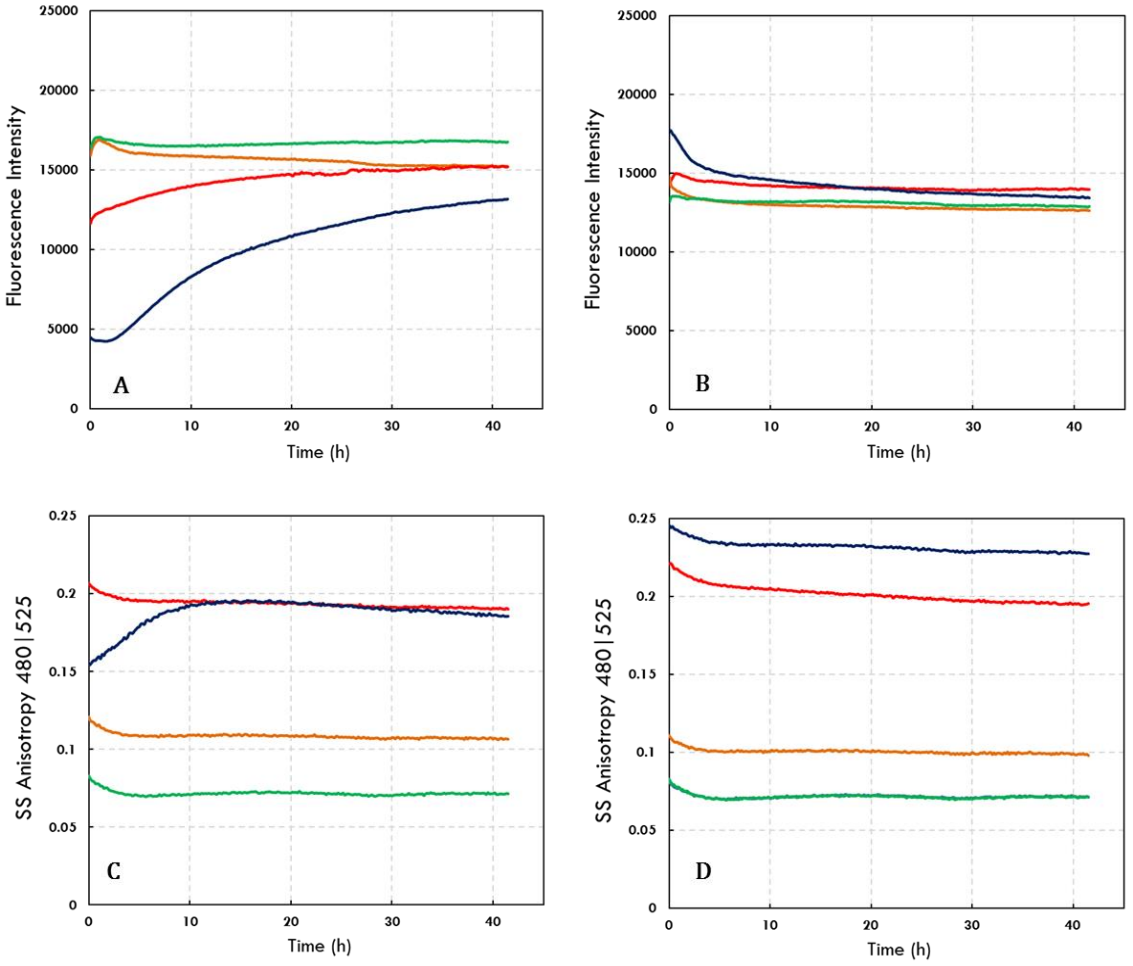

Figure 3.20: Changes in **(A and C)** the steady-state fluorescence intensity and **(B and D)** anisotropy of 0.2µM sCT-HL488 in interaction with 0mM (green curve), 0.1mM (orange curve), 1.0mM (red curve) and 3mM (blue curve) POPC:POPS 80:20 LUVs over time. (A and B) The samples were prepared using method A/stock II (direct injection from the diluted stock solution) or (C and D) using method B/stock II (using a HFIP evaporation step). The results obtained using samples prepared using method A/stock I were similar to the ones presented for method B/stock II, i.e. both the fluorescence intensity and anisotropy of the samples were constant over the incubation time.

3.2.2.3. hCT-HL488 Partition

The partition behaviour of hCT-HL488 towards anionic lipid vesicles was then studied using method B in the preparation of samples. As occurred in the intrinsic fluorescence study of hCT, described in section 3.1, no changes in the UV-vis absorption spectra or emission fluorescence (Figure 3.22A) upon addition of POPC:POPS 70:30 vesicles were detected for 1μM hCT-HL488. In addition, its steady-state anisotropy was independent of the phospholipid concentration used ($< r >= 0.079 \pm 0.002$ ($n = 11$)), revealing no interaction with the anionic lipid membranes (Figure 3.22B).

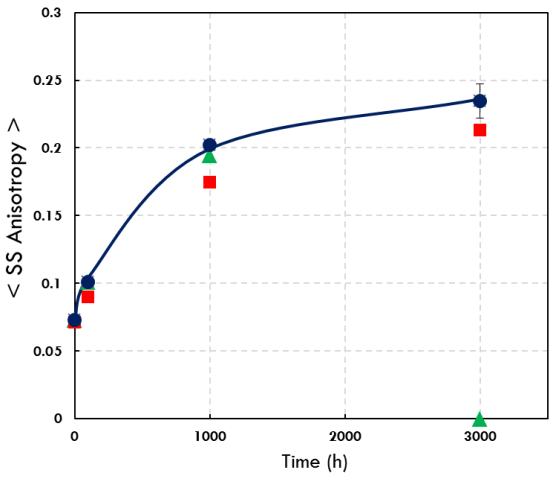

Figure 3.21: Average equilibrium steady-state fluorescence anisotropy values measured for 0.2 μM sCT-HL488 in interaction with POPC:POPS 80:20 LUVs after incubating the samples for 40h at T= 25°C. The methods used in preparing the samples were method A/stock I (red squares), method A/stock II (green triangles) and method B (blue circles), respectively. The solid line is the best fit of equation 2.5 to experimental data obtained suing method B.

In fact, even when POPC:POPS 50:50 LUVs were used in the partition study to force their interaction with hCT-HL488, still no alterations on any of the fluorescence parameters measured for hCT-HL488 were noticed ($e.g.$, $< r >= 0.084 \pm 0.003$ ($n = 11$)). Together with the results obtained from the intrinsic fluorescence studies (section3.1), our data shows that human calcitonin does not interact with POPS-containing vesicles.

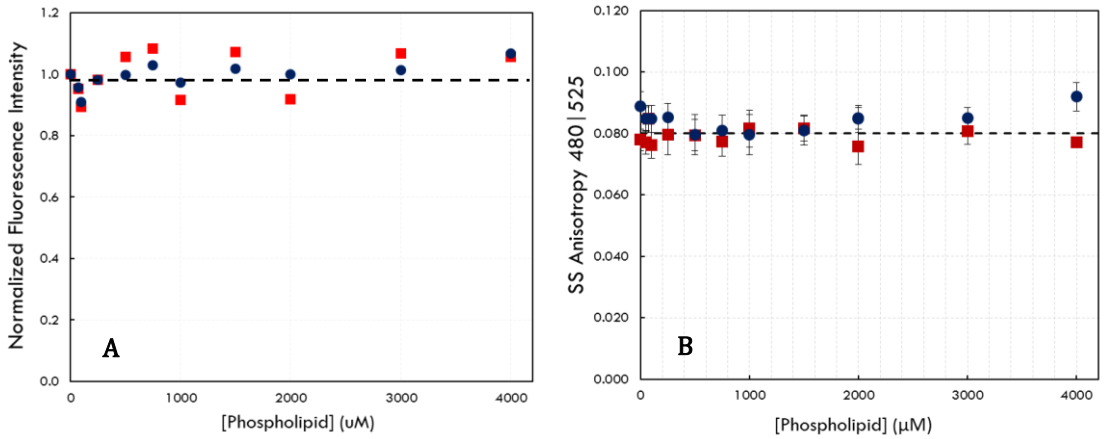

Figure 3.22: (A) The steady-state anisotropy values and **(B)** relative steady state fluorescence intensities presented a constant value upon increasing the phospholipid concentration using POPC:POPS 70:30 (blue circles) or POPC:POPS 50:50 (red squares) showing no interaction/binding of 1μM hC-HL488 to the negatively-charged phospholipids. The dashed line represented in A is the mean anisotropy value of $\langle r \rangle \sim 0.081$.

Chapter IV

Concluding Remarks

4. CONCLUDING REMARKS

In the past few years, accumulated evidence supports the conclusion that lipid membranes can catalyse the conversion of several amyloidogenic protein/peptides into toxic aggregates (amyloid assemblies) (Zhao et al. 2004; Butterfield & Lashuel 2010; Relini et al. 2013; Relini et al. 2014). The anionic phospholipid content of the lipid membranes is considered to be a major factor controlling the binding of several amyloidogenic peptides/proteins to the membrane surface and the subsequent conformational change that ultimately leads to amyloid fibril formation (King et al. 1999; Apostolidou et al. 2008; Jayasinghe & Langen 2005; Orte et al. 2008; Zhao et al. 2004). However, the detailed mechanism(s) involved in this process is (are) not yet fully understood, nor the intermediate species formed along these pathways have been completely characterized (Zhao et al. 2004; Gorbenko & Kinnunen 2006). The aim of this work was to investigate the ability of negatively-charged lipid membranes to induce the formation of amyloid assemblies under conditions close to physiological using calcitonin as model polypeptide, in order to elucidate the features that govern the formation of peptide-membrane toxic species. Hopefully, the understanding of these mechanisms will help unravelling the pathways that cause several human diseases like Alzheimer's and Parkison's diseases.

CT is a 32-amino acid peptide hormone with an *N*-terminal disulphide bridge between Cys 1 and Cys 7 and a C-terminal proline amidated residue (Figure 2.1). Both the human and salmon variants of this peptide hormone were used in this study as the time scale of their fibrillogenesis kinetics in solution is quite distinct (Diociaiuti et al. 2011). Previous studies have also already revealed prominent contributions of membrane interactions toward CT fibrillization (Arvinte & Drake 1993; Stipani et al. 2001; Diociaiuti et al. 2011) and indicated the formation of CT-induced oligomeric pores in lipid bilayers (Diociaiuti et al. 2006). However, most of these studies have been essentially qualitative, and an integrative quantitative model describing hCT and sCT interactions with membranes is still missing.

Two complementary fluorescence approaches were employed in this work when studying CT interaction with POPC LUVs containing variable mol% of POPS: the extrinsic fluorescence properties of both HL488-labeled CT variants were used for sensing their membrane binding/oligoerization and these results were compared with previously ones obtained for the unlabelled CT peptides by exploring their intrinsic fluorescence properties due to their Tyr residue (Y22 and Y12 in sCT and hCT, respectively (Figure 2.1).

Although this last methodology is non-invasive, as the auto fluorescence of both unmodified CT variants eliminates the possible perturbation introduced by the fluorescent label, its application to peptide-membrane partition studies can be compromised by the conjugation of two factors, namely the highly scattering properties of the liposome suspensions used in these studies and the characteristic low brightness of Tyr residues. After establishing a correction procedure for the impact of light-scattering on the steady-state fluorescence anisotropy measurements used to monitor CT binding to POPC LUVs containing 20mol% of POPS, a $K_p = (5.5 \pm 0.3)\text{x}10^5$ was recovered for sCT. Under the same experimental conditions, no evidence was found for hCT binding to membranes prepared with the same lipid composition.

In the second part of this work, the extrinsic fluorescence properties of both HL488-labelled CT variants were used to gain information about the polypeptide dynamics in homogeneous solution and their interaction with membranes prepared with variable anionic lipid content. As this fluorescent dye has been recently commercialized, a small set of solvents was first used to explore the environmental effects on the photophysics of both the free HL488 dye and HL488-labelled CTs. This was important to provide an interpretation framework for the spectroscopic data obtained later when studying the interaction of both HL488-labelled calcitonin variants with liposomes.

The results obtained in the solvatochromic study performed with a number of alcohols with different lengths of aliphatic chain (methanol, ethanol, propanol and butanol) and fluoro alchools (TFE and HFIP) do not conform to the general solvent effects. In fact, usually absorption spectra are less sensitive to changes in the solvent polarity, but fluorescence emission spectra are seen to shift dramatically to longer wavelengths with the increasing solvent polarity. This effect is related with the larger dipole moment in the excited state that interacts with the polar solvent molecules and reduces the energy of excited state (Lakowicz 2006). Our data, however, suggest that specific solvent effects such as hydrogen bonding, acid-base chemistry or charge transfer interactions, must be at play here due to the progressive bathochromic shift detected in the absorption and fluorescence emission spectra of both free dye and the fluorescently-labelled peptides upon reducing the dielectric constant of the medium from $\varepsilon = 80.4$ (water) to $\varepsilon = 47.0$ (glycerol), and a pronounced hypsochromic shift measured when both were solubilized in the fluoroalchools (TFE and HFIP). Since the chemical structure of the dye is unknown, it is not possible to further speculate on this topic.

At contrast with what was observed for the free dye, the fluorescence intensity decays measured for sCT-HL488 and hCT-HL488 in homogeneous medium were critically influenced by the solvent used. The dynamical fluctuations of the polypeptide chain must allow for close contact with nearby amino acids, resulting in a photon induced electron transfer (PET) quenching mechanism of HL488 caused by transient nearby residues such as tyrosine, methionine and histidine. Therefore, the fluorescence emission kinetics of the derivatized peptides reflect their conformational dynamics in the solvent used (Vaiana et al. 2009; Doose et al. 2005; Chen et al. 2010). In fact, over the last years, the effect of alcohols on the fibrillation mechanism of polypeptides in solution has been increasingly investigated. Changes in the conformational sampling of peptides depending on high, intermediate and low dielectric environments of peptides have been reported (Munishkina et al. 2003; Tanizaki et al. 2008). Fluoroalchools (HFIP and TFE) have been used to mimic the effects of membranes on proteins since these solvents destabilize the native states of proteins allowing the formation of partially unstructured forms in the case of folded proteins and partially folded forms in the case of unstructured proteins (Munishkina et al. 2003; Sekhar & Udgaonkar 2011). In addition, it has been shown that high concentrations of HFIP and TFE stabilize the helical content of some peptides (Chen & Wetzel 2001; Mukhopadhyay et al. 2006; Natalello et al. 2011) as expected from a strengthening of hydrogen-bonding interactions in lower dielectric environments, and high concentrations of methanol, ethanol and propanol stabilized the β-structure content in proteins. Wang and co-workers have recently shown that HFIP and TFE can induce almost 100% of α-helical content on bovine calcitonin, but in aqueous solution (several buffer systems were studied) only 20% of α- helical content was identified in this peptide (Wang et al. 2005). Furthermore, it has been shown that although sCT and hCT adopt a random coil conformation in aqueous solution, they easily acquire an α-helical secondary structure in the presence of organic solvents (Arvinte & Drake 1993; Diociaiuti et al. 2011).

In the near future we plan to study the conformational equilibria of both sCT and hCT as a function of the solvent used with circular dichroism (CD) as a complementary tool. Hopefully, we will be able to relate the data obtained in these studies with the complexity described for the fluorescence intensity decays obtained here for sCT-HL488 and hCT-HL488 in each solvent, which will contribute to further elucidate the dynamics of salmon and human calcitonins in homogeneous solution.

The steady-state and time-resolved fluorescence studies performed with both fluorescently-labeled CT variants further provided important information about their aggregation state in aqueous solution. The steady-state anisotropy values were found to be independent of the sCT-HL488 and hCT-HL488 concentration used (Figure 3.7). Together with the prevision from the Perrin equation, it was concluded that both peptides behave as compact monomers in aqueous solution within a wide range of concentrations (from ~1nM to ~8μM).

In the last part of our work, we were able to show that the interaction of sCT-HL488 with lipid membranes was dependent on (*i*) the method used to prepare the samples, (*ii*) the concentration of the fluorescently-labeled peptide used, and (*iii*) the mol% of POPS included on the POPC liposomes. By far, the most intriguing result obtained in this study was finding that a 8-fold dilution of the stock solution I of sCT-HL488 in HFIP critically affected the kinetics of its interaction with POPC liposomes prepared with a variable content of negatively-charged phospholipid. It was shown that upon increasing the proportion of HFIP relatively to the fluorescently-labeled peptide in stock solution II prior to its direct injection into each sample, the fluorescence measurements took a much longer time to reach an equilibrium value. This effect was apparently more pronounced upon increasing the total phospholipid concentration of the sample/anionic lipid content of the liposomes, suggestion that it was liposome-mediated. It seems that sCT-HL488 interacted very fast with the lipid vesicles used in each assay but was initially trapped in a highly quenched state, eventually with a distinct conformation/aggregation state, that slowly evolved into the usual fluorescent species. To overcome these effects, the method used to prepare the samples was therefore changed and the organic solvent was eliminated by evaporation prior to sample preparation (method B) (Rolinski et al. 2010; Amaro et al. 2011). Despite the fact that the problem was solved (i.e. slow interaction kinetics of sCT-Hl488 with the membranes), we still need to perform further studies to fully understand the origin of these effects.

Regarding the influence of sCT-HL488 concentration on its interaction with POPC:POPS 80:20 LUVs, the data obtained could be adequately described by a coupled partition/oligomerization equilibria. Briefly, using 1 and 3.4μM of sCT-HL488, the UV-Vis absorption spectrum was found to progressively red-shifted upon increasing the phospholipid concentration (Figure 3.10A), but a shoulder was detected in the blue region of their absorption spectra at low lipid concentrations (high P/L molar ratio) (Figure 3.10B).

These findings were explained by the exciton theory where the dipole-dipole interactions between interacting fluorophores in parallel geometry (H-type) generate a blue-shifted band in the absorption spectrum, showing sCT-HL488 oligomerization upon crowding of the membrane surface. Concomitantly, there was a drop in the fluorescence intensity of sCT-HL488, which was not accompanied by significant changes in its mean fluorescence lifetime. Thus, the peptide-peptide interactions that occurred at a high P/L ratio produced non-fluorescent membrane-bound oligomers (Figure 3.16).

Finally, we were able to show that CT binding to negatively-charged liposomes was dominantly driven by electrostatic interactions. The apparent partition coefficient obtained for sCT-HL488 increased exponentially with the mol% of POPS included in the LUVs, in agreement with its net charge of +3. However, no spectroscopic evidence was obtained for either sCT-Hl488 binding to POPC vesicles, nor for hCT-HL488 (with a net charge of +1) binding to 30 or 50mol% POPS-containing POPC LUVs. The possible interference of the fluorescent label used on the partition behaviour of the modified peptides was also ruled out since very similar partition coefficients were obtained for sCT and sCT-HL488 in the intrinsic and extrinsic fluorescence studies performed with POPC:POPS 80:20 LUVs. The absence of human calcitonin interaction with negatively-charged vesicles, the opposite of some other mechanisms already described in the literature (Stipani et al. 2001; Wagner et al. 2004; Herbig et al. 2005) can arise from differences on the membrane compositions, such as the use of cholesterol-rich and ganglioside-containing vesicles, which usually resulted in substantial conformational changes and substantial increase in its membrane binding affinity, as described earlier for other peptides (Jayasinghe & Langen 2005; Apostolidou et al. 2008; Knight et al. 2008; Fantini & Yahi 2010).

The intermediate oligomers formed on the fibrillization pathway of several amyloidogenic peptides/proteins (Gorbenko & Kinnunen 2006; Diociaiuti et al. 2011), often with a β-sheet structure (Relini et al. 2004; Chimon et al. 2007; Ono et al. 2009) have been identified as the main cytotoxicity species instead of the mature amyloid fibrils *per se*. The performance of additional studies using thioflavin T (ThT) binding (Ryan et al. 2008; Biancalana & Koide 2010) and CD measurements will eventually allow the detection of potential conformational changes of sCT/hCT to β-sheet rich structures as a function of (i) the peptide and phospholipid concentrations used, and (ii) lipid composition of the liposomes.

REFERENCES

Ahmed, M., Davis, J., Aucoin, D., Sato, T., Ahuja, S., Aimoto, S., Elliott, J.I., Van Nostrand, W.E. & Smith, S.O., 2010. Structural conversion of neurotoxic amyloid-beta(1-42) oligomers to fibrils. *Nature Structural & Molecular Biology*, 17(5), pp.561–7.

Amaro, M., Birch, D.J.S. & Rolinski, O.J., 2011. Beta-amyloid oligomerisation monitored by intrinsic tyrosine fluorescence. *Physical Chemistry Chemical Physics : PCCP*, 13(14), pp.6434–41.

Andreassen, K.V., Hjuler, S.T., Furness, S.G., Sexton, P.M., Christopoulos, A., Nosjean, O., Karsdal, M.A. & Henriksen, K., 2014. Prolonged calcitonin receptor signaling by salmon, but not human calcitonin, reveals ligand bias. *PloS one*, 9(3), p.e 92042.

Andreotti, G., Vitale, R.M., Avidan-Shpalter, C., Amodeo, P., Gazit, E. & Motta, A., 2011. Converting the highly amyloidogenic human calcitonin into a powerful fibril inhibitor by three-dimensional structure homology with a non-amyloidogenic analogue. *The Journal of Biological Chemistry*, 286(4), pp.2707–18.

Apostolidou, M., Jayasinghe, S.A. & Langen, R., 2008. Structure of alpha-helical membrane-bound human islet amyloid polypeptide and its implications for membrane-mediated misfolding. *The Journal of Biological Chemistry*, 283(25), pp.17205–10.

Arvinte, T. & Drake, a F., 1993. Comparative study of human and salmon calcitonin secondary structure in solutions with low dielectric constants. *The Journal of Biological Chemistry*, 268(9), pp.6408–14.

Bauer, H.H., Mueller, M., Goette, J., Merkle, H.P. & Fringeli, U.P., 1994. Interfacial Adsorption and Aggregation Associated Changes in Secondary Structure of Human Calcitonin Monitored by ATR-FTIR Spectroscopy. *Biochemistry*, 33(40), pp.12276–12282.

Bellotti, V. & Chiti, F., 2008. Amyloidogenesis in its biological environment: challenging a fundamental issue in protein misfolding diseases. *Current Opinion in Structural Biology*, 18(6), pp.771–9.

Berberan-Santos, M.N., Prieto, M.J.E. & Szabo, A.G., 1991. Excited-state intramolecular relaxation of the lipophilic probe 12-(9-anthroyloxy)stearic acid. *The Journal of Physical Chemistry*, 95(14), pp.5471–5475.

Bergström, F., Mikhalyov, I., Hägglöf, P., Wortmann, R., Ny, T. & Johansson, L.B.A., 2002. Dimers of dipyrrometheneboron difluoride (BODIPY) with light spectroscopic applications in chemistry and biology. *Journal of the American Chemical Society*, 124(2), pp.196–204.

Biancalana, M. & Koide, S., 2010. Molecular mechanism of Thioflavin-T binding to amyloid fibrils. *Biochimica et Biophysica acta*, 1804(7), pp.1405–12.

Blackley, H.K., Sanders, G.H., Davies, M.C., Roberts, C.J., Tendler, S.J. & Wilkinson, M.J., 2000. In-situ atomic force microscopy study of beta-amyloid fibrillization. *Journal of Molecular Biology*, 298(5), pp.833–40.

Bucciantini, M., Giannoni, E., Chiti, F., Baroni, F., Formigli, L., Zurdo, J., Taddei, N., Ramponi, G., Dobson, C.M. & Stefani, M., 2002. Inherent toxicity of aggregates implies a common mechanism for protein misfolding diseases. *Nature*, 416(6880), pp.507–11.

Butterfield, S.M. & Lashuel, H.A., 2010. Amyloidogenic protein-membrane interactions: Mechanistic insight from model systems. *Angewandte Chemie - International Edition*, 49(33), pp.5628–5654.

Castanho, M.A.R.B. & Prieto, M.J.E., 1992. Fluorescence study of the macrolide pentaene antibiotic filipin in aqueous solution and in a model system of membranes. *European Journal of Biochemistry*, 207(1), pp.125–134.

Castanho, M.A.R.B., Santos, N.C. & Loura, L.M.S., 1997. Separating the turbidity spectra of vesicles from the absorption spectra of membrane probes and other chromophores. *European Biophysics Journal*, 26(3), pp.253–259.

Castro, B.M., de Almeida, R.F.M., Fedorov, A. & Prieto, M., 2012. The photophysics of a Rhodamine head labeled phospholipid in the identification and characterization of membrane lipid phases. *Chemistry and Physics of Lipids*, 165(3), pp.311–9.

Chamberlain, A.K. & Bowie, J.U., 2004. Analysis of side-chain rotamers in transmembrane proteins. *Biophysical Journal*, 87(5), pp.3460–9.

Chen, H., Ahsan, S.S., Santiago-Berrios, M.B., Abruña, H.D. & Webb, W.W., 2010. Mechanisms of quenching of Alexa fluorophores by natural amino acids. *Journal of the American Chemical Society*, 132(21), pp.7244–5.

Chen, S. & Wetzel, R., 2001. Solubilization and disaggregation of polyglutamine peptides. *Protein Science : a publication of the Protein Society*, 10(4), pp.887–91.

Chi, E.Y., Ege, C., Winans, A., Majewski, J., Wu, G., Kjaer, K. & Lee, K.Y.C., 2008. Lipid membrane templates the ordering and induces the fibrillogenesis of Alzheimer's disease amyloid-beta peptide. *Proteins*, 72(1), pp.1–24.

Chimon, S., Shaibat, M.A., Jones, C.R., Calero, D.C., Aizezi, B. & Ishii, Y., 2007. Evidence of fibril-like β-sheet structures in a neurotoxic amyloid intermediate of Alzheimer's β-amyloid. *Nature Structural & Molecular Biology*, 14(12), pp.1157–64.

Chiti, F. & Dobson, C.M., 2009. Amyloid formation by globular proteins under native conditions. *Nature Chemical Biology*, 5(1), pp.15–22.

Chiti, F. & Dobson, C.M., 2006. Protein misfolding, functional amyloid, and human disease. *Annual review of Biochemistry*, 75, pp.333–66.

Chiti, F., Taddei, N., Baroni, F., Capanni, C., Stefani, M., Ramponi, G. & Dobson, C.M., 2002. Kinetic partitioning of protein folding and aggregation. *Nature Structural Biology*, 9(2), pp.137–43.

Cleary, J.P., Walsh, D.M., Hofmeister, J.J., Shankar, G.M., Kuskowski, M.A., Selkoe, D.J. & Ashe, K.H., 2005. Natural oligomers of the amyloid-beta protein specifically disrupt cognitive function. *Nature Neuroscience*, 8(1), pp.79–84.

Cleland, W.W., 1964. Dithiothreitol, a New Protective Reagent for SH Groups. *Biochemistry*, 3(4), pp.480–482.

Conway, K.A., Lee, S.J., Rochet, J.C., Ding, T.T., Williamson, R.E. & Lansbury, P.T., 2000. Acceleration of oligomerization, not fibrillization, is a shared property of both alpha-synuclein mutations linked to early-onset Parkinson's disease: implications for pathogenesis and therapy. *Proceedings of the National Academy of Sciences of the United States of America*, 97(2), pp.571–6.

Davidson, W.S., Jonas, A., Clayton, D.F. & George, J.M., 1998. Stabilization of alpha-synuclein secondary structure upon binding to synthetic membranes. *The Journal of biological chemistry*, 273(16), pp.9443–9.

Diociaiuti, M., Gaudiano, M.C. & Malchiodi-Albedi, F., 2011. The Slowly Aggregating Salmon Calcitonin: A Useful Tool for the Study of the Amyloid Oligomers Structure and Activity. *International Journal of Molecular Sciences*, 12(12), pp.9277–9295.

Diociaiuti, M., Polzi, L.Z., Valvo, L., Malchiodi-Albedi, F., Bombelli, C. & Gaudiano, M.C., 2006. Calcitonin forms oligomeric pore-like structures in lipid membranes. *Biophysical Journal*, 91(6), pp.2275–2281.

Domingues, M.M., Santiago, P.S., Castanho, M. a R.B. & Santos, N.C., 2008. What can light scattering spectroscopy do for membrane-active peptide studies? *Journal of Peptide Science : an official publication of the European Peptide Society*, 14(4), pp.394–400.

Doose, S., Neuweiler, H. & Sauer, M., 2005. A close look at fluorescence quenching of organic dyes by tryptophan. *Chemphyschem : a European Journal of Chemical Physics and Physical Chemistry*, 6(11), pp.2277–85.

Doose, S., Neuweiler, H. & Sauer, M., 2009. Fluorescence quenching by photoinduced electron transfer: a reporter for conformational dynamics of macromolecules. *Chemphyschem : a European Journal of Chemical Physics and Physical Chemistry*, 10(9-10), pp.1389–98.

Durell, S.R., Guy, H.R., Arispe, N., Rojas, E. & Pollard, H.B., 1994. Theoretical models of the ion channel structure of amyloid beta-protein. *Biophysical Journal*, 67(6), pp.2137–45.

Easter, J.H., DeToma, R.P. & Brand, L., 1976. Nanosecond time-resolved emission spectroscopy of a fluorescence probe adsorbed to L-alpha-egg lecithin vesicles. *Biophysical Journal*, 16(6), pp.571–83.

Eisinger, J. & Flores, J., 1985. Fluorometry of turbid and absorbant samples and the membrane fluidity of intact erythrocytes. *Biophysical Journal*, 48(1), pp.77–84.

Ellis, J.P., Culviner, P.H. & Cavagnero, S., 2009. Confined dynamics of a ribosome-bound nascent globin: Cone angle analysis of fluorescence depolarization decays in the presence of two local motions. *Protein Science : a publication of the Protein Society*, 18(10), pp.2003–15.

Fantini, J. & Yahi, N., 2010. Molecular insights into amyloid regulation by membrane cholesterol and sphingolipids: common mechanisms in neurodegenerative diseases. *Expert reviews in Molecular Medicine*, 12, p.e27.

Faustino, A.F., Carvalho, F. a, Martins, I.C., Castanho, M. a R.B., Mohana-Borges, R., Almeida, F.C.L., Da Poian, A.T. & Santos, N.C., 2014. Dengue virus capsid protein interacts specifically with very low-density lipoproteins. *Nanomedicine : Nanotechnology, Biology, and Medicine*, 10(1), pp.247–55.

Ferreon, A.C.M., Gambin, Y., Lemke, E.A. & Deniz, A.A., 2009. Interplay of alpha-synuclein binding and conformational switching probed by single-molecule fluorescence. *Proceedings of the National Academy of Sciences of the United States of America*, 106(14), pp.5645–50.

Fery-Forgues, S. & Lavabre, D., 1999. Are Fluorescence Quantum Yields So Tricky to Measure? A Demonstration Using Familiar Stationery Products. *Journal of Chemical Education*, 76(9), p.1260.

Freire, J.M., Domingues, M.M., Matos, J., Melo, M.N., Veiga, A.S., Santos, N.C. & Castanho, M.A.R.B., 2011. Using zeta-potential measurements to quantify peptide partition to lipid membranes. *European Biophysics Journal*, 40(4), pp.481–487.

Frisken, B.J., 2001. Revisiting the method of cumulants for the analysis of dynamic light-scattering data. *Applied Optics*, 40(24), pp.4087–91.

García-Sáez, A.J. & Schwille, P., 2010. Surface analysis of membrane dynamics. *Biochimica et Biophysica acta*, 1798(4), pp.766–76.

Glabe, C.G., 2008. Structural classification of toxic amyloid oligomers. *The Journal of Biological Chemistry*, 283(44), pp.29639–43.

Gorbenko, G.P. & Kinnunen, P.K.J., 2006. The role of lipid-protein interactions in amyloid-type protein fibril formation. *Chemistry and Physics of Lipids*, 141(1-2), pp.72–82.

Green, B., Uniuersity, S. & September, R., 1989. Aggregation Phenomena in Xanthene Dyed. Acc. Chem. Res., (23), pp.171–177.

Haidekker, M. a, Brady, T.P., Lichlyter, D. & Theodorakis, E. a, 2005. Effects of solvent polarity and solvent viscosity on the fluorescent properties of molecular rotors and related probes. *Bioorganic Chemistry*, 33(6), pp.415–25.

Hamada, D. & Dobson, C.M., 2002. A kinetic study of beta-lactoglobulin amyloid fibril formation promoted by urea. *Protein science : a publication of the Protein Society*, 11(10), pp.2417–26.

Hartl, F.U. & Hayer-Hartl, M., 2009. Converging concepts of protein folding in vitro and in vivo. *Nature Structural & Molecular Biology*, 16(6), pp.574–81.

Hebda, J. a & Miranker, A.D., 2009. The interplay of catalysis and toxicity by amyloid intermediates on lipid bilayers: insights from type II diabetes. *Annual review of Biophysics*, 38, pp.125–52.

Herbig, M.E., Weller, K., Krauss, U., Beck-Sickinger, A.G., Merkle, H.P. & Zerbe, O., 2005. Membrane surface-associated helices promote lipid interactions and cellular uptake of human calcitonin-derived cell penetrating peptides. *Biophysical Journal*, 89(6), pp.4056–66.

Hipp, M.S., Park, S.-H. & Hartl, F.U., 2014. Proteostasis impairment in protein-misfolding and -aggregation diseases. *Trends in Cell Biology*. Vol 24.,No. 9.

Itoh-Watanabe, H., Kamihira-Ishijima, M., Kawamura, I., Kondoh, M., Nakakoshi, M., Sato, M. & Naito, A., 2013. Characterization of the spherical intermediates and fibril formation of hCT in HEPES solution using solid-state (13)C-NMR and transmission electron microscopy. *Physical Chemistry Chemical Physics : PCCP*, 15(39), pp.16956–64.

Jahn, T.R. & Radford, S.E., 2005. The Yin and Yang of protein folding. *The FEBS Journal*, 272(23), pp.5962–70.

Jayasinghe, S.A. & Langen, R., 2005. Lipid membranes modulate the structure of islet amyloid polypeptide. *Biochemistry*, 44(36), pp.12113–9.

Jha, A., Narayan, S., Udgaonkar, J.B. & Krishnamoorthy, G., 2012. Solvent-induced tuning of internal structure in a protein amyloid protofibril. *Biophysical Journal*, 103(4), pp.797–806.

Jo, E., McLaurin, J., Yip, C.M., St George-Hyslop, P. & Fraser, P.E., 2000. alpha-Synuclein membrane interactions and lipid specificity. *The Journal of Biological Chemistry*, 275(44), pp.34328–34.

Jonsson, A., Ståhl, S., Ha, T., Hoyer, W. & Gro, C., 2008. Stabilization of a Beta-hairpin in monomeric Alzheimer's amyloid-beta peptide inhibits amyloid formation, *PNAS*, 105(13), pp.5099–5104.

Jungbauer, L.M., Yu, C., Laxton, K.J. & LaDu, M.J., 2009. Preparation of fluorescently-labeled amyloid-beta peptide assemblies: the effect of fluorophore conjugation on structure and function. *Journal of molecular Recognition : JMR*, 22(5), pp.403–13.

Kanaori, K. & Nosaka, A.Y., 1995. Study of human calcitonin fibrillation by proton nuclear magnetic resonance spectroscopy. *Biochemistry*, 34(38), pp.12138–43.

Kasha, M., Rawls, H.R. & Ashraf El-Bayoumi, M., 1965. The exciton model in molecular spectroscopy. *Pure and Applied Chemistry*, 11(3-4), pp.371–392.

Kelly, J.W., 1998. The alternative conformations of amyloidogenic proteins and their multi-step assembly pathways. *Current opinion in Structural Biology*, 8(1), pp.101–6.

Kim, W. & Hecht, M.H., 2005. Sequence determinants of enhanced amyloidogenicity of Alzheimer A{beta}42 peptide relative to A{beta}40. *The Journal of Biological Chemistry*, 280(41), pp.35069–76.

King, M.E., Ahuja, V., Binder, L.I. & Kuret, J., 1999. Ligand-dependent tau filament formation: implications for Alzheimer's disease progression. *Biochemistry*, 38(45), pp.14851–9.

Knight, J.D. & Miranker, A.D., 2004. Phospholipid catalysis of diabetic amyloid assembly. *Journal of Molecular Biology*, 341(5), pp.1175–87.

Knight, J.D., Williamson, J.A. & Miranker, A.D., 2008. Interaction of membrane-bound islet amyloid polypeptide with soluble and crystalline insulin. *Protein Science : a publication of the Protein Society*, 17(10), pp.1850–6.

Lakowicz, J.R., 2006. *Principles of fluorescence spectroscopy*, Boston, MA.

Lundberg, K.M., Stenland, C.J., Cohen, F.E., Prusiner, S.B. & Millhauser, G.L., 1997. Kinetics and mechanism of amyloid formation by the prion protein H1 peptide as determined by time-dependent ESR. *Chemistry & biology*, 4(5), pp.345–55.

Mäler, L. & Gräslund, A., 2009. Artificial membrane models for the study of macromolecular delivery. *Methods in Molecular Biology (Clifton, N.J.)*, 480, pp.129–39.

Marcon, G., Plakoutsi, G., Canale, C., Relini, A., Taddei, N., Dobson, C.M., Ramponi, G. & Chiti, F., 2005. Amyloid formation from HypF-N under conditions in which the protein is initially in its native state. *Journal of Molecular Biology*, 347(2), pp.323–35.

Mayer, L.D., Hope, M.J. & Cullis, P.R., 1986. Vesicles of variable sizes produced by a rapid extrusion procedure. *Biochimica et Biophysica Acta*, 858(1), pp.161–168.

McClare, C.W.F., 1971. An accurate and convenient organic phosphorus assay. *Analytical Biochemistry*, 39(2), pp.527–530.

Melo, A.M., Fedorov, A., Prieto, M. & Coutinho, A., 2014. Exploring homo-FRET to quantify the oligomer stoichiometry of membrane-bound proteins involved in a cooperative partition equilibrium. *Physical Chemistry Chemical Physics : PCCP*.

Melo, A.M., Prieto, M. & Coutinho, A., 2011. The effect of variable liposome brightness on quantifying lipid-protein interactions using fluorescence correlation spectroscopy. *Biochimica et Biophysica Acta*, 1808(10), pp.2559–68.

Melo, A.M., Ricardo, J.C., Fedorov, A., Prieto, M. & Coutinho, A., 2013. Fluorescence detection of lipid-induced oligomeric intermediates involved in lysozyme "amyloid-like" fiber formation driven by anionic membranes. *Journal of Physical Chemistry B*, 117(10), pp.2906–2917.

Mobley, D.L., Cox, D.L., Singh, R.R.P., Maddox, M.W. & Longo, M.L., 2004. Modeling amyloid beta-peptide insertion into lipid bilayers. *Biophysical Journal*, 86(6), pp.3585–97.

Mukhopadhyay, S., Nayak, P.K., Udgaonkar, J.B. & Krishnamoorthy, G., 2006. Characterization of the formation of amyloid protofibrils from barstar by mapping residue-specific fluorescence dynamics. *Journal of Molecular Biology*, 358(4), pp.935–42.

Muller, J.M., van Ginkel, G. & van Faassen, E.E., 1996. Effect of lipid molecular structure and gramicidin A on the core of lipid vesicle bilayers. A time-resolved fluorescence depolarization study. *Biochemistry*, 35(2), pp.488–97.

Munishkina, L.A. & Fink, A.L., 2007. Fluorescence as a method to reveal structures and membrane-interactions of amyloidogenic proteins. *Biochimica et Biophysica Acta*, 1768(8), pp.1862–85.

Munishkina, L.A., Phelan, C., Uversky, V.N. & Fink, A.L., 2003. Conformational behavior and aggregation of alpha-synuclein in organic solvents: modeling the effects of membranes. *Biochemistry*, 42(9), pp.2720–30.

Murphy, R., 1997. Static and dynamic light scattering of biological macromolecules: what can we learn? *Current opinion in Biotechnology*, 8(1), pp.25–30.

Natalello, A., Benetti, F., Doglia, S.M., Legname, G. & Grandori, R., 2011. Compact conformations of α-synuclein induced by alcohols and copper. *Proteins*, 79(2), pp.611–21.

Nath, A. & Rhoades, E., 2013. A flash in the pan: Dissecting dynamic amyloid intermediates using fluorescence. *FEBS Letters*, 587(8), pp.1096–1105.

Noronha, M., Lima, J.C., Paci, E., Santos, H. & Maçanita, A.L., 2007. Tracking local conformational changes of ribonuclease A using picosecond time-resolved fluorescence of the six tyrosine residues. *Biophysical Journal*, 92(12), pp.4401–14.

Ono, K., Condron, M.M. & Teplow, D.B., 2009. Structure-neurotoxicity relationships of amyloid beta-protein oligomers. *Proceedings of the National Academy of Sciences of the United States of America*, 106(35), pp.14745–50.

Orte, A., Birkett, N.R., Clarke, R.W., Devlin, G.L., Dobson, C.M. & Klenerman, D., 2008. Direct characterization of amyloidogenic oligomers by single-molecule fluorescence. *Proceedings of the National Academy of Sciences of the United States of America*, 105(38), pp.14424–14429.

Pace, C.N., Vajdos, F., Fee, L., Grimsley, G. & Gray, T., 1995. How to measure and predict the molar absorption coefficient of a protein. *Protein science : a publication of the Protein Society*, 4(11), pp.2411–2423.

Pal, S.K., Peon, J. & Zewail, A.H., 2002. Biological water at the protein surface: dynamical solvation probed directly with femtosecond resolution. *Proceedings of the National Academy of Sciences of the United States of America*, 99(4), pp.1763–8.

Pastor, I., Ferrer, M.L., Lillo, M.P., Gomez, J. & Mateo, C.R., 2007. Structure and dynamics of lysozyme encapsulated in a silica sol-gel matrix. *Journal of Physical Chemistry B*, 111(39), pp.11603–11610.

Poirier, M.A., Li, H., Macosko, J., Cai, S., Amzel, M. & Ross, C.A., 2002. Huntingtin spheroids and protofibrils as precursors in polyglutamine fibrilization. *The Journal of Biological Chemistry*, 277(43), pp.41032–7.

Poveda, J.A., Prieto, M., Encinar, J.A., Gonz??lez-Ros, J.M. & Mateo, C.R., 2003. Intrinsic tyrosine fluorescence as a tool to study the interaction of the Shaker B "ball" peptide with anionic membranes. *Biochemistry*, 42(23), pp.7124–7132.

Quintas, A., 2013. What drives an amyloid protein precursor from an amyloidogenic to a native-like aggregation pathway?. OA *Biochemistry* (1), pp.1–8.

Quist, A., Doudevski, I., Lin, H., Azimova, R., Ng, D., Frangione, B., Kagan, B., Ghiso, J. & Lal, R., 2005. Amyloid ion channels: a common structural link for protein-misfolding disease. *Proceedings of the National Academy of Sciences of the United States of America*, 102(30), pp.10427–32.

Raffen, R., Dieckman, L.J., Szpunar, M., Wunschl, C., Pokkuluri, P.R., Dave, P., Wilkins Stevens, P., Cai, X., Schiffer, M. & Stevens, F.J., 1999. Physicochemical consequences of amino acid variations that contribute to fibril formation by immunoglobulin light chains. *Protein Science : a publication of the Protein Society*, 8(3), pp.509–17.

Relini, A., Marano, N. & Gliozzi, A., 2013. Misfolding of amyloidogenic proteins and their interactions with membranes. *Biomolecules*, 4(1), pp.20–55.

Relini, A., Marano, N. & Gliozzi, A., 2014. Probing the interplay between amyloidogenic proteins and membranes using lipid monolayers and bilayers. *Advances in Colloid and Interface Science*, 207, pp.81–92.

Relini, A., Torrassa, S., Rolandi, R., Gliozzi, A., Rosano, C., Canale, C., Bolognesi, M., Plakoutsi, G., Bucciantini, M., Chiti, F. & Stefani, M., 2004. Monitoring the process of HypF fibrillization and liposome permeabilization by protofibrils. *Journal of Molecular Biology*, 338(5), pp.943–57.

Rennella, E., Cutuil, T., Schanda, P., Ayala, I., Gabel, F., Forge, V., Corazza, A., Esposito, G. & Brutscher, B., 2013. Oligomeric states along the folding pathways of β2-microglobulin: kinetics, thermodynamics, and structure. *Journal of Molecular Biology*, 425(15), pp.2722–36.

Rochet, J.C. & Lansbury, P.T., 2000. Amyloid fibrillogenesis: themes and variations. *Current opinion in Structural Biology*, 10(1), pp.60–8.

Rolinski, O.J., Amaro, M. & Birch, D.J.S., 2010. Early detection of amyloid aggregation using intrinsic fluorescence. *Biosensors & Bioelectronics*, 25(10), pp.2249–52.

Royer, C.A., Mann, C.J. & Matthews, C.R., 1993. the fluorescence equilibrium unfolding profile. *Protein science: a publication of the Protein Society in Science*, pp.1844–1852.

Rusinova, E., Tretyachenko-Ladokhina, V., Vele, O.E., Senear, D.F. & Alexander Ross, J.B., 2002. Alexa and Oregon Green dyes as fluorescence anisotropy probes for measuring protein-protein and protein-nucleic acid interactions. *Analytical Biochemistry*, 308(1), pp.18–25.

Ryan, T.M., Howlett, G.J. & Bailey, M.F., 2008. Fluorescence detection of a lipid-induced tetrameric intermediate in amyloid fibril formation by apolipoprotein C-II. *The Journal of Biological Chemistry*, 283(50), pp.35118–28.

Rymer, D.L. & Good, T.A., 2001. The role of G protein activation in the toxicity of amyloidogenic Abeta-(1-40), Abeta-(25-35), and bovine calcitonin. *The Journal of Biological Chemistry*, 276(4), pp.2523–30.

Santos, N.C., Prieto, M. & Castanho, M.A.R.B., 2003. *Quantifying molecular partition into model systems of biomembranes: An emphasis on optical spectroscopic methods*, Biochimica et Biophysica Acta - Biomembranes, 1612, (2), pp. 123-135.

Schauerte, J.A., Wong, P.T., Wisser, K.C., Ding, H., Steel, D.G. & Gafni, A., 2010. Simultaneous single-molecule fluorescence and conductivity studies reveal distinct classes of Abeta species on lipid bilayers. *Biochemistry*, 49(14), pp.3031–3039.

Schröder, G.F., Alexiev, U. & Grubmüller, H., 2005. Simulation of fluorescence anisotropy experiments: probing protein dynamics. *Biophysical Journal*, 89(6), pp.3757–70.

Seelig, J., 2004. Thermodynamics of lipid – peptide interactions. Biochimica et biophysica acta, 1666, pp.40–50.

Sekhar, A. & Udgaonkar, J.B., 2011. Fluoroalcohol-induced modulation of the pathway of amyloid protofibril formation by barstar. *Biochemistry*, 50(5), pp.805–819.

Sirangelo, I., Malmo, C., Iannuzzi, C., Mezzogiorno, A., Bianco, M.R., Papa, M. & Irace, G., 2004. Fibrillogenesis and cytotoxic activity of the amyloid-forming apomyoglobin mutant W7FW14F. *The Journal of biological chemistry*, 279(13), pp.13183–9.

Sparr, E., Engel, M.F.M., Sakharov, D. V, Sprong, M., Jacobs, J., de Kruijff, B., Höppener, J.W.M. & Killian, J.A., 2004. Islet amyloid polypeptide-induced membrane leakage involves uptake of lipids by forming amyloid fibers. *FEBS letters*, 577(1-2), pp.117–20.

Stipani, V., Gallucci, E., Micelli, S., Picciarelli, V. & Benz, R., 2001. Channel formation by salmon and human calcitonin in black lipid membranes. *Biophysical journal*, 81(6), pp.3332–8.

Tanizaki, S., Clifford, J., Connelly, B.D. & Feig, M., 2008. Conformational sampling of peptides in cellular environments. *Biophysical Journal*, 94(3), pp.747–59.

Tomski, S.J. & Murphy, R.M., 1992. Kinetics of aggregation of synthetic β-amyloid peptide. *Archives of Biochemistry and Biophysics*, 294(2), pp.630–638.

Torres-lugo, M. & Peppas, N.A., 2000. Transmucosal delivery systems for calcitonin : a review. Biomaterials, 21, 1191-1196.

Uversky, V.N., 2013. Unusual biophysics of intrinsically disordered proteins. *Biochimica et Biophysica Acta*, 1834(5), pp.932–51.

Vaiana, A.C., Neuweiler, H., Schulz, A., Wolfrum, J., Sauer, M. & Smith, J.C., 2003. Fluorescence quenching of dyes by tryptophan: interactions at atomic detail from combination of experiment and computer simulation. *Journal of the American Chemical Society*, 125(47), pp.14564–72.

Vaiana, S.M., Best, R.B., Yau, W.-M., Eaton, W.A. & Hofrichter, J., 2009. Evidence for a partially structured state of the amylin monomer. *Biophysical Journal*, 97(11), pp.2948–57.

Valeur, B., 2002. *Molecular Fluorescence*, Wiley-VCH Verlag GmbH.

Vilar, M., Chou, H.-T., Lührs, T., Maji, S.K., Riek-Loher, D., Verel, R., Manning, G., Stahlberg, H. & Riek, R., 2008. The fold of alpha-synuclein fibrils. *Proceedings of the National Academy of Sciences of the United States of America*, 105(25), pp.8637–42.

Wagner, K., Van Mau, N., Boichot, S., Kajava, A. V, Krauss, U., Le Grimellec, C., Beck-Sickinger, A. & Heitz, F., 2004. Interactions of the human calcitonin fragment 9-32 with phospholipids: a monolayer study. *Biophysical Journal*, 87(1), pp.386–95.

Wang, S.S.-S., Good, T.A. & Rymer, D.L., 2005. The influence of phospholipid membranes on bovine calcitonin secondary structure and amyloid formation. *Protein science : a publication of the Protein Society*, 14(6), pp.1419–1428.

Wong, P.T., Schauerte, J.A., Wisser, K.C., Ding, H., Lee, E.L., Steel, D.G. & Gafni, A., 2009. Amyloid-beta membrane binding and permeabilization are distinct processes influenced separately by membrane charge and fluidity. *Journal of Molecular Biology*, 386(1), pp.81–96.

Yamaguchi, K., Naiki, H. & Goto, Y., 2006. Mechanism by which the amyloid-like fibrils of a beta 2-microglobulin fragment are induced by fluorine-substituted alcohols. *Journal of Molecular Biology*, 363(1), pp.279–88.

Zanin, L.M.P., Dos Santos Alvares, D., Juliano, M.A., Pazin, W.M., Ito, A.S. & Ruggiero Neto, J., 2013. Interaction of a synthetic antimicrobial peptide with model membrane by fluorescence spectroscopy. *European Biophysics Journal : EBJ*, 42(11-12), pp.819–31.

Zhao, H., Tuominen, E.K.J. & Kinnunen, P.K.J., 2004. Formation of amyloid fibers triggered by phosphatidylserine-containing membranes. *Biochemistry*, 43(32), pp.10302–7.